UNIVERSITAT
POLITÈCNICA
DE VALÈNCIA

Impact Evaluation of Future Climate and Land Use Scenarios on Water and Sediment Regime using Distributed Hydrological Modelling in a Tropical Rainforest Catchment in West Java (Indonesia)

Dissertation of Doctor

SHANTOSA YUDHA SISWANTO

Advisor:

Dr. FÉLIX FRANCÉS GARCÍA

Valencia, July, 2020

ACKNOWLEDGEMENTS

Abstract

Climate change has occurred in Indonesia, for example, increasing the surface air temperature, including in the Upper Citarum watershed. This phenomenon leads to a lack of water in the dry season, which lowers agriculture production and remains a great obstacle for agricultural activity. Meanwhile, human activity has produced severe LULC changes within the Upper Citarum watershed. This occurs due to the demands of the ever-increasing population growth in the region. As a result, rice field and forested areas have been sacrificed to compensate the urban increment. The general objective of this dissertation is to understand and analyze the impact of climate and LULC changes on the hydrological process and their relationship with historical and future changes by using spatially distributed modeling on the Upper Citarum tropical catchment. The distributed model TETIS has been implemented to obtain the results of past and future scenarios on the water and sediment cycles. Annual historical bathymetries in the reservoir were used to calibrate and validate the sediment sub-model involving Miller's density evolution and trap efficiency of Brune's equation. Climate change has been considered under RCP 4.5 and RCP 8.5 trajectories. Meanwhile, to overcome the LULC problem, historical and future LULCs have been studied. LCM model was used to forecast the LULC in 2029. The forecasted results of LCM model show, on one hand, a continuation in the expansion of urban areas at the expense of the contiguous rice fields. The results determined that deforestation and urbanization were the most influential factors for the alteration of the hydrological and sedimentological processes in the Upper Citarum Catchment. Thus, it decreases evapotranspiration, increases water yield by increasing all its components; overland flow, interflow and baseflow. The changes in LULC are currently producing and will produce in the future, a relatively small increment of erosion rates, increasing the area exceeds *Tsl* erosion. Sediment yield will increase in 2029 as the result of erosion increment. Other LULC scenarios such as conservation, government plan and natural vegetation scenarios are expected to have an increment in total evapotranspiration, the water yield is expected to decrease. Flood regime, erosion and sedimentation are reduced dramatically. Hence, it leads to a massive increment of reservoir and hydropower lifetime signed by a very long period of the lifetime. Climate change alters the magnitude of water balance and can be identified from the shift of infiltration, overland flow, interflow, baseflow and water yield. Those increments finally change the flood regime, catchment erosion. RCP 8.5 trajectory gives a bigger impact compared to RCP 4.5 trajectory on hydrological and sediment cycle. . LULC change results a bigger impact on water balance, flood regime, erosion and sedimentation. The combination of climate and LULC change give a bigger impact on the flows of water balance, erosion, flood, sedimentation and will be catastrophic for the hydropower operation of the Saguling Dam.

Resumen

El cambio climático ha afectado a Indonesia, por ejemplo, incrementando la temperatura del aire en la superficie, incluso en la cuenca del Upper Citarum. Este fenómeno conduce a la falta de agua en la estación seca, reduciendo la producción agrícola lo que es un gran obstáculo para su actividad. Además, la actividad humana ha producido cambios severos en LULC en la cuenca del Upper Citarum, Indonesia. Esto se debe al elevado crecimiento de la población en la región, por el que se han convertido campos de arroz y áreas boscosas en suelo urbano. De esta forma, el objetivo general de esta tesis es comprender y analizar el impacto de los cambios climáticos y LULC en el proceso hidrológico y su relación con los cambios históricos y futuros mediante el uso de modelos distribuidos espacialmente en la cuenca tropical del Upper Citarum. El modelo distribuido TETIS se ha implementado para obtener los resultados de escenarios pasados y futuros en los ciclos de agua y sedimentos. Se usaron batimetrías históricas anuales en el embalse para calibrar y validar el submodelo de sedimentos que involucra la evolución de la densidad de Miller y la eficiencia de retención de la ecuación de Brune. Con el fin de arrojar más luz sobre estos problemas, el escenario de cambio climático se ha implementado en base al modelo de cambio climático bajo las trayectorias RCP 4.5 y RCP 8.5. Además, para intentar resolver el problema LULC, también se ha implementado el LULC histórico y futuro. El modelo LCM se usó para pronosticar el LULC en 2029 y los resultados muestran, por un lado, una continuación en la expansión de las áreas urbanas a expensas de los arrozales contiguos. Los resultados determinaron que la deforestación y la urbanización fueron los factores más influyentes para la alteración de los procesos hidrológicos y sedimentológicos en la cuenca del Upper Citarum. Por lo tanto, disminuye la evapotranspiración, aumenta la producción de agua al aumentar todos sus componentes; escorrentía, interflujo y flujo base. Los cambios en LULC están produciendo y producirán, un incremento relativamente pequeño de las tasas de erosión, aumentando el área excede la erosión de Tsl. La producción de sedimentos aumentará en 2029 como resultado del incremento de la erosión. Se espera que otros escenarios de LULC como la conservación, el plan gubernamental y los escenarios de vegetación natural tengan un incremento en la evapotranspiración total, y se espera que la producción de agua disminuya. El régimen de inundación, la erosión y la sedimentación se reducen drásticamente. Por lo tanto, habrá un incremento de la vida útil del embalse y la energía hidroeléctrica. El cambio climático altera la magnitud del equilibrio hídrico y puede identificarse a partir del cambio de infiltración, escorrentía, interflujo, flujo base y producción de agua. Esos incrementos finalmente cambian el régimen de inundación y erosión de la cuenca. La trayectoria RCP 8.5 tiene un mayor impacto en comparación con la trayectoria RCP 4.5 en el ciclo hidrológico y de sedimentos. El cambio de LULC tiene un mayor impacto en el balance hídrico, el régimen de inundación, la erosión y la sedimentación. La combinación del cambio climático y LULC tiene un mayor impacto en los flujos de equilibrio hídrico, erosión, inundación, sedimentación y será catastrófico para la operación hidroeléctrica de la presa Saguling.

Resum

El canvi climàtic ha afectat Indonèsia, per exemple, incrementant la temperatura de l'aire en la superfície, inclús en la conca de l'Upper Citarum. Aquest fenomen conduïx a la falta d'aigua en l'estació seca, reduint la producció agrícola, el que és un gran obstacle per a la seua activitat. A més, l'activitat humana ha produït canvis severs en LULC en la conca de l'Upper Citarum, Indonèsia. Açò es deu a l'elevat creixement de la població en la regió, motiu pel qual s'han anat convertint camps d'arròs i àrees boscoses en sòl urbà. D'aquesta manera, l'objectiu general d'aquesta tesi és comprendre i analitzar l'impacte dels canvis climàtics i LULC en el procés hidrològic i la seua relació amb els canvis històrics i futurs per mitjà de l'ús de models distribuïts espacialment en la conca tropical de l'Upper Citarum. El model distribuït TETIS s'ha implementat per a obtindre els resultats d'escenaris passats i futurs en els cicles de l'aigua i sediments. Es van usar batimetries històriques anuals en l'embassament per a calibrar i validar el submodel de sediments que involucra l'evolució de la densitat de Miller i l'eficiència de retenció de l'equació de Brune. Amb la finalitat de donar més llum a aquests problemes, l'escenari de canvi climàtic s'ha implementat basant-se en el model de canvi climàtic davall les trajectòries RCP 4.5 i RCP 8.5. A més, per a intentar resoldre el problema LULC, també s'ha implementat el LULC històric i futur. El model LCM es va usar per a pronosticar el LULC en 2029 i els resultats mostren, d'una banda, una continuació en l'expansió de les àrees urbanes a costa dels arrossars contigus. Els resultats van determinar que la desforestació i la urbanització van ser els factors més influents per a l'alteració dels processos hidrològics i sedimentològics en la conca de l'Upper Citarum. Per tant, disminuïx l'evapotranspiració, augmenta la producció d'aigua en augmentar tots els seus components; escorrentia, interflux i flux base. Els canvis en LULC estan produint i produiran, un increment relativament xicotet de les taxes d'erosió, augmentant l'àrea excedix l'erosió de Tsl. La producció de sediments augmentarà en 2029 com a resultat de l'increment de l'erosió. S'espera que altres escenaris de LULC com la conservació, el pla governamental i els escenaris de vegetació natural tinguen un increment en l'evapotranspiració total, i s'espera que la producció d'aigua disminuïsca. El règim d'inundació, l'erosió i la sedimentació es reduïxen dràsticament. Per tant, hi haurà un increment de la vida útil de l'embassament i l'energia hidroelèctrica. El canvi climàtic altera la magnitud de l'equilibri hídric i pot identificar-se a partir del canvi d'infiltració, escorrentia, interflux, flux base i producció d'aigua. Eixos increments finalment canvien el règim d'inundació i erosió de la conca. La trajectòria RCP 8.5 té un major impacte en comparació amb la trajectòria RCP 4.5 en el cicle hidrològic i de sediments. El canvi de LULC té un major impacte en el balanç hídric, el règim d'inundació, l'erosió i la sedimentació. La combinació del canvi climàtic i LULC té un major impacte en els fluxos d'equilibri hídric, erosió, inundació, sedimentació i serà catastròfic per a l'operació hidroelèctrica de la presa Saguling.

Table of Contents

List of Figures

List of Tables

CHAPTER 1. INTRODUCTION

1.1   Background of the study and problem statement

The study area is the Upper part of Citarum Catchment, which drains into the Saguling reservoir located in West Java, Indonesia. The Upper Citarum Catchment provides the water supply for agricultural and urban areas as well as supplying the hydroelectricity for the region. Together with the Middle and Lower Citarum Catchment, the entire watershed provides 7,650 million cubic meters of water per year (m^3 y^{-1}); approximately 5,750 million m^3 y^{-1} (75%) comes from Citarum Catchment dams (Saguling, Cirata and Jatiluhur) and 1,950 million m^3 y^{-1} (25%) comes from other rivers. Saguling reservoir itself provides 1.008 MW of electricity (Hidayat *et al.*, 2013). Currently, approximately 78% of the water is used for irrigation, 14% for industrial activities and electricity generation and 8% for domestic consumption (Boer *et al.*, 2012).

Land use change has been identified clearly in Upper Citarum Catchment from 1990 to 2010 as the result of economical anthropogenic activity (Noda *et al.*, 2017). It results in a massif changes of water balance. Hence, it disturbs human activity such as scarcity of water for consumption and irrigation, flood, erosion and lower dam capacity that lowers the electricity and water lifetime. Moreover, the evidence of climate change can be seen from the climatological records of several numbers of climatology stations in the Upper Citarum Catchment over the last few decades (Kuntoro, Cahyono and Soentoro, 2018). For example, annual rainfall amount has decreased between 1896 and 1991 and declines its annual water discharge by 9.8% and 3.2% (Boer *et al.*, 2012).

1.1.1   Land use land cover change

Land use change refers to a change in the use or management of land by humans, which may lead to a change in land cover (Mach, Stechow and Planton, 2014) and (Mukundan *et al.*, 2013). The increase in urban and agricultural cultivation areas will attribute the rapid population increment. Furthermore, the forest will be impacted by this occurrence (Figure 1). The decline in the number of forest areas will negatively affect the balance of the nature, such as the rising of carbon content in the atmosphere, increase

evaporation, reduce transpiration of plants, etc. These phenomena can be found in Figure 2 resulted from three Integrated Science Assessment Model (ISAM) data sets. ISAM-HYDE refers to different data sets on cropland and pastureland based on historical database of the global environment by Klein Goldewijk et al. (2011). ISAM-RF is a dataset based on new pastureland estimates and updated cropland estimates by Ramankutty and Foley (1999). Meanwhile, ISAM-HH is a dataset of regional estimates based on Houghton (2008).
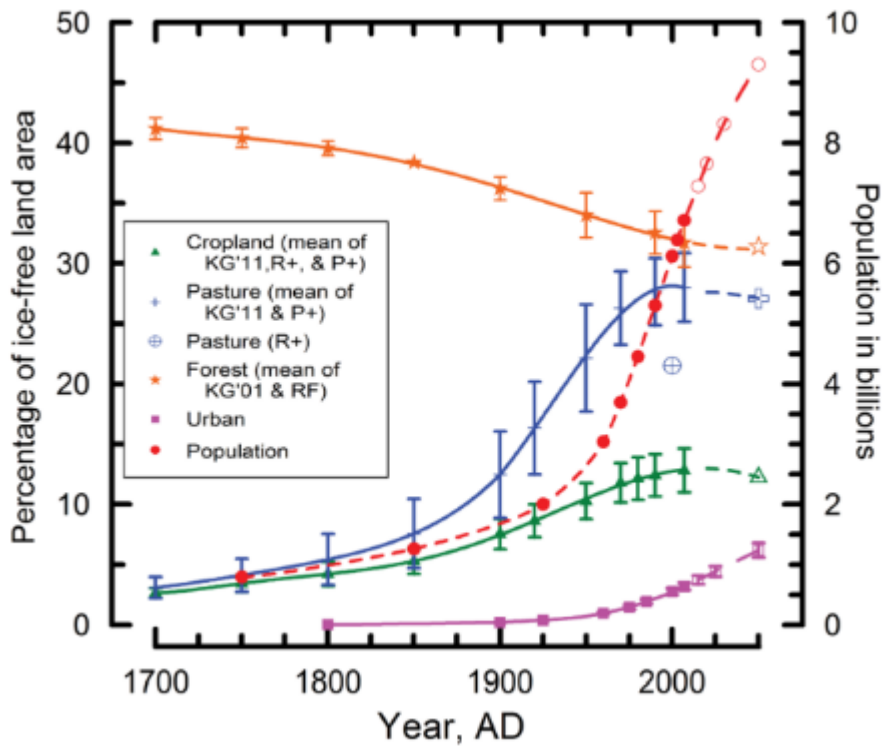
Figure 1. LULC changes of the historical period to future extrapolation (2050) of agricultural land in the world. Source: (Hooke, 2012)
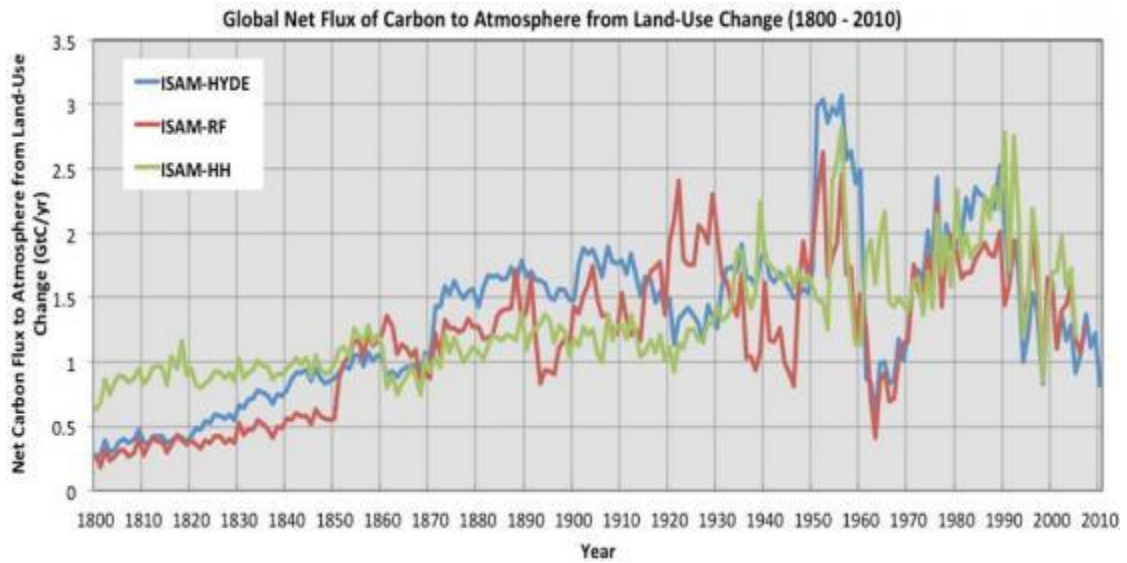
Figure 2. Escalation of carbon emission in the world during 1800-2010.
Source: (Meiyappan, 2013)

Nowadays, the environment has been severely affected on a global scale by Land Use/Land Cover (LULC) changes (Price, 2011; Baker and Miller, 2013; Bosmans *et al*., 2017; Rogger *et al*., 2017). In a global extent, the LULC conversion over the last three centuries (since 1950) has increased significantly (Goldewijk and Ramankutty, 2010). LULC change also exists in West Java, Indonesia for about 15,000 ha in 2010 which is converted to housing, rice field and agricultural land (Siswanto, 2010). The decline of the cover crop of 1.170 ha was detected by Change Vector Analysis in Citarum Catchment between 1994 to 2001 (Wikantika, Utama and Riqqi, 2005). The LULC changes in Upper Citarum Catchment can be identified by 40% of deforestation that occurred between 1997 and 2005 and 35% between 2005 and 2014. Meanwhile, the increase of agricultural areas was noted 8% and 2% from 1997 to 2005 and from 2005 to 2014, respectively (Agatona *et al*., 2015). The decline of both paddy field and forest area in Upper Citarum Catchment has noted 0.2-0.3% annually. Meanwhile, the urban area increases by 2-4.5% annually. The dominant decline occurs in the forest, paddy field and mixed plantation. Meanwhile, the annual upland crop and the developed area will increase in the future (Watung, Tala'ohu and Dariah, 2005).

4

LULC change impacts the hydrology of a watershed, affecting the quality and quantity of water (Siswanto and Francés, 2019). LULC changes pose a significant threat to watershed sustainability and negatively affect many human activities due to the possible exacerbation of water scarcity, flood frequency, soil erosion, sediment transport, higher river water turbidity and reservoir siltation (Defra, 2004; Kheereemangkla *et al.*, 2016; Garg *et al.*, 2017; Boongaling *et al.*, 2018). LULC change shifts the hydrological processes of a basin by altering its soil infiltration, surface runoff and evapotranspiration (McColl and Aggett, 2007). Moreover, Chang and Franczyk (2008) explain that deforestation, urbanization, and cultivation reduce infiltration capacity, lowers soil porosity, lowers evapotranspiration rates due to loss of vegetation, fewer interception losses and decrease groundwater recharge.

In the early stages, the replacement of vegetation covers such as deforestation, urbanization and cultivation, will lead to a significant increase in overland flow. For example, deforestation leads to various negative impacts such as a decrease in rainfall, an increase in overland flow, an increase in sediment yield, triggers floods in the rainy season and drought in the dry season (Delang, 2002). LULC changes scenario in Upper Citarum Catchment such as replacement of forests to the urban area by 10% decreases lateral flow (interflow), percolation and evapotranspiration by 83.51, 146.66 and 1.50 mm, respectively. Meanwhile, it increases overland flow by 232.64 mm (Salim, Dharmawan and Narendra, 2019). Moreover, LULC change in Upper Citarum Catchment decreases the 2-year return period and increases sharply the return period of more than 2 years (Dasanto *et al.*, 2014). Moreover, deforestation affects water yield in the downstream of the Upper Citarum Catchment based on a study using the HEC-RAS model.

Soil erosion is largely determined by the absence of protective land cover (Bakker *et al.*, 2008). Vegetation cover is known as the most effective protector for erosion. Removal of cover crop for agriculture purposes, creation of pasture lands, or construction purposes leave land vulnerable to wind and water erosion (Happ, 2014). The decline of the land cover area will lead to a heavier and faster

kinetic impact of rain splash. If these occur, the detachment of soil aggregate will occur. Eroded soil particles from areas experiencing severe erosion will decrease the soil quality of the area since the particle of soil will cover the surface and reduces the permeability of the soil. Hence, the overland flow is generated and more erosion is created. As a result, the area that exceeds the tolerable soil loss (Tsl) increases. In the lower part, sedimentation is generated and accelerated linearly with the increment of erosion. Thus, LULC destruction or natural land cover restoration will affect erosion rates (Fenli *et al*., 2002; Happ, 2014; Mushtaq and Lala, 2017; Vaighan *et al*., 2017; Zare *et al*., 2017; Valentine *et al*., 2008 in Noda *et al.*, 2017), sediment yield (Budiyono *et al*., 2016) and eco-environmental change (Fenli *et al*., 2002). Dasanto *et al*. (2014) stated that deforestation in a large catchment, such as the Upper Citarum Catchment, will definitely generate more overland flow and finally increase the catchment erosion as well as the reservoir sedimentation rates. In fact, the erosion rate in the Upper Citarum Catchment had increased from 62.04 to 137.66 ton ha^{-1} yr^{-1} between 1990 and 2013 (Chaidar *et al*., 2017).

Developing countries in South East Asia had an increment of annual sediment yield by 1.6 times the rate of population increment due to LULC change (Abernethy, 1990). For example, runoff in Malaysia caused by logging can carry sediments 8-17 times larger than before logging (Kiersch, 2000). Moreover, in the Dong Nai watershed (38,788 km2) in Vietnam, the sediment yield had increased from 24.96 to 38.66 ton ha^{-1} yr^{-1} between 2000 and 2008 (Loi, 2010). In particular, five times increment of sedimentation rate in Citarum Catchment was found in almost 20 years of period (Asdak, 2006). LULC changes from 1990 to 2010 in Upper Citarum Catchment has increased sediment storage from hillslope to the lower area for about 0.7 Mton year^{-1} and sediment yield in the depositional area for about 0.02 Mton year^{-1} ((Noda *et al.*, 2017).

In terms of an outlet of a reservoir, such as a dam, the land cover change will determine the lifetime of a sanctuary such as a dam or a lake due to the increment of sedimentation. Lake and reservoir are highly dependent on the quantity and quality of river water. Sediment export to rivers or outlet is

6

determined by on-site sediment production and the connectivity of sediment sources and rivers (Bakker *et al.*, 2008). The total suspended solids (TSS) can increase suddenly when a sub-watershed land cover has decreased below 30% and in case of opening of the agricultural land of more than 50% (Deutsch and Busby, 2000). For a reservoir, this increase in sediment yield will reduce its effective storage by sediment accumulation (Fonseca *et al.*, 2016). On average, the annual reduction of global reservoir storage due to sediment deposition is around 0.5–1% (Verstraeten *et al.*, 2003) and in tropical regions is 1% each year (Nagle *et al.*, 1999). Moreover, for many reservoirs, the annual storage reduction rates are much higher: they can even reach 4% or 5% such that they lose the majority of their capacity after only twenty-five to thirty years. The sedimentation rate of the Saguling reservoir (outlet of Upper Citarum Catchment) had increased from 1.05 to 4.80 million tons yr^{-1} from 1982 to 2004 (Apip *et al.*, 2010). As pointed out by Ilyas (2002), this increase in sedimentation will decrease the reservoir lifetime, concluding that in 100 years from 1984, this reservoir will lose its storage capacity by 21%. Thus, the Citarum Catchment in West Java is considered as one of the supercritical watershed area (Asdak, 2006).

Land use land cover change may have an impact on the surface albedo, evapotranspiration, sources and sinks of greenhouse gases (GHGs), or other properties of the climate system and may thus give rise to radiative forcing and other impacts on climate, locally or globally (Mach, Stechow and Planton, 2014). Thus, it potentially impacts water resources (Stonestrom, Scanlon and Zhang, 2009). Moreover, the severity and frequency of flash floods have been increasing in many parts of the world, recently. As mentioned before, this increasing trend has been associated with widespread uncontrolled anthropogenic activities that negatively impact the environment. Such activities include the destruction of forest area, increased agricultural activities, draining of wetlands which are known to moderate floods and an increase in unplanned urbanization which contributes to high flood peak discharges (Wiskow *et al.*, 2003).

The presence of land conversion from forest to agriculture or from agriculture to non-agricultural land will certainly affect the hydrological

characteristics concerned. By monitoring and evaluating changes in land cover types and study the characteristics of the discharge and its impact on the water balance and lake sedimentation rate, then the problem of watershed damage can be detected and anticipated earlier. The negative effects of these LULC changes must be predicted immediately to avoid the negative impact in Upper Citarum Catchment. Therefore, we need to analyze the historical LULC change as well as project a future LULC as a base to analyze the hydrological condition of the watershed. In addition, alternative scenarios of LULC are also required as an effort to prevent negative impacts. These scenarios play a role as an alternative for LULC management and to give illustration to mitigate the impact of LULC. Regarding the future state of LULC, a model is required to predict future LULC. Land Change Modeler (LCM) with Artificial Neural Network (ANN) based is an alternative to predict future LULC. LCM has been widely used to assess LULC changes for various purposes as implemented by Leh *et al*. (2013), Calijuri *et al*. (2015) and *Sinha and Eldho (2018)*. Only a few numbers of studies related to LCM implementation in Upper Citarum Catchment. Among them is a study that analyzes LULC change from 2000 to 2010 using the Artificial Neural Network and logistic regression approach (Ridwan, Ardiansyah and Gandasasmita, 2017). Analysis of LULC change dynamics and prediction of LULC in 2050 in Upper Citarum Catchment using CA-Markov principle as part of the LCM model has been done by Yulianto, Maulana, & Khomarudin (2018). Yulianto, Suwarsono, & Sulma (2019) then improve the previous result in 2018 by implementing more accuracy and reliability of the model. Meanwhile, another implemented model in Upper Citarum Catchment has been implemented by Yusuf *et al*. (2018) who analyze and predict LULC change by using CA-M model. Meanwhile, Riza Siregar (2018) used HEC-RAS to analyze LULC change in the Upper Citarum Catchment. Unfortunately, none of those studies incorporate LCM with hydrological model and climate change to analyze more parameters such as water balance, flood, erosion and sedimentation which is conducted in this study.

1.1.2   Climate change

The existence of climate change has become the world's attention today due to a negative future long-term effect on the earth. The sign of climate change has been many identified, such as one reported on IPCC report: Warming of the climate system is unequivocal and since the 1950s, many of the observed changes are unprecedented over decades to millennia. The atmosphere and ocean have warmed, the amounts of snow and ice have diminished, sea level has risen and the concentrations of greenhouse gases have increased (IPCC, 2014). Climate change is caused by direct or indirect human activities that change the global atmosphere condition over a period of time (Intergovernmental and Legal Affairs Climate Change Secretariat, 2006). As noted by the Framework Convention on Climate Change (UNFCCC), in its Article 1, defines climate change as: "a change of climate which is attributed directly or indirectly to human activity that alters the composition of the global atmosphere and which is in addition to natural climate variability observed over comparable periods." The UNFCCC thus makes a distinction between climate change attributable to human activities altering the atmospheric composition and climate variability attributable to natural causes (IPCC, 2014)

Fossil fuels used for human activities that are formed from a long period of a fossil of plants and animals are the main source of greenhouse gases (GHGs). Burning of fossil products releases billion tons of carbon, methane and nitrous oxide yearly into the atmosphere (Maximillian *et al*., 2019). Moreover, carbon dioxide is released as well into the atmosphere through deforestation. Meanwhile, livestock will produce methane, agricultural fertilizer produces nitrous oxide. Gases such as HFCs, PFCs and CFCs, which are normally found in air conditioners and refrigerators are also contributing as dangerous gases in the atmosphere. Human activities that emit GHG into the atmosphere are currently very essential in global activity and are part of the human lifestyle.

The most identified result of global warming is the change in temperature. For example, the melting of icebergs in parts of the polar ice due to temperature

increment. Each of the last three decades has been successively warmer at the Earth's surface than any preceding decade since 1850 (Figure 3a). In the Northern Hemisphere, 1901–2012 was likely the warmest 30-year period of the last 1400 years, considered as medium (Figure 3b). Ultimately, these changes will affect the climatological condition. Higher and faster evaporation from the soil results in a drier soil. These changes initiate the shift of other elements in the water cycle.
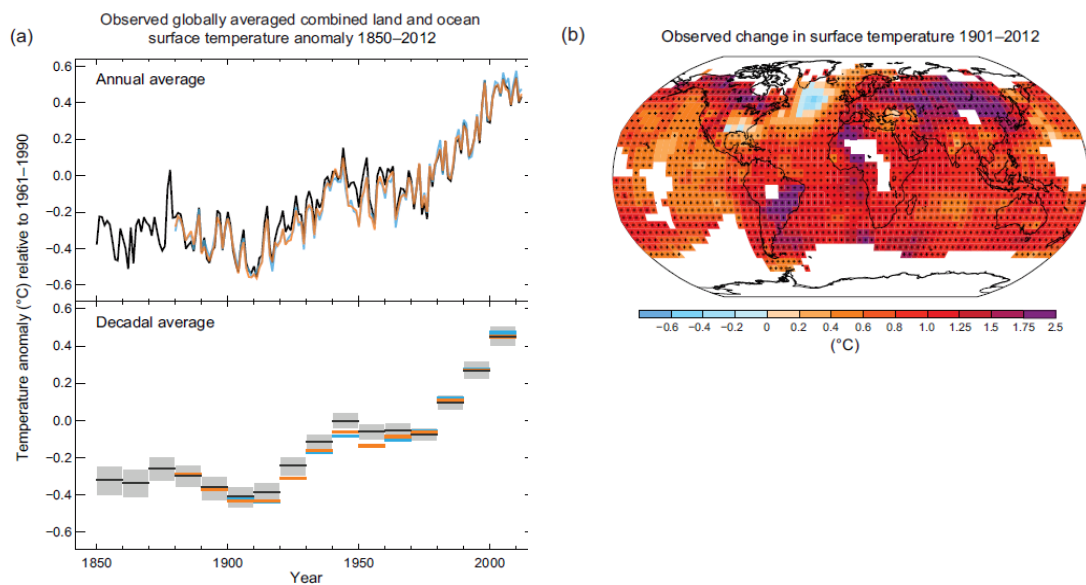
Figure 3. Historical temperature of the earth. (a) Temperature anomaly, (b) surface temperature of the world. Source: Field *et al.* (2014)

Data from climate observation has shown the increase of global annual precipitation by ±0.2 mm yr^{-1} during the 20th century (Piao *et al.*, 2007). Meanwhile, the temperature increased at a rate of ±0.8 °C (Hansen *et al.*, 2006). Moreover, in the past 30 years, the temperature increased significantly with a decadal trend of 2°C. The increase in temperature will escalate evaporation, increase the moisture-holding capacity at a rate of about 7% per 1°C and finally transport more amount of water favour in the atmosphere. These changes will ultimately accelerate the hydrological process (Menzel and Burger, 2002) and stimulating more frequent precipitation events (Trenberth *et al.*, 2003). In Indonesia, the increasing surface air temperature by around 0.5°C during the past 100 years shows the existence of climate change (Poerbandono, Julian and

10

Ward, 2014). Future temperature is predicted to increase from 1.3 to 4.6 °C by the end of 2100 with a trend of 0.1 to 0.4 °C per year (Berliana *et al.*, 2010).

Climate change will impact the hydrological cycle of a watershed. The increment of temperature on the land surface will increase the temperature of the waterbody. This increment will lead to c. Accompanied by high humidity, the rainfall event will increase for a long period in a certain place. Confidence in precipitation change averaged over global land areas since 1901 is low before 1951 and medium afterward (Figure 4). For other latitudes area-averaged long-term positive or negative trends have low confidence (IPCC, 2014). The shift of hydrological cycle changes the pattern and quantity of precipitation, together with the change of temperature, are considered as the initial part of the increasing rate of overland flow (Chiew *et al.*, 1995); Mkankam Kamga, 2001). The annual overland flow and water yield are predicted to increase by 10% - 40% and 10% - 30% in some wet tropical areas and dry tropics, respectively (Kundzewicz *et al.*, 2007).
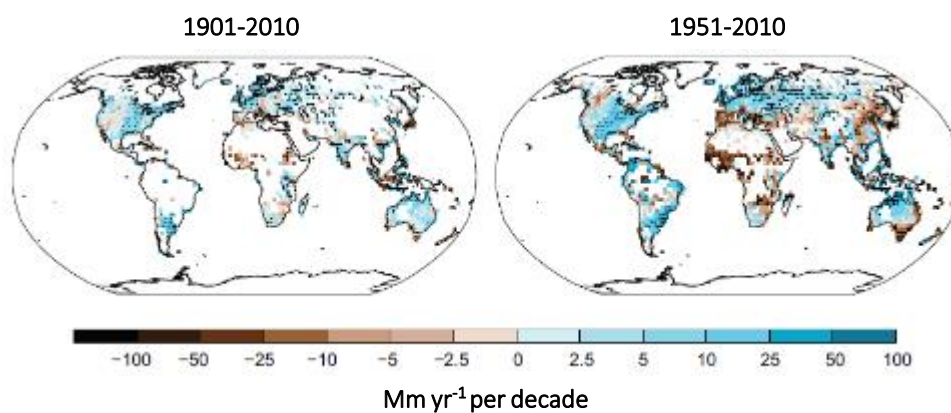
Figure 4. The observed change in annual precipitation with a different initial period.
Source: (Field *et al.*, 2014)

The unexpected abundance of water as a result of climate change leads to flooding occurrences in the rainy season. Likewise, lack of water in the dry season become a common fact in Indonesia (Stocker *et al.*, 2013). In the capital of Indonesia, Jakarta, the increasing precipitation can be detected from monthly precipitation data of about 100 mm in 1955-1985 compared to the period 1885-1915 (1900s). Moreover, Jakarta suffered major floods in both 2002

and 2007, the later causing at least 58 deaths and direct economic damages of US$ 453 million (Poerbandono, Julian and Ward 2014). In particular, the output of the ECHAM model suggests that rainfall in Upper Citarum Catchment is expected to decrease in the future. Meanwhile, another model such as HADGEM shows a different behaviour by showing a fluctuating rainfall amount in the future. Another two GCM models, CCSR and CSIRO, suggested that the seasonal rainfall would increase consistently over the period from 2020 to 2080 under both scenarios (Boer *et al.*, 2012).

Citarum Catchment is predicted to provide insufficient water demand after 2010 (Hernowo, 2001 in Boer *et al.*, 2012). Recently, all of the sub-districts of Upper Citarum Catchment already experience water deficit problems (i.e., not enough supply to meet the demands), particularly in the lower areas of the catchment cover such as Kerawang, Bekasi and Purwakarta, even without a changing climate and if the level of water extraction from the streamflow was limited to 10% of the mean annual flow. In 2080, the water deficit for most of the sub-districts in this lower area would be even more severe. (Kusuma, Kuntoro and Silasari, 2011). Therefore, the impact of climate changes on the hydrological and sediment cycles in a tropical watershed can be significant and studying this process is extremely important (Gyamfi, Ndambuki and Salim, 2016). Further study in data sharing, management, data acquisition of climate projection, together with the construction of a robust hydrological model needs to be conducted (Kusuma, Kuntoro and Silasari, 2011). To achieve this, especially regarding climate change, it is necessary to use a trajectory of future climate change to describe the future state. Climate change projections are important not only to attribute and detect the process but also to adjust and mitigate through establishing strategies for the future (Solomon *et al.*, 2007).

Moreover, climate change will affect the erosion rate as it changes the rate and amount of precipitation as the initial agent of erosion occurrence. Enhancement of rainfall amount as the result of climate change, increase the erosion since greater erosivity is a direct consequence of climate change (Favis-Mortlock and Guerra 1999; M.A. Nearing 2001; Nearing *et al*. 2005). The

sedimented material of erosion will create another problem such as lower permeability due to the clogging of soil's macro and micropores. Hence, runoff is generated and discharge of the river in the watershed is fluctuating so greatly and widely affect the supply of irrigation and household water in the downstream area (Hidayat *et al.*, 2013). Moreover, erosion that occurs in the watershed will lead to rapid sedimentation development. The present sediment yield is increasing compared to the past (Figure 5). In the lower part or certain location such as a dam, the sediment infilling will initially decrease the volume of water and eventually decrease the electrical capacity. Therefore, the authority of the dam will face the increasing cost of maintenance (Hunt, Stilpen and de Freitas, 2018). Finally, the community will be in a high-risk condition due to receiving the negative impact of lower electricity production and an inadequate amount of water.
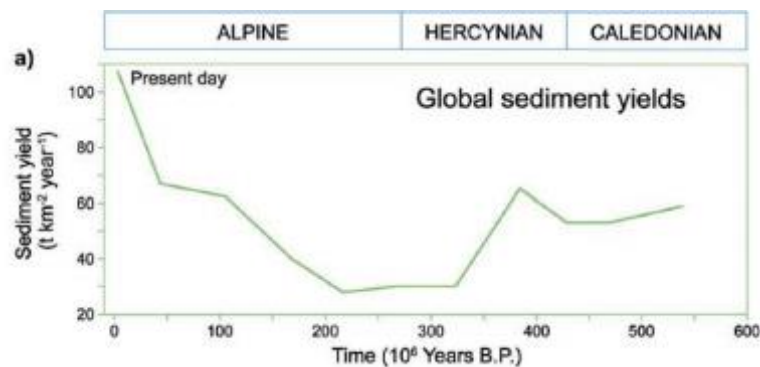
Figure 5. Tentative reconstructions of the variation of sediment yield from the land surface of the globe during the past 500 million years (Tardy, N'kounkou and Probst, 1989)

A future trajectory data source provider such as the Global Circulation Model (GCM) can be used to study climate change. GCM is known as a recent and robust tool to construct climate change projection (Kundzewicz *et al.*, 2007; Huebener *et al.*, 2007). Utilization of GCM in earlier studies related with the climate change and many aspects has been conducted for example by Mullan, Favis-Mortlock and Fealy (2012) in the Northern Ireland, Bussi *et al.* (2014) in the Ésera River catchment, central southern Pyrenees, Spain, Cousino *et al.* (2015) in the Maumee River watershed, Ohio, Michigan, Indiana, USA, Budiyono *et al.* (2016) in the Jakarta, Indonesia and Mukundan *et al.* (2013) in the Cannonsville

watershed, New York, USA. Only a few studies of climate change have conducted in Upper Citarum Catchment. For example, a research conducted by Santikayasa, Babel and Shrestha (2015) which analyzes the impact of climate change on water availability using statistical downscaling in Citarum Catchment. Another research has been done by Boer *et al*. (2012) which implement SRESA and SRESB scenarios adopted from ICCP 2007 to analyze the water supply scenario in Upper Citarum Catchment. SRES stands for Special Report on Emissions Scenarios. SRES is a scenario characterised by regionalisation of economic development, with A2 being a more regionally oriented scenario and B2 a more locally oriented scenario (Bussi *et al*., 2014).

M Syahril Badri *et al*., (2011) implement a trend of meteorological data to mitigate future climate change in Upper Citarum Catchment. However, most of them have not implemented the GCM from the newest IPCC (IPCC 2014) to project climate change in the future. The fifth assessment report of IPCC (published in 2014) provide scenarios based on different technical approach. These new scenarios called representative concentration pathways (RCP), consist of greenhouse gas concentration and emission pathways. It is also considering the impact caused by LULC change. It is a better scenarios compared to a previous method such as SRES which only consider a forcing by greenhouse gas and aerosol from artificial climate change factors (Kim *et al*., 2013). Trajectories of RCP 4.5 and 8.5 adopted from ICCP 2014 is important to be implemented in this study. Those RCP will give a projection of climate change for a long period. Hence, we can observe and mitigate the future climate status. In this study, the selection of RCP 4.5 was based on the necessity to analyze the climate change which stabilized before 2100. Meanwhile, RCP 8.5 is also included in the analysis because it provides the continuous increment of climate change even beyond 2100, which shows no stabilization in 2100. Regarding soil erosion and sedimentation, only a few numbers of studies related to the climate change impact on soil erosion and sedimentation in Upper Citarum Catchment (M.A. Nearing 2001; O'Neal, *et al*. 2005; Mer, & Clark 201;(Maeda *et al*., 2010); Nunes, Seixas, & Keizer 2013). This fact leads to the importance of this study to overcome the gap. The study of erosion and sedimentation is important to be

conducted since those elements affect the environment and activity of the people in West Java. Lack of water supply and electricity due to enormous erosion and sedimentation results in a significant negative impact on the community. it will also affect other sectors such as the agricultural which plays a role as the backbone for the community in Java.

1.1.3 Climate and LULC changes

Individual study of climate change and LULC change has been conducted worldwide. However, a combined study of climate and land use change scenarios showed a significant synergistic impact on hydrology, relative to implement the individual study (Molina-Navarro *et al.*, 2014). Through interaction, LULC change deteriorate or may soften climate change effect. Therefore, the implementation of LULC change under climate change scenarios is important (US EPA National Center for Environmental Assessment, 2009). Hence, many researchers have conducted studies related to the combination of LULC and climate change such as conducted by Rodriguez-Lloveras, Buytaert, & Benito (2016), Asselman, Middelkoop, & van Dijk (2003), Molina-Navarro *et al.* (2014), Kuntoro *et al.* (2018); (Notebaert, Verstraeten, Ward, Renssen, & Van Rompaey (2011), Wilson & Weng, (2011), Khoi & Suetsugi (2014), López-Moreno *et al.* (2014) and Fan and Shibata (2015). An example study has been implemented in Upper Aragón River, Spanish Pyrenees which combines the impact of climate and land use change on water availability and reservoir management. The results of the study show that the individual impact of reforestation could decrease annual streamflow by 16%. Moreover, the implementation of the individual impact of future projection of climate change under Regional Climate Model (RCM) results a 13.8% decrease in annual streamflow. Meanwhile, the combined effects of reforestation and climate change are expected to reduce annual streamflow by 29.6%. Another study in Be River Catchment, Vietnam shows a bigger delta change magnitude of evapotranspiration, streamflow, sediment load, surface runoff, groundwater discharge resulted from the combination of land use change and climate change. Those are bigger than the result of the individual impact of both land

use and climate change. Unfortunately, the study of the combined impact of LULC and climate change in Upper Citarum Catchment is rarely implemented. The example of this study can be found from a study by Kuntoro, Cahyono, & Soentoro (2018). They used historical spatial analysis to examine the future LULC change (linear method) and climate projection from GCM to see the climate status in the future. This combination results in a more severe drought and flooding event compared to the individual effect. Beyond the satisfaction result of the study, this study lack of temporal scale as the study was implemented with only monthly scale based. Moreover, none of them analyze the combined impact of erosion and sedimentation.

Considering the important result of the combined impact of LULC and climate change, the study related to the combination of LULC and climate change is extremely important to understand its impact on water balance, flood, erosion and sedimentation in Upper Citarum Catchment.

Tropical regions are located in the mid-latitude zone, an area mainly characterized by its large energy input for evapotranspiration and intense rainfall (De Graff *et al*., 2012; Sinha and Eldho, 2018; Wohl *et al*., 2012). During the rainy season, rainfall amounts can be 100 times more than during the dry season (Bruijnzeel, 2004). These characteristics generate numerous environmental problems such as frequent flooding and high erosion rates (Gupta, 2011). Humid tropical watersheds are considered unique due to their rapid evolution that affects the hydrological cycle (Calijuri *et al*., 2015). However, human activities in humid tropical regions have profoundly altered the LULC conditions due to economic activities (Costa, 2005). In general, these changes decrease canopy interception, evapotranspiration (Marhaento *et al*., 2018), soil productivity and soil water storage (Zuazo and Pleguezuelo, 2008). As a consequence, it is clear that in most cases they increase water yield, overland flow (Marhaento *et al*., 2018) and flood occurrence (Wheater and Evans, 2009; Sinha and Eldho, 2018). Regarding climate change, the change in LULC together with climate change will directly affect larger the global river runoff than increased CO_2 (Miao *et al*., 2011).

A model is required to understand the impact of LULC and climate change on the hydrological process. Meanwhile, it is also necessary to simplify the hydrological processes in a mathematical model (Xu, 2002). Physically-based distributed models are preferred as they better reflect the impact of climate and LULC changes on the model's parameters (Legesse *et al*., 2003; Ghaffari *et al*., 2010; Naabil *et al*., 2017). Furthermore, a distributed model has more advantages, such as the ability to explore the spatial variability of inputs, processes and characteristics and also the capability to obtain results from any specific location (Carpenter and Gergakakos, 2006). This study has used the TETIS distributed model which has been satisfactorily applied in different catchment areas (from less than 1 km^2 up to 60,000 km^2), hydrological problems, spatial resolutions (cells from 5 m to 500 m) and climate types all around the world, including implementation in the humid tropical climate of the Combeima River in Colombia (Peña *et al*., 2016).

Previous studies related with the water cycle in Upper Citarum Catchment have been addressed by Agus *et al*. (2004), Harlan *et al*. (2009), Poerbandono *et al*. (2009), Tommi (2011), Hidayat *et al*. (2013) and Julian *et al*. (2013). Flood frequency studies in Upper Citarum Catchment have been performed by Dharma *et al*. (2011) and Mauliana (2016). Ayuningtyas (2012) and Chaidar *et al*. (2017) have studied catchment erosion in Upper Citarum Catchment by implementing the USLE method, while Wibowo (2011) has deployed a model to interpret the sediment cycle in Upper Citarum Catchment. However, these studies have dealt with different hydrological aspects separately. Moreover, none of these studies have considered the future evolution of the LULC and the historical reservoir sedimentation data. Those gaps have been incorporated in our study. Hence, our study is valuable to fill the gap of the conducted researches in Upper Citarum Catchment.

1.2 Objectives

The general objective of this study is to understand and analyze the impact of climate and LULC changes on the hydrological process and their

relationship with historical and future changes by using spatially distributed modeling on the Upper Citarum Catchment. Therefore, the specific objectives this study are:

1. Assessment of implemented scenarios of LULC to mitigate the negative impact of erosion and sedimentation as well as observing its water balance.
2. Analysis of historical LULC changes and its water and sediment cycle.
3. Analysis of climate changes and its impact on water and sediment cycle.
4. Assessment of combined LULC and climate changes on water and sediment cycle.

and main tasks of this study are:

1. Generating scenarios of LULC, including future LULC using a spatial model (covered by chapter 2).
2. Analysis of two historical LULC to find out LULC change impact on water balance, flood regimes, catchment erosion and reservoir sedimentation (covered by chapter 3).
3. Implementing (i.e. calibration and validation) a robust distributed hydrological and sediment model for the study area with LULC historical changes (covered by chapter 3).
4. Analysing the climate data from trajectories (climate change scenarios), as well as projecting the future climatological input (covered by chapter 3).
5. Comparing and combining the impact of LULC and climate changes on water balance, flood regimes, catchment erosion and reservoir sedimentation (covered by chapter 4, 5 and 6)

CHAPTER 2. MATERIALS AND METHODS

Chapter Overview

This chapter describes the area where this study is implemented. Upper Citarum Catchment is located in a tropical watershed and plays an important role for the community in West Java. The relevant information regarding the theory and mechanism of the implemented model is briefly explained, including the input data of the model. An open-source regional climate model called Regional Climate Model CORDEX East Asia has been implemented to predict climate change. Representative Concentration Pathway (RCP 4.5 and 8.5) were chosen to illustrate the possibility of future climate change in the study area. To eliminate the deviation of climate data information on the global climate model, a proper bias correction is required. The main model which is used in this study, called TETIS distributed hydrological models, was intended to describe the hydrological cycle. The mechanism of TETIS is briefly described in this chapter, including the water and sediment sub-models. AFINS software has been used to assess the flood regime of different scenarios. The input data for the model (TETIS, LCM and AFINS) consists of hydrometeorological, spatial and sediment data. A spatial model (called Land Change Modeler) which principally based on Artificial Neural Network and Markov Chains has been implemented to predicts future LULC. LULC scenarios (conservation, government plans, natural vegetation and future scenarios) are briefly explained in this chapter, especially regarding its spatial content and how those scenarios were produced.

2.1   The study area

2.1.1   General description

The Upper Citarum Catchment is part of West Java (Figure 6) and located in the upstream part of the Citarum River. The Upper Citarum Catchment covers an area of 2,316 km^2 or 1.8% of total Java island (BPS, 2017). Bandung is the main city and the total population within the catchment is about nine million. Upper Citarum Catchment covers some regions as follow: Cimahi Municipality, Bandung Municipality, Bandung Regency, West Bandung Regency, Sumedang Regency and Garut Regency and consisted of eight sub-watersheds i.e. Cikapundung, Cipamokolan, Cikeruh, Cisangkuy, Citarik, Cirasea, Ciwidey, Ciminyak and Tjihaur (Agatona, Setiawan and Effendi, 2016). The topography is described as being relatively flat in the central area and mountainous at the outer limits of the catchment area, especially in the northern and southern parts. The river network configuration is a "bowl shape" and it is highly vulnerable to flooding.
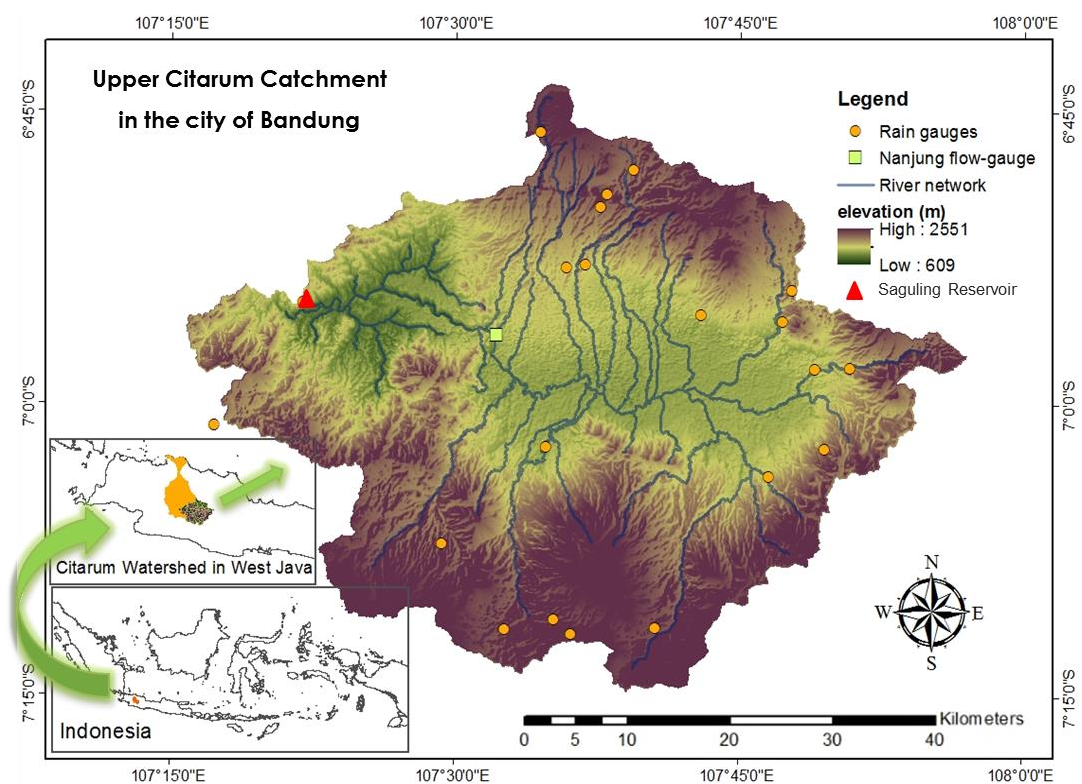
Figure 6. Digital Elevation Model of Upper Citarum Catchment (outlet at Saguling reservoir), including main river network and hydrometeorological stations.

21

The Saguling reservoir is the outlet for this watershed with an initial capacity of 889 Hm^3. It is considered to be important as it acts as the main hydroelectricity and water supply source for people who live in Java and Madura islands. Together with hydropower of Jatiluhur and Cirata, the hydropower of Saguling produce electricity of a total 5.000 Gigawatt. It also provides water for state water suppliers (PDAM and PAM Jaya) for 473 million m^3 areas (Suripin, 2001) and irrigation water for 296 ha rice fields in the northern coastal zone (Pantura). The Saguling reservoir itself provides water of 875 million m^3. The Upper Citarum Catchment has a humid tropical climate characterized by two different seasons (Molion, 1993): a rainy season from November to April and a dry season from May to October. The mean rainfall and temperature have been recorded as 1840 mm yr-1 and 25.6 °C, respectively. It has 6 orders of soil consisting of Entisols, Inceptisols, Andisols, Mollisols, Alfisols and Ultisols. These orders are then divided into 8 sub-orders, 19 great groups, 40 sub-groups and 72 families (ICALRRD, 1993). LULC is constituted by primary and secondary forests (Pinus merkusii, Calliandra callothyrsus, Bambusa sp.), shrubs, grass, dry cultivations (corn, soybean, cassava), plantations (tea and coffee), rice fields, residential areas, industrial zones, mining, bare lands and water bodies. Forests, plantations and dry cultivations areas generally occupy the hilly parts of the catchment. Meanwhile, urban areas and rice fields occupy the central flat part. The remaining LULC types are spread throughout the catchment. However, LULC is highly dynamic as described later in the sub-section analysing its historical evolution. Overview of the study area is presented in Figure 7.
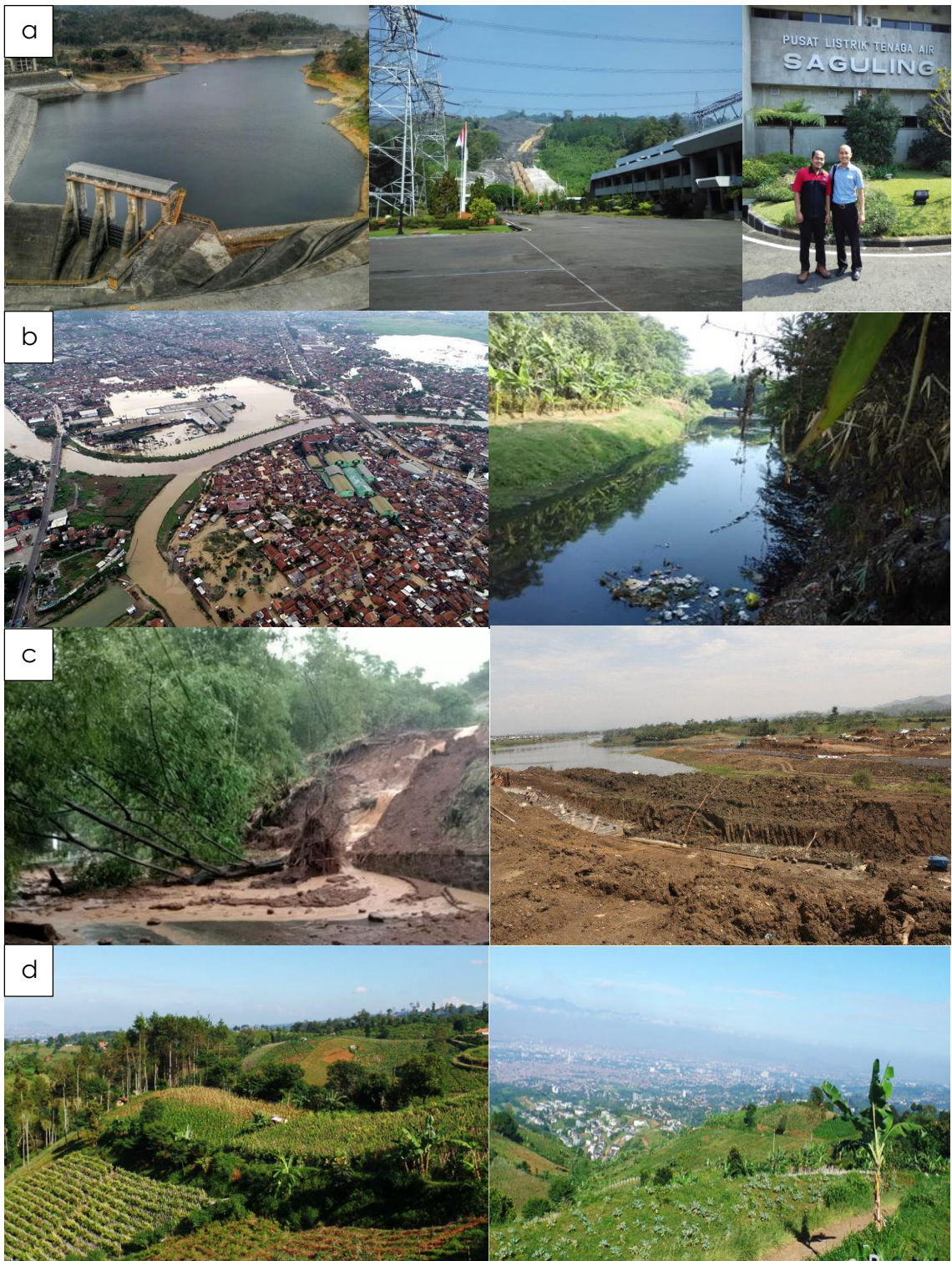
Figure 7. Overview of the study area. a) Saguling reservoir and the electricity plant, b) example of river in Upper Citarum Catchment, c) erosion and the depositional area, d) landscape in the Northern part of the study area.
some figures are downloaded from various source: https://ekonomi.bisnis.com, https://bandung.bisnis.com, https://republika.co.id, https://finance.detik.com, https://bersapedahan.wordpress.com

2.1.2 Hydrometeorology

This study used twenty stations of daily rainfall from 1985 to 2014 (Table 1). The highest altitude belongs to Cipeusing station with 1563 m above sea level. Meanwhile, the lowest is possessed by Saguling station with 638 m above sea level and this station act as the outlet of the watershed. The highest yearly precipitation amount was recorded 4,500 mm yr^{-1} in Kertamanah station. Meanwhile, the lowest precipitation was noted 1,259 mm yr^{-1} in Jatiroke station. The gaps were found in Saguling station for two years and Cipeusing station for one year. The gap of precipitation and temperature data was filled by the inverse of the square of distance method in the TETIS model.

Table 1. Selected rainfall station in the Upper Citarum Catchment

Station	Altitude (m)	Yearly Precipitation Amount (mm yr^{-1})	Gap (year)
Saguling	638	1510	2010, 2011
Ciherang	670	2057	-
Rancaekek	680	1668	-
Paseh	696	1771	-
Cibiru	710	1965	-
Cicalengka	757	1643	-
Jatiroke	776	1259	-
Dago Pakar	802	1912	-
Tanjungsari	844	1919	-
Cikancung	856	1858	-
Cidadap/Montoya	1000	2153	-
Cisondari	1179	1582	-
Margahayu	1195	2672	-
Kayu ambon	1218	1740	-
Lembang	1228	1816	-
Cileunca	1432	1841	-
Cipanas	1466	2606	-
Cibereum	1510	2486	-
Kertamanah	1514	4500	-
Cipeusing	1563	1412	2014

Figure 8 illustrates the monthly precipitation in the study area. The rainy season normally occurs around November to April.

24

Meanwhile, the summer season occurs from May to October. The higher daily precipitation occurs in January, February, March, April, May, November and December. Meanwhile, June, July, August, September and October being the driest season. Likewise, the same pattern also found in the data of discharge. The maximum daily precipitation was noted 7.98 mm in March. Meanwhile, the minimum daily precipitation was noted at 1.16 mm in August. The maximum daily discharge was noted 32.18 m³s⁻¹ in March. Meanwhile, August being the lowest minimum daily discharge with 6.23 m³s⁻¹
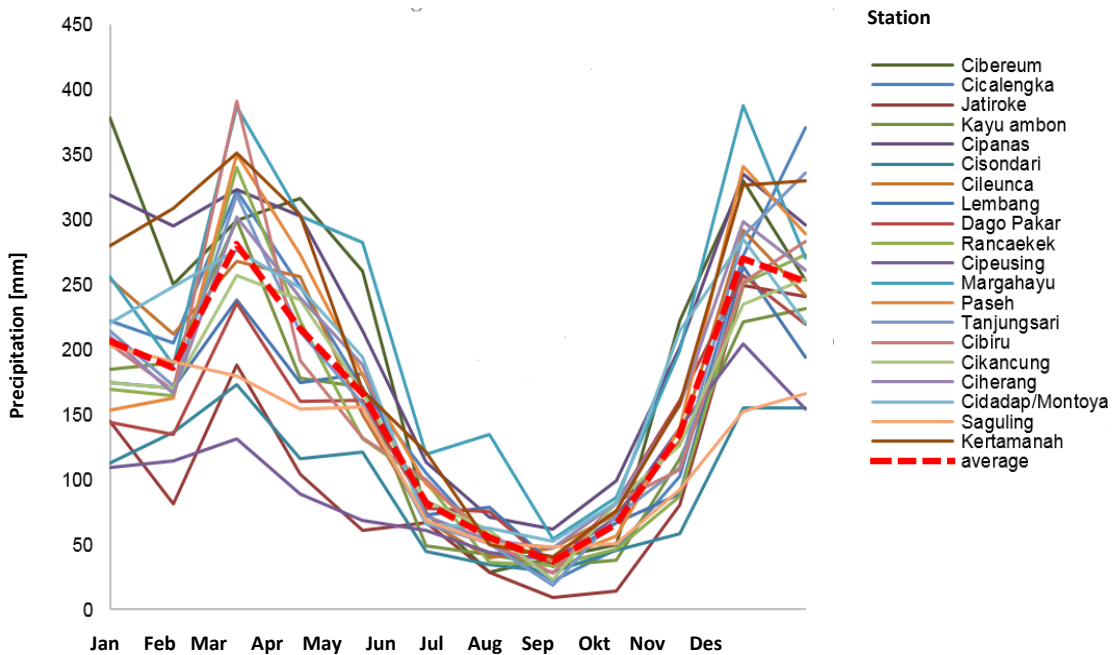
Figure 8. Monthly rainfall amount of 20 stations in Upper Citarum Catchment (1985-2014)

The reference evapotranspiration (ET0) was estimated using the Hargreaves equation method based on mean, maximum and minimum temperatures (Berti *et al.*, 2013) as follow:

$$ET_0 = 0.0023 \cdot (t_{med} + 17.78) \cdot R_0 \cdot \sqrt{t_{max} - t_{min}} \qquad [1]$$

However, daily temperature datasets were only available from 1985 to 2014 at the Bandung meteorological station. Due to this data limitation, the temperature data from that station was processed into nine modified

25

temperature points based on altitude using the ISA method (Field *et al.*, 2014). The equation of ISA is described as follow:

$$T = T_0 - 6.5 \frac{h(m)}{1000}$$ [2]

Where T_O refers to the temperature of standard sea-level conditions ($\circ$K or $\circ$C) and *h* refers to altitude (m or ft). The higher ET0 can be found in the mid-year due to higher temperature, meanwhile the lower ET0 in the beginning and the end of the year.

The mean temperature spatially results in the narrow range of 22.6-23.7$\circ$C and a relatively constant ET0 of approximately 130 mm month^{-1} was computed. To obtain the precipitation and ET0 at each pixel, TETIS performs spatial interpolation by the inverse of the square of the distance method.

The peak of reference evapotranspiration occurs in September with 150 mm month^{-1}. Meanwhile, the lowest was found in January with 108 mm month^{-1}. The high value of ET0 in September is caused by the high temperature on that month. Meanwhile, January has the lowest ET due to lower temperatures.

The average monthly precipitation and discharge are illustrated in Figure 9. The discharge dataset in the period 1985 to 2014 Nanjung station was used for the model input. The TETIS model used 19 discharge stations as input data. The same pattern with no delay between precipitation and discharge was found. The highest and lowest mean daily discharge was noted 151 m^{3}s^{-1} and 47 m^{3}s^{-1} in March and August, respectively. Meanwhile, March and November being the highest mean monthly discharge due to a bigger rainfall amount.
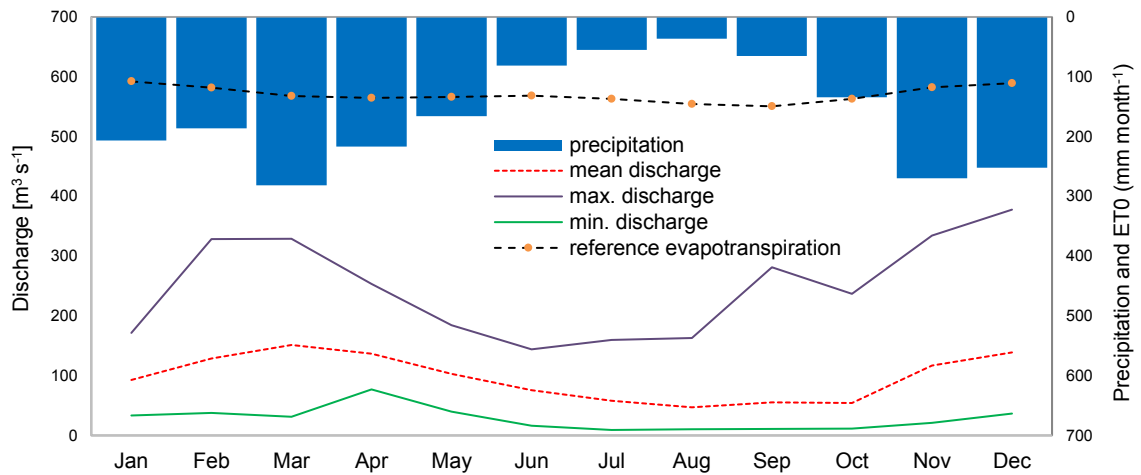
Figure 9. Monthly average of catchment rainfall, reference evapotranspiration and outlet discharge (1985-2014)

2.1.3 Sediment information

The data of deposited sediment volume from the Saguling reservoir was collected from a related reservoir institution in West Java. Yearly deposited sediment was derived from the bathymetry method. Figure 10 shows the volume of deposited sediment in the reservoir from 1985 to 2013. The sediment volume in the period 1985-1987 was measured only once in 1987. Thus, the annual sediment volume has the same amount in that period due to the division into 3 years from a single amount. The lowest and highest sediment amount was noted in 1988 and 2010, respectively. The sediment yield has increased since the first time the dam was built in 1985 and the clear increasing trend was found from 1985 to 1991. Meanwhile, the rest of the years were fluctuating with a small increasing number.
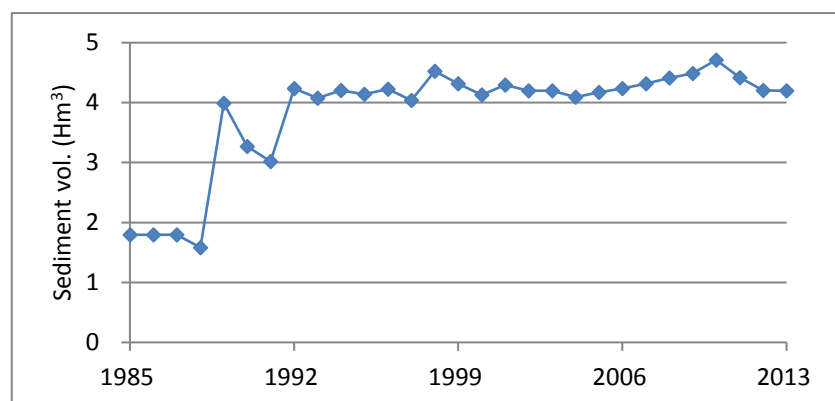
Figure 10. Escalation of deposited sediment in Saguling dam in the period 1985-2013

27

2.2 Spatial Information for the input of the model

Basic spatial inputs for TETIS parameterization are comprised of topography (in the form of a DEM), soil, geology and LULC maps (Table 2). All map manipulations were done using ArcGIS with a final spatial resolution of 90 m.

The required maps for TETIS such as flow accumulation, flow direction, overland flow velocity and slope maps were extracted directly from a DEM. Soil data were derived from 77 samples with depths of approximately 200 cm. Soil unit map of family level based on soil taxonomy classification (soil survey staff, 1990) with scale 1: 50,000 was used.

Table 2. Spatial information for the input of TETIS models

Data Type	Scale (resolution)	Source	Input, driver or parameter
Topographic map	2 arc-second (90m)	Digital Elevation Model USGS	- Slope - Flow - Direction - Flow accumulation - Overland flow velocity - Elevation
Soils (survey) map	1:50,000	Indonesian Center for Agricultural Land Resources Research and Development (ICALRRD) Report	- Static storage - Infiltration capacity - Percolation capacity - Available water content - Texture - Erodibility
Geology/hydrogeology map of Bandung	1: 100,000	Ministry of Public Work, Indonesia	- Percolation capacity - Aquifer permeability
LULC 1994, 2009 and 2014	Landsat TM 30 meters (supervised classification)	Planning Board of West Java, Indonesia	- Vegetation coefficient - Static storage capacity - Infiltration capacity - Interception

From this soil information, infiltration capacity, field capacity and available water content were calculated using the pedotransfer function developed by Saxton and Rawls (2006). Pedotransfer function is a simple model to understand and forecast hydrological characteristics related to soil (Saxton *et al.*, 2006). Erodibility was estimated using the formula proposed by Wischmeier *et al.* (1971). The hydrogeological map of Bandung Regency with a scale of 1: 100,000 was transformed into the value of percolation by lithology and used to estimate deep percolation capacities and aquifer saturated conductivities.

28

The LULC maps for 1994, 2009 and 2014 have been corrected manually by comparing it with Landsat TM imagery. Since the LULC maps did not have the same classification, a proper reclassification has been implemented (Table 3). As part of the implemented LULC scenario in the study area, the government scenario has also different LULC classification with the one which is used for TETIS implementation. Therefore, it is required to be transformed to have the same classification (Table 4). Practice management indices (P) as an input of sediment sub-model was set to the value of one (1) due to the limitation of data.

Table 3. LULC classification of 1994, 2009, 2014 and its standardization.

LULC 1994	LULC 2009 & 2014	Standardized LULC
Bare land	Building	Bare land
Building	Bush/Shrub	Bush/Shrub
Bush/Shrub	Dry Cultivation	Dry Cultivation
Dry Cultivation	Forest	Forest
Forest primary	Grass	Grass
Forest secondary	Plantation	Industrial zone
Grass	Rice Field Irrigated	Plantation
Mix Plantation	Rice Field Non-Irrigated	Rice field
Mining	Soil with Gravel	Urban
Plantation	Urban area	Waterbody
Rice Field	Waterbody	
Urban Area		
Waterbody		

Table 4. Transformation LULC of government plan scenario

Government Plan Scenario	Standardized LULC
City urban	Urban (original LULC)
Protected Forest	Forest
Enclave for urban	Urban
Rice field	Rice field
Forest Conservation	Forest
Geology Protection Area	All except urban and industrial zone
Limited forest production	Forest
Production forest	Forest
Prone to Mountain eruption	All except urban and industrial zone
Prone to Soil Movement	All except urban and industrial zone
Suitable for Conservation Forest	Forest
Villages urban	Urban (original LULC)
Water Absorber Area	Forest
Waterbody	water

2.3 Sediment information for the input of the model

The annual deposited sediment was computed by the differential bathymetry method, taking into account the temporal evolution of the sediment density using the Miller (1953). Reservoir bathymetries were collected annually by a public company responsible for the reservoir management from 1985 to 2013. A mean decrease in reservoir volume was noted 3.83 Hm^3 yr^{-1}. After sediment density correction, the mean deposition is recorded at 3.44 Mton yr^{-1}. As explained in the methodology section, for the calibration and validation of the TETIS sediment sub-model, it is necessary to determine the catchment sediment yield. Therefore, the annual deposited sediment was modified due to the un-trapped sediment in the reservoir using the Dendy (1974) equation, resulting in a mean of 3.68 Mton yr^{-1} during the historical period of observations. No dredging of sediment occurred in the reservoir during the observational period.

Sediment calibration uses LULC map of 2009 and the trapped sediment data in the same year. This calibration is done by comparing deposited sediment mass with the calibration result in the Saguling reservoir. Fortunately, this reservoir has completed the annual reservoir bathymetry data from 1985 to 2014. Deposited sediment data (volume) from the bathymetry measurement should be corrected in advance because it is not in the real volume. This happens because it is affected by gravity (compaction) for certain years and entrapped sediment which flows out from the reservoir. To calculate the effect of compaction, the formula (Miller, 1953) is used:

$$W_t + 0.4343K\left[\left(\frac{t}{t-1}\right)Lnt - 1\right], t > 1 \qquad [3]$$

Where: W_t = average sediment specific weight (kg m^{-3})
    W_1 = specific weight of sediment in the first year
    K = consolidation constant

initial bulk density is calculated using (Lara and Pemberton, 1965). This is supported by the statement from (Lane and Koelzer, 1943) which underlined that the W_1 and K Both are functions of the type of reservoir operation and the size of

the sediment. For sediment mixture, a weighted average of specific weights and constant consolidation must be used (Lara and Pemberton, 1965):

$$W_1 = 0.01[W_1(c)P(c) + W_1(m)P(m) + W_1(s)P(s)] \qquad [4]$$

$$K = 0.01[K(c)P(c) + K(m)P(m) + K(s)P(s)] \qquad [5]$$

Where: $W_{1(c)}$, $W_{1(m)}$, $W_{1(s)}$ = initial specific weight;
$K_{(c)}$, $K_{(m)}$, $K_{(s)}$ = consolidation constants;
$P_{(c)}$, $P_{(m)}$, $P_{(s)}$ = percentage of clay, silt and sand respectively

Because the reservoir has a large area, sediment always submerged or nearly submerged is used as the value of the initial specific weight and constant consolidation (Table 5). Then, yearly deposited sediment (yearly layer) bulk density can be calculated by using a Miller's formula. The bulk density of the deposited sediment is calculated by averaging all layers of sediment. Compaction indicates an increase in bulk density for the older layers. To calculate the loss due to deposited sediments (trap efficiency), the Brune's curve is used (Bussi *et al.*, 2014). This is important to be applied to see how much sediment flows out from the reservoir or not deposited.

Table 5. Initial specific weight (kg m^{-3}) and constant consolidation of three soil texture

Type of reservoir operation	Clay		Silt		Sand	
	$W_1(c)$	K(c)	$W_1(m)$	K(m)	$W_1(s)$	$K_1(s)$
Sediment always submerged or nearly submerged	416	256	1120	91	1500	0
Moderate to considerable reservoir drawdown	561	135	1140	29	1550	0
Reservoir normally empty	641	0	1150	0	1550	0
Riverbed sediment	941	0	1170	0	1550	0

Brune's curve requires two data i.e. the data mean annual inflow and storage capacity to calculate the capacity-inflow ratio (Figure 11). Nowadays, Brune's curve has been transformed into a better equation, one of them is a modification made by Dendy (Dendy, 1974) with the equation as follow:

$$TE\ Dendy = 100 \left[0.97^{0.19^{log(\frac{C}{I})}} \right] \qquad [6]$$

Where: I = water inflow ($m^3\ s^{-1}$)

C = reservoir capacity (m^3)
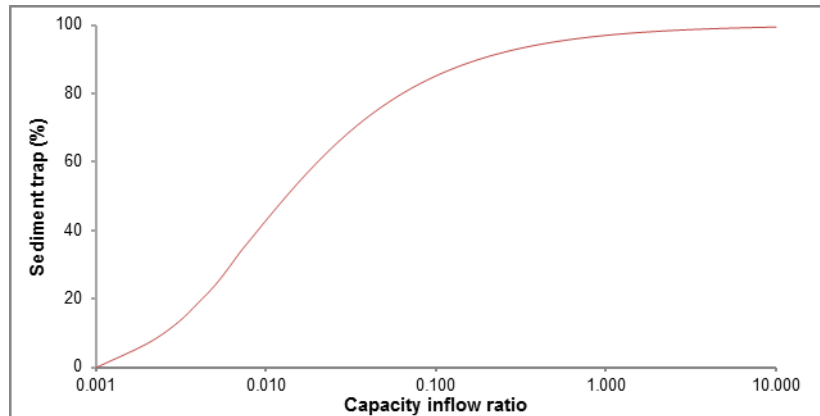
Figure 11. Brune's curve for estimating trap efficiency, modified by Dendy (1974)

2.4 Climate change scenarios

2.4.1 CORDEX

Global Climate Models (GCM) provide us with projections of how the climate of the earth may change in the future (Khan *et al.*, 2018). These results are the main motivation for the international community to take decisions on climate change mitigation. GCM provides reliable prediction information with scales of around 1000 by 1000 km (Cochran, Bokuniewicz and Yager, 2019). It is covering what could be a vastly differing landscape (from very mountainous to flat coastal plains for example) with greatly varying potential for floods, precipitation, temperature or other extreme events.

However, the impacts of a changing climate and the adaptation strategies required to deal with them, and will occur on more regional and national scales. This is where Regional Climate Downscaling (RCD) has an important role to play by providing projections with much greater detail and more accurate representation of localized extreme events (Lambert, 2017). Regional Climate Models (RCM) represents the climatological data in much greater detail compared to GCM as illustrated in Figure 12.
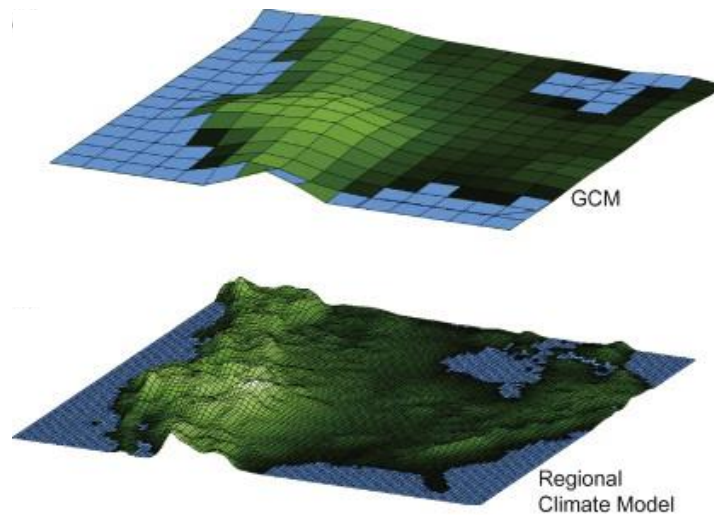
Figure 12. Illustration of GCM and RCM regarding its spatial resolution.
Source: Hannah (2015)

RCM and Empirical Statistical Downscaling (ESD) applied over a limited area and driven by GCMs. It provides information on much smaller scales supporting a more detailed impact and adaptation assessment and planning, which is vital in many vulnerable regions of the world (Wolf and Collins, 2015).

Assisting the necessity of regional climate change projection, CORDEX was created for whole regions of the world to comply with the Fifth Assessment Report (AR5) and beyond. The main goal of CORDEX creation is to provide a coordinated model evaluation framework, a projection of climate change implementation, impact and mitigation studies. CORDEX was created by The World Climate Research Program (WCRP) in 2009 in the Task Force for Regional Climate Downscaling (Asia, 2017). Fulfilling the need for the East Asian climate change projection, CORDEX created the CORDEX-East Asia branch (Figure 13).

Figure 13. Coverage Area of Cordex-EA Phase 1.
Source: *http://cordex-ea.climate.go.kr/cordex/mainPage.do*

CORDEX-East Asia provides the ensemble climate simulations within the timeline of multiple dynamical and statistical downscaling models forced by multiple global climate models for the East Asia region. Cordex East Asia consists of 5 RCM:

1. HadGEM-RA developed by the National Institute of Meteorological Research (NIMR),

2. The Regional Climate Model version 4 (RegCM4) developed by the International Centre for Theoretical Physics (ICTP),

3. Seoul National University Meso-scale Model version 5 (SNU-MM5) developed by of Penn State University / National Center for Atmospheric Research Meso-scale model (MM5) produced by Seoul National University,

4. The Weather Research and Forecasting (SNU-WRF) was made by Seoul National University.

5. Regional Spectral Model (YSU-RSM) produced by Yongsei University.

As usually exist in the climate projection data, RCM from Cordex East Asia contains a Radiative Forcing (RF) indicator. RF value is used as one of the inputs for simulation of the global climate model, whereas the output from the model is utilized to observe the projections of the various elements in climate change. In the IPCC AR5 report (IPCC, 2014), a new terminology called Representative

Concentration Pathways (RCP) has been introduced as the latest generation of climate change scenarios (Moss *et al.*, 2010). The RCP scenario has a complete representation of the estimated RF ranges in the future. This RCP is divided into four classifications, starting from the lowest scenario (optimistic) to the most extreme scenario (pessimistic): RCP 2.6 (aggressive mitigation strategy, the increment of RF 2.6 W m^{-2}), RCP 4.5 (intermediate - light, the increment of RF 4.5 W m^{-2}), RCP 6.0 (intermediate - high, the increment of RF 6.0 W m^{-2}) and RCP 8.5 (the increment of RF 8.5 W m^{-2}). Trajectories of RCP 4.5 and 8.5 were implemented for this study. RCP 4.5 is a state where radiative forcing is in the range ~650 ppm CO_2 eq and the condition is stable after 2100. Meanwhile, RCP 8.5 is a condition where radiative forcing is in the range of ~ 1370 ppm CO_2 eq in 2100 and continues to increase (van Vuuren *et al.*, 2011)

In this study, observation of future climate change used RCM CORDEX East Asia database from EAS-44 with coverage area to East Asia with boundaries -40.92° - 47.96° East and -26.84° - 46.20° North with a resolution of 0.44°. Type of data that useful for the study from CORDEX East Asia (http://cordex-ea.climate.go.kr/cordex/) is precipitation (Pr, unit in kg m^{-2} s-1), maximum temperature (Tasmax, unit in Kelvin), the mean temperature (Tas, unit in Kelvin) and minimum temperature (Tasmin, unit in Kelvin) of RCP 4.5 and 8.5. Those raw data were downloaded from the CORDEX East Asia website in Net CDF file type (resolution: 50x50 km) and then converted to an excel database using NetCDF4Excel software. Two nearest points of the CORDEX East Asia data with averaged areal values of observation data were compared to choose the best fitting between both distributions of data. This method was implemented because the correction cannot be carried out by comparing each meteorological station with the nearest grid point of the climatological field, but it should be done by comparing areal averaged values (Déqué, 2007). Hence, the mean daily precipitation and temperature of the watershed were compared with CORDEX data. The best-fitting point data was used in the data processing to project the future climate including bias correction. Five models consisted of SNU MM 5, SNU-WRF, YSU-RSM, RegCM4 and HadGEM-3RA were analyzed. The analysis was done by comparing those models with observation data. After

having bias correction, the HadGEM-3RA climate model was selected as the best model to be used in future analysis. The correction was implemented through linear regression (linear scaling). The method has been used by many researchers for example by Bussi *et al*. (2014). This method is applied to all climatology aspects such as precipitation, maximum temperature, mean temperature and minimum temperature. To take into account seasonal variations, bias correction is separated under rainy and dry season.

Bias correction was implemented based on the difference between linear interpolation with 1 : 1 line of the q-q plot. Biases were corrected through a comparison between historical data of CORDEX East Asia in 1975-2005 (30 years) with observational data in the same period. The correction factor was then implemented to the raw data of future climate for the period 2011 to 2100. These new corrected data were then used as input for hydrological and sedimentation model to examine the impact of future climate change on hydrological and sediment cycle.

2.4.2 Bias correction

Nowadays, the Regional Climate Model (RCM) is widely used in hydrological studies for the catchment scale. RCM produces climate projection with a resolution of 25-50 Km generated from GCM which is suitable for large catchment study. Unfortunately, the climate variables contained in RCM are often inconsistent with streamflow observation data (Teutschbein and Seibert, 2010). Thus, RCM raw data is not directly used in hydrological studies (Bergström *et al.*, 2001). Moreover, precipitation and temperature data experience a large bias (Christensen *et al*., 2008; Teutschbein and Seibert, 2012; Varis, Kajander, and Lemmela, 2004). Hence, it is very risky if the RCM raw data is used directly in hydrological studies because it will result in a non-accurate characteristic of the catchment and could lead to a false prediction.

The occurrence of bias can be caused by errors in the process of imperfect conceptualization, discretization and spatial averaging within grid cells (Teutschbein and Seibert, 2012). Common biases encountered are the low

intensity of rainfall in wet days, imperfect extreme temperature estimation (Ines and Hansen, 2006) and under-overestimation of seasonal temperatures and precipitation (Christensen *et al.*, 2008; Terink *et al.*, 2009; Teutschbein and Seibert, 2010). Therefore, correction of bias is necessary to be conducted to provide a reliable climatological data of RCM (Christensen *et al.*, 2008; Teutschbein and Seibert, 2010; Varis, Kajander, and Lemmela, 2004). The bias correction method diminishes the bias in RCM so that RCM data is more accurate. The bias method varies from simple to complex methods. The bias correction uses an algorithm transformation method to adjust RCM raw data. The process is carried out based on the identification of the difference between observed and simulated climate parameters. The methods commonly used to make bias correction include:

1. Linear scaling for precipitation and temperature

The linear scaling method uses monthly precipitation or temperature data as the basis for the correction (Lenderink, Buishand and Deursen, 2007). The difference between simulated (RCM raw data) and observed precipitation or temperature values is used in the process of correction. Raw data is corrected based on the ratio of mean monthly and control period (Teutschbein and Seibert, 2012).

2. Local intensity scaling (LOCI) for precipitation

LOCI is presented by (Schmidli, Frei and Vidale, 2006) and meant to correct the bias in wet-day frequency and intensity (Teutschbein and Seibert, 2012). LOCI fill the gap which linear scaling cannot do, such as for certain periods (wet period). LOCI adjust the mean value of wet days frequency and intensity and correct the linear method. LOCI accomplished the correction in two steps:

a. RCM Calibration of a certain precipitation threshold, such as the number of RCM days exceeding this threshold which fit observed data greater than 0. The number of precipitation days is corrected by using the calibrated threshold. Hence all days less than the threshold is assigned as dry days with 0 mm of precipitation.

b. The linear scaling factor, estimated by calculating the mean value of monthly mean wet-day intensities.

3. Power transformation of precipitation

This method corrects the difference of variance for time series of precipitation (Leander and Buishand, 2007; Leander *et al.*, 2008). The monthly distribution-free approach is the base of this method.

4. Variance scaling for temperature

A stepwise approach of mean and variance of temperature correction is implemented in the variance scaling method. This method is different from linear and LOCI methods which correct the mean and variance limited to a power function of precipitation data. In the first step, the mean of RCM raw data is adjusted using linear scaling. Then, the standard deviation is scaled following the ratio of observed and control run. And finally, the corrected time series is readjusted using the corrected mean. The adjusted RCM in the control period has equal standard deviation and the mean of the observed value.

5. Distribution mapping for precipitation and temperature

The correction of the RCM raw-data distribution function (corresponds to the observed distribution function) is the aim of this method. The shifting function of the occurrence of precipitation and temperature distribution function is required in this method. Quantile-quantile mapping, probability mapping, histogram equalization and statistical downscaling are a technique to fulfil this method (Ines and Hansen, 2006; Rojas *et al.*, 2011)

6. Delta-change for precipitation and temperature

Instead of using RCM simulation of future conditions, RCM simulated future data is used in the correction of this method. In this method of control period (base-line climate/observed climate) cannot be used. Observation of time series

is conducted through an overlay process between RCM simulated future data and scenario run.

2.5 TETIS distributed hydrological model

2.5.1 Water sub-model description

TETIS (Francés *et al.*, 2007) is a distributed conceptual hydrological model with physically-based parameters. TETIS simulates the water and sediment cycle through unit cell as process-based. Thus, to perform the model, TETIS required data of hydrometeorological time series and spatial map (elevation, soils and vegetation). For each cell, TETIS conceptualizes the water cycle in a set of interconnected virtual tanks (Figure 14-left). The interception tank (T6) represents the amount of rainfall intercepted by the plant canopy that subsequently experiences evaporation. The static tank (T1) represents water detention in puddles and capillary water storage (below field capacity) in the upper soil. The infiltration capacity below field capacity is assumed to be infinite and the only output from this tank is evapotranspiration. The surface tank (T2) conceptualizes the amount of water over the surface that moves either in the form of gravitational infiltration (above field capacity) or overland flow. The gravitational tank (T3) represents the storage in the upper soil between field capacity and saturation and its outputs are deep percolation and interflow. This deep percolation recharges the aquifer tank (T4). The aquifer flow can be connected with the river network within the watershed (baseflow) or not (deep aquifer flow). Finally, the river channel tank (T5) collects overland flow, interflow and baseflow and then distributes them through the catchment drainage network.
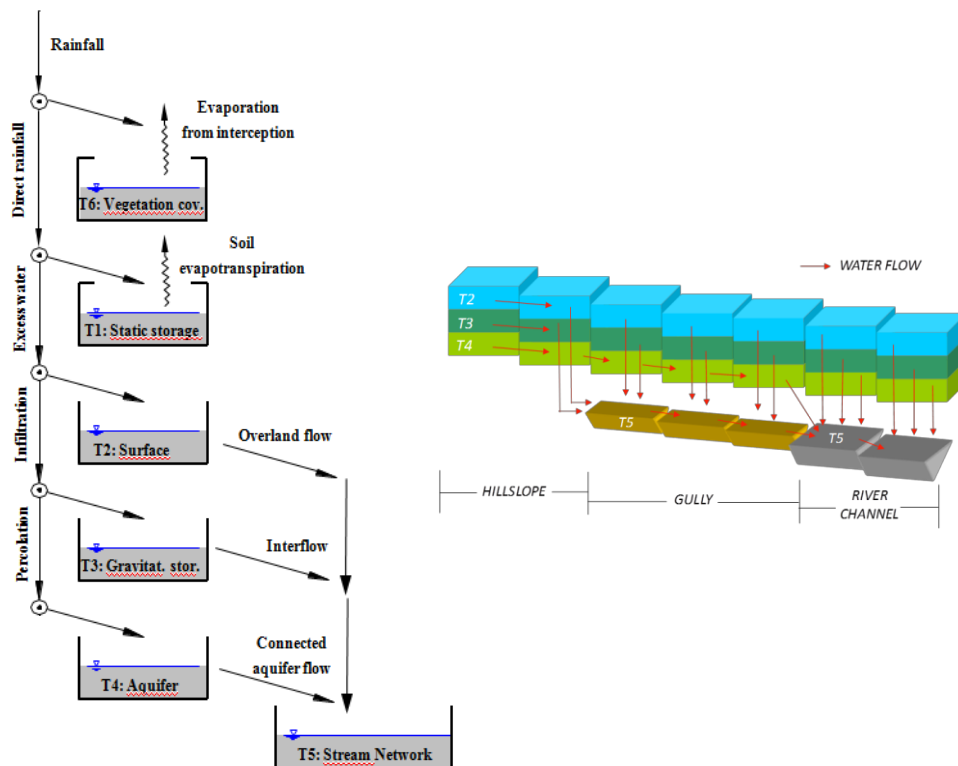
Figure 14. Left: Vertical tank conceptualization of the TETIS model for each cell.
Right: Water movement scheme of the TETIS model

As stated by Francés *et al.* (2007), TETIS is a distributed conceptual model, developed for continuous simulation of the hydrological cycle. Water movement on the land in the TETIS model are generated in the sequence of cell network in the form of transported downstream. The water flow of the channel in the TETIS is generated by a conceptual simplification called Kinematic Wave. Gully and river channels are differentiated in the stream network according to a certain threshold of drainage area. Each cell with these different criteria collects water from upstream and delivers water downstream as described in Figure 14-right. This figure explains the interconnected horizontal and vertical water propagation that represents the overland flow, interflow and baseflow. The translation of runoff over the basin is done by considering non-retained water flows over the hillslopes until it reaches a channel of the natural drainage network. When the water reaches this point, it flows through the catchment drainage network.

TETIS deals with effective model parameters using a split parameter structure (Francés and Benito, 1995). In this way, the effective parameters of each cell are the result of the multiplication of the initially estimated parameter map by nine correction factors (static storage, evapotranspiration, infiltration, overland flow, percolation, interflow, deep aquifer flow, connected aquifer flow and channel flow velocity). As there will be only nine variables to be calibrated (the CFs), this internal structure is extremely effective with regards to the calibration process. For this reason, in TETIS it is possible to use optimization algorithms for the automatic calibration of the model. In addition to that, TETIS allows the adjustment of parameter maps without interfering with the calibrated CFs in different LULC situations. Parameters that need to be altered for the changes of LULC are monthly vegetation coefficients for evapotranspiration, the canopy interception capacity, the static storage capacity due to changes in the effective root depth and puddle retention capacity and the gravitational infiltration capacity in the case of urbanization.

2.5.2 Sediment sub-model description

The TETIS sediment sub-model is based on the model formulation developed for the CASC2D-SED (Francés, Vélez and Vélez, 2007). A CASC2D-SED model is an event scale hydrological and sediment model that reproduces the hillslope processes in two dimensions, while the channel approach is mono-dimensional. In the TETIS adaptation, both processes are mono-dimensional (Francés *et al.,* 2017).

Soil erosion, sediment transport and deposition are determined by combining the sediment availability and the sediment total transport capacity. The availability of the sediment confines the transport of fine sediment. Meanwhile, flow transport capacity confines the coarse material of the sediment (Julien, 2010). Still following Julien (2010), the hillslope transport capacity follows the appropriate textural composition of sediment which is separated on three textural classes namely sand, silt and clay. Those textural classes indicate different diameters and settling velocity. The gravitational characteristics of these

textures determine the behaviour of each texture in the stream. The transport capacity mechanism in the hill slope is differentiated into three parts. First of all, transport capacity is used to lift suspended sediment downstream, then the residual capacity is used to lift deposited sediment and finally, if the residual transport capacity is still available, it will be used to erode the soil parent material. Further deposition and suspension will be depending on settling velocity characteristics of sediment. The gully and channel erosion and transport processes are described by the Engelund and Hansen equation (Engelund and Hansen, 1967), where the streamflow transport capacity depends on the hydraulic radius, flow velocity, friction force and grain characteristics. The characteristic of gully and channel erosion and transport processes is the same as the characteristic of hillslope except for the non-existence of parent material erosion.

The transport capacity for hill slopes is determined by the Kilinc and Richardson (1973) equation and modified by Julien (2010) by implementing the USLE (Universal Soil Loss Equation; factors of soil erodibility, soil cover and soil practice-management (K, C, P indices) following Wischmeier and Smith (1961). To accomplish the modification, these factors were introduced into the equation as presented in the equation below:

$$Q_h = \frac{1}{\gamma_s} W \, \alpha \, S_o^{1.66} \left(\frac{Q}{W} \right)^{2.035} \frac{K}{0.15} \, C \, P \qquad [7]$$

Where: Q_h = water discharge in the hillslope (m^3 s^{-1})
γ_s = the specific weight of the sediment (tons m^{-3})
W = width (m)
α = a dimensional and empirical parameter
S_o = the terrain slope (m/m)
Q = water discharge per unit width (m^3 s^{-1})

K = USLE indices for soil erodibility (unitless)
C = USLE indices for cropping management (unitless)
P = USLE indices for support practice factors (unitless)

The Engelund and Hansen equation (Engelund and Hansen, 1967) is used for the total transport capacity of the gully and river channels, where grain

characteristics, flow velocity, hydraulic distance and friction force define the sediment transport. Sediment erosion, transport and deposition are defined by sediment availability on one hand and sediment total transport capacity, on the other hand. All the transport process of gully and channel is equal with the characteristic of hillslope process, except the non-existence of erosion from the parent material.

TETIS uses two total transport capacities, one for hill slopes and the other for river channels. Each of these transport capacities has its corresponding CF that can be calibrated, namely α (hillslope transport capacity) and β, consist of β1 (gully transport capacity) and β (river channel transport capacity). Regarding the implementation of TETIS with different LULC, the correction factor is not necessary to be modified. The parameter that required to be changed is only the map of the USLE land cover factor and with regards to urbanization, the soil erodibility factor is also needed to be changed.

The sediment sub-model of TETIS will be implemented to compare the observed and the simulated sediment data in the calibration phase. After that, the validation phase is required to check the certainty of the calibration process. After the calibration and validation phase is completed, the accepted model can be simulated on a certain time series to study the erosion and sedimentation.

2.5.3 Indices for performance evaluation of predictive models

One of the model performance indicators that can be used to measure the robustness of the TETIS model output is the Nash Sutcliffe Efficiency index (NSE), Standard Deviation Ratio (RSR) and Volume Error (VE) (Moriasi *et al.*, 2007).

Nash Sutcliffe Efficiency (NSE)

The NSE is a normalized statistic that determines the relative magnitude of the residual variance compared to the measured data variance. The NSE equation is illustrated as follow:

$$NSE = \left| 1 - \frac{\sum_{i=1}^{n}(\hat{Q}_i - Q_i)^2}{\sum_{i=1}^{n}(Q_i - Q_i)^2} \right.$$

Where $\hat{Q}_i$ is simulated discharge, Q_i is observed discharge and $\bar{Q}$ is the mean observed discharge. Based on NSE, a calibration can be accepted if the index is greater or equal to 0.6 (Bussi *et al.*, 2014). A perfect fit provides an NSE = 1. An NSE = 0 indicates that the model results are not better than the results of a model with only one variable (for example the mean value). Negative values indicate that the model performs worse than the mean value (Beven, 2000).

Calibration can be accepted if the NSE index greater or equals to 0.6 (Francés *et al.*, 2017). Meanwhile, a perfect fit provides NSE equal to one. NSE equal to zero indicates that the result of the model is not better than the result of a model with only one variable (for example the mean value). Negative values indicate that the model performs worse than the mean value (Beven, 2000). RSR represents the ratio of the RMSE and standard deviation of measured data Meanwhile, the VE calculates the average tendency of the simulated data to be larger or smaller than its observed counterpart.

RMSE-observations standard deviation ratio (RSR)

RSR is widely used as an indicator to quantify the statistical error by calculating RMSE based on the standard deviation (Singh, Knapp and Demissie, 2004). The model is better along with the lower RSR. RSR is calculated by dividing RMSE with a standard deviation of measured data, as shown in the formula as follow:

$$RSR = \frac{RMSE}{STDEV_{obs}} = \frac{\left[\sqrt{\sum_{i=1}^{n}\left(Y_i^{obs} - Y_i^{sim}\right)^2} \right]}{\left[\sqrt{\sum_{i=1}^{n}\left(Y_i^{obs} - Y^{mean}\right)^2} \right]} \qquad [9]$$

Volume error

The equation of volume error is as follows:

$$\%errVol = \frac{V_o - \hat{V}_p}{V_o} \times 100\%$$

[10]

Where V_o refers to total observed volume, V_p refers *to* total simulated volume. A positive index indicates underestimation while negative index overestimation. The optimum index is 0%.

2.5.4 Water sub-model Implementation

The calibration and validation of TETIS were performed by using parameter maps corresponding to the appropriate historical LULC. Therefore, the model validation can be classified as a Differential Split-Sample test (Klemes 1986). The calibration and validation of the water component of TETIS were achieved by comparing the discharge simulation of TETIS with the discharges of a flow gauge station located in the downstream of the Saguling reservoir.

The calibration of the water sub-model has been performed with parameter maps corresponding to LULC 2009 in the period 2008 to 2010 in Nanjung flow gauge station and with one year of the warm-up period. The NSE, RSR and VE were used to measure the model performance. Warming up period was introduced at the beginning of the calibration period to find the best initial moisture condition in soil, aquifer and channel discharge.

The calibration of the model was started manually by adjusting the CFs to find realistic values based on an acceptable threshold of NSE. Once these values were obtained, the calibration continued automatically using the SCE-UA optimization algorithm (Duan *et al.*, 1994) implemented in TETIS version 8.3.1 (Figure 15). Adjustment of correction factors in manual and automatic calibration was conducted through a trial and error procedure until the best fitting between estimated and observed discharge is achieved. Correction factors consist of evapotranspiration, static storage, percolation, overland flow,

45

infiltration, interflow, baseflow and flow velocity. Deep aquifer flow was assumed as zero due to the assumption of non-water loss from the aquifer. Calibrated CFs were satisfactorily validated for the periods 2012-2014 and 1994-1996, corresponding to LULC 2014 and LULC 1994, respectively. The selected periods for calibration and validation were based on the availability of common and complete hydrometeorological and LULC data. Temporal validation is done by implementing the model in the different time ranges of the calibration process.

After model validation, a long period of meteorological data (1985-2014) was simulated using historical LULC (1994, 2009 and 2014) and scenarios to determine the impact of LULC changes on water balance, flood regime, catchment erosion and reservoir sedimentation. To accurately predict the expected lifetime of the reservoir, the recirculation of this historic meteorological input is required to obtain long-term results.
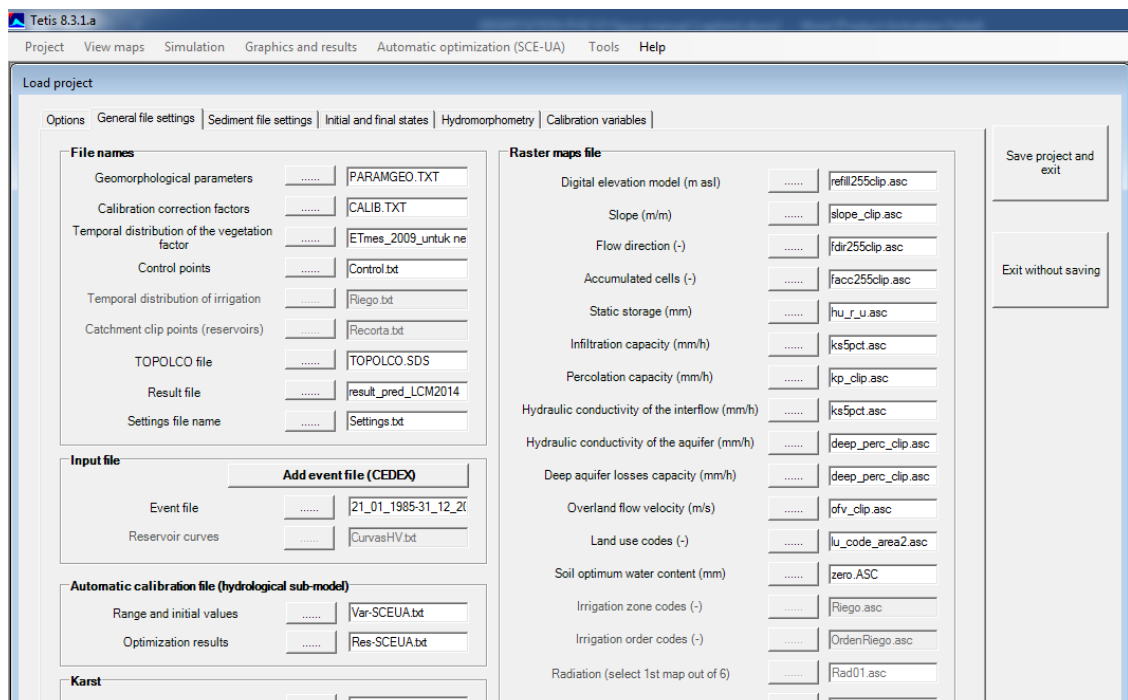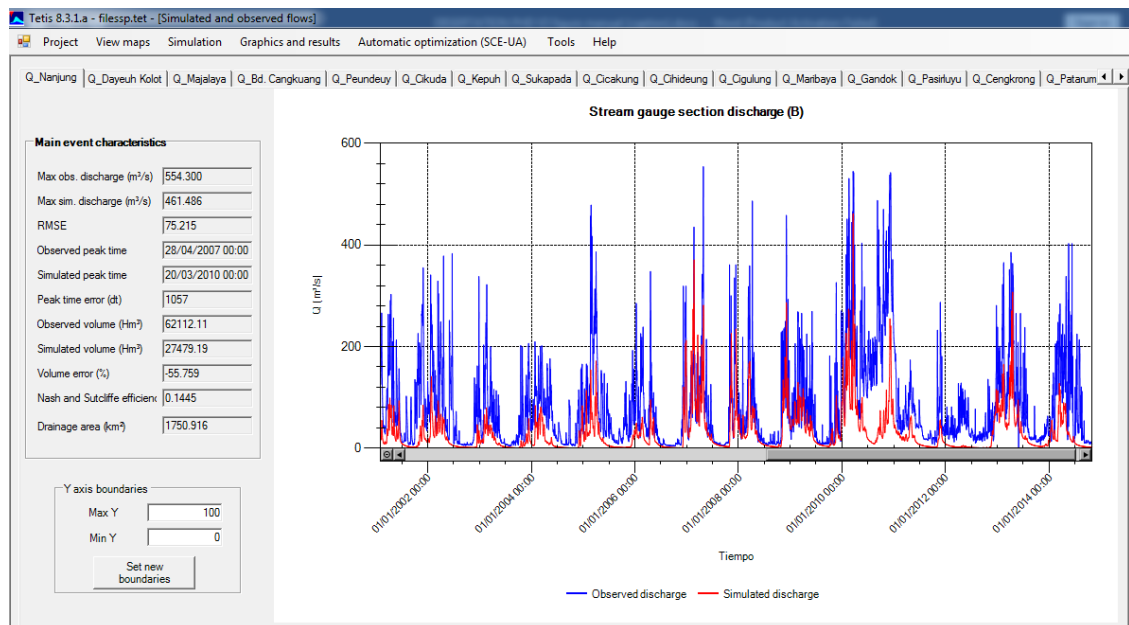
Figure 15. Input data and example of a water discharge result in TETIS software as the main tool of the study.

2.5.5   Sediment sub-model Implementation

The calibration of the TETIS sediment sub-model was implemented by comparing the observed and the simulated sediment volume. After calibration, the validation phase is required to check the certainty of calibration. In the calibration and validation of the sediment sub-model, the bathymetric information of the reservoir has been used. This type of information has already been studied in depth by many authors, such as (Alatorre, Beguería and García-Ruiz, 2010) or Bussi *et al.* (2014).

The sediment sub-model calibration was done for the year 2009, comparing the observed sediment yield (obtained from the reservoir data) and the output TETIS simulation using LULC 2009. Meanwhile, the validation was conducted by comparing the observed deposited sediment volume during the period 2008-2012 with corresponding simulations using TETIS.

In this case, volume error was used to measure the model's performance for sediments. Calibration involved the adjustment of correction factors of

47

hillslope transport capacity (α), gully and stream channel network (β) until the best result was achieved. After the model validation was completed, a long period of simulation using different historical LULC (1994, 2009 and 2014) and scenarios were implemented. These simulations used the same correction factor as on the final calibration. Unfortunately, spatial validation was not done due to the absence of another sediment gauges data in the watershed. Nevertheless, the model can be considered satisfactorily validated in time.

After both water and sediment model was successfully calibrated and validated, a long period of meteorological data (1985-2014) is simulated using historical LULC and scenarios. To accurately predict the expected design life of reservoirs in this region, the historical meteorological input was repeatedly used in the future long run of the model.

2.6 AFINS

Flood frequency analysis deal with flood event and frequency analysis. It engages with the statistical approach involved flood magnitudes and flood probabilities in the analysis process. Thus, flood frequency analysis able to analyze flood (discharge) in certain years of return periods. This study used Maximum-Likelihood-method with AFINS tool (Botero and Francés, 2006) to estimate the return period.

A mathematician from German, Emil Gumbel (1891-1966) has introduced for the Gumbel distribution as an alternative to analysing data frequency. This distribution is useful to analyze non-normal distribution data as it is usually found in hydrometeorological data. Therefore, the application of Gumbel distribution to analyze non-normal distribution data becomes very frequent. The main focus of Gumbel is the application of extreme value theory to modify a phenomenon or problem. For example, those which are found in hydrometeorological modeling of events such as annual flood (Onen and Bagatur, 2017) and annual discharge (Pal and Pani, 2016). Therefore, Gumbel distribution is known as a tool

to analyze the distribution of extreme values data. Gumbel equation is presented as follow:

$$F(x) = \exp\left\{-\exp\left[-\frac{(x-\alpha)}{\beta}\right]\right\}$$
$$f(x) = \frac{1}{\beta}\exp\left\{\left[-\frac{(x-\alpha)}{\beta}\right] - \exp\left[-\frac{(x-\alpha)}{\beta}\right]\right\}$$

[11]

where:

$F(x)$ = cumulative probability distribution function

$f(x)$ = probability density function

α = parameter of location

β = parameter of scale (larger than zero)

x = continuous random variable (define from negative infinity to positive infinity)

Flood frequency analysis in this study follows a standard approach (see for example the book of Kottegoda and Rosso (2008), using the software AFINS (http://lluvia.dihma.upv.es/EN/software/software.html) to: i) estimate the parameters of different probability distribution functions by the Maximum-Likelihood-Method; and ii) to perform the statistical model selection, mainly using the comparison with the sample plotting positions (also called empirical distribution). Gumbel function has been implemented to analyze flood frequency in 5 to 100 years. Gumbel function has been selected due to the ability of the function on flood frequency analysis. The example of Gumbel distribution analysis implementation in tropical regions has done by Clarke (2002) to detect and predict annual maximum river discharges in a tropical watershed in Brazil.

To describe flood regimes, Saguling station was selected as a station for calculating annual maximum daily discharges. The output of annual maximum discharge has been simulated by TETIS using the input of daily discharge for the period 1985-2014. Historical LULC (1994, 2009 and 2014) and scenarios were used as samples for this flood frequency analysis. Prior to the implementation of the AFINS tool, the annual maximum discharges from TETIS simulation were sorted as

a requirement for the input. The distribution of maximum discharge is then used to describe the maximum discharge for the return period from 5 to 100 years.

2.7 Land change modeler

Land Change Modeler for ArcGIS (version 2.0) is a powerful machine learning procedure (empiric model) developed by Clark Labs to analyze historical spatial variables, model and predict future change (Eastman, 2016). Among other methods, LCM uses a multi-layer perceptron (MLP) neural network to model the transition potentials based on the analysis of physic, environment and socio-economy of historical LULC evolution.

The mechanism of MLP is described in Figure 16. MLP uses layers (green and blue boxes) with each layer containing neurons. MLP receives a data input and propagates the data on the network to produce output. A weight is existing on each connection between two adjacent layers of neurons, it determines the quality of the relationship. A linear operation with the existing weight value is performed on each input data of the layer, then the computational results will be transformed using a non-linear operation called activation
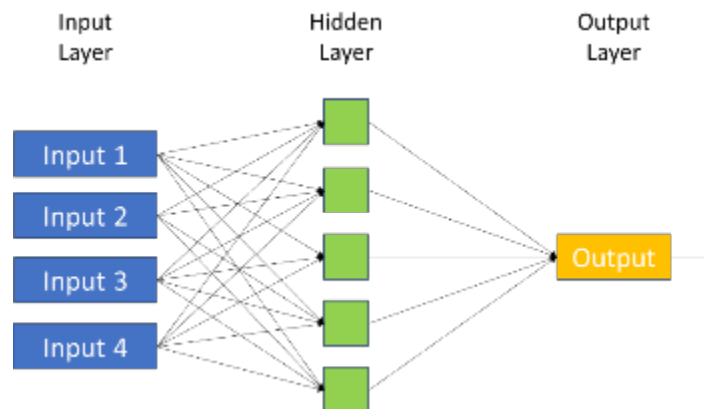
Figure 16. Multi-layer perceptron (MLP) neural network mechanism adopted by LCM.

In the predictions process, LCM uses a spatio-temporal Markov Chain to quantify the change based on transition potentials (Figure 17). The Markov Chain Model was discovered in 1906 by a Russian expert, A.A. Markov. Markov Chain is

a discrete random process with the assumption that the next state depends only on the current state (Eastman, 2016). Markov Chain is a mathematical technique to model various systems and processes. This technique can be used to estimate changes in the future with dynamic variables based on changes from dynamic variables in the past. This technique can also be used to analyze future events mathematically. Markov chain explains the activity of variables in the future based on the activity of variable at present. The process of the Markov chain can be reviewed as follow (Weng, 2002):

$$Kt_{(j)} = P \times Kt_{(j-1)} \qquad [12]$$

Where: $Kt_{(j)}$ = chance of occurrence at $t_{(j)}$
        P = Transitional Probability
        $t_{(j)}$ = time of j

     Kt is an event in a certain time and all the previous events are defined as $Kt_{(j)}$, ..., $Kt_{(j-n)}$. The probability of all future events $Kt_{(j)}$ depends only on the event $Kt_{(j-1)}$ and does not depend on previous events such as $Kt_{(j-2)}$, $Kt_{(j-3)}$, ..., $Kt_{(j-n)}$. The activity of variables in the future can be predicted based on the activity of the variable in the past. For example, Kt_6 is affected by the event Kt_5, Kt_5 affected by the event Kt_4 and so forth and this change is affected by the transition probability. For example, events Kt_3 will not affect the event Kt_6. The above process is usually connected like a chain. Therefore, this theory is known as the Markov Chain. If a particular event from a series of experiments depends on several possible events, then the series of experiments is called the "Stochastic Process"
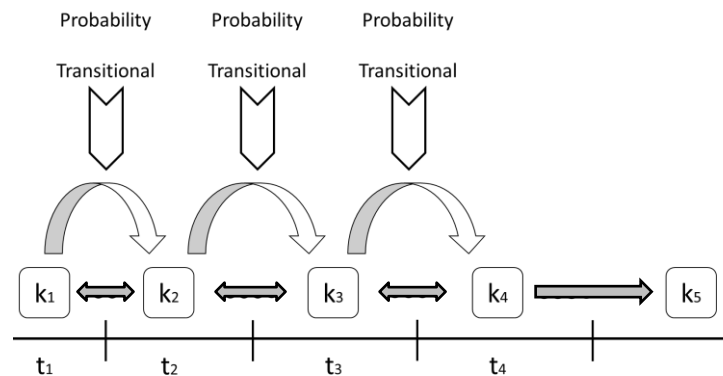
Figure 17. The process of Markov chain analysis in LCM

According to (Render, Stair and Hanna, 2012), there are 4 assumptions in Markov analysis:

1. A limited number from each possible state, where the probability of the transitions from an initial system state equal to one
2. The probability of the change in state is constant for all time.
3. Ability to predict each future state based on current state analysis using matrix probability transition
4. The size of the system or the number of objects is fixed during the analysis.

The LCM is included within the IDRISI GIS and Image Processing software and is available as a software extension for use with ESRI's ArcGIS product. LCM provides:

- A certain set of tools to perform land cover change analysis
- A relatively simple modeling environment, to create predictions for future scenarios, integrating drivers of change as well as constraints, such as protected areas.
- Specific tools for the implementation of REDD projects (such as estimation of baselines and modeling deforestation)

The LCM application consists of three main steps: change analysis, transition potential and prediction. The change analysis step identifies gains and losses, persistence and transition trends from one previous land cover state (T1) to another (T2). The transition potential step determines the potential of the area to transition based on the transition trend. The transition may consist of a single or a group of land cover categories related to its driver variable called the sub-model. For the transition potential modeling, the MLP performs the training and testing by identifying two groups. The first one is the group of pixels that have been transitioned from T1 to T2, meanwhile the other group consists of persisted pixels. The performance of training and testing is expressed in the accuracy rate. Based on historical changes and the transition potential model, the prediction process will determine the relative change of transition in the future. The validation step is conducted by comparing the predicted and observed maps to determine whether the transitioned pixels are correctly predicted or not. Three

results exist under validation: hits (model correctly predicted the change), false alarms (model predicted the change, but it did not occur) and misses (model did not predict the change, but it occurred).

2.8   Scenarios of LULC

2.8.1   Conservation scenario

The used conservation scenario for this study is presented in Figure 18. LULC conservation scenario was developed based on the principle of soil conservation. Therefore, this scenario is associated with an index to prevent soil erosion, in this case, the threshold of *Tsl*. The threshold for the study area is adopted from the threshold of *Tsl* specifically proposed for Indonesia by Arsyad (2000) with a value of 13.5 ton ha^{-1} yr^{-1}. Hence, in this scenario, the erosion rate of a location exceeds the *Tsl* will be replaced by the forest as it is able to combat erosion. The conservation scenario was built upon LULC 2014 as the newest available LULC. Beforehand, an erosion map in 2014 was generated to determine the exact location of the area that exceeds *Tsl*, which will be replaced by forest vegetation. Thus, the sediment sub-model from TESIS was used to generate this erosion map. After the replacement process is finished, the TETIS sediment sub-model was implemented once again to produce a new erosion distribution map and water balance conditions for further analysis.
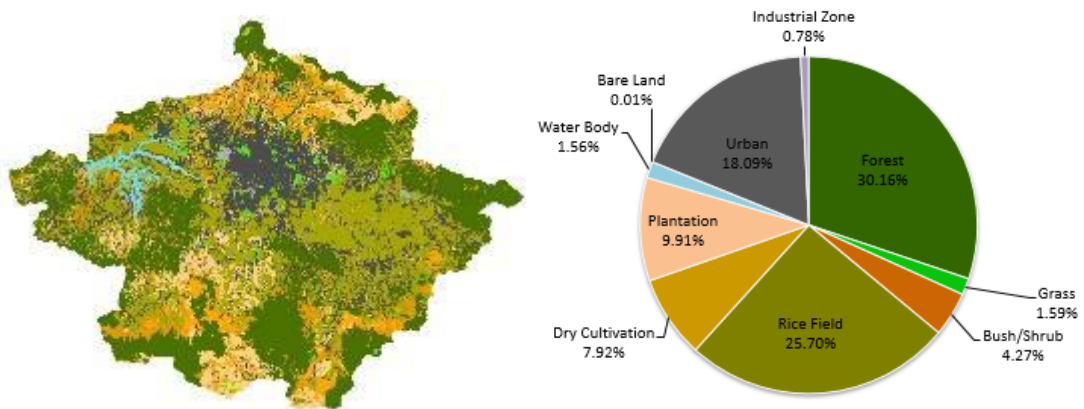
Figure 18. LULC of conservation scenario

From the generated erosion map, many parts in the northern, southern and eastern parts of the study area exceed the *Tsl*, thus many sites on those areas

53

have been replaced by forest as explained previously. Meanwhile, the western and central parts of the area did not experience many changes because those areas show a low erosion rate. Thus, the original LULC in those areas has remained.

2.8.2 Government plan scenario

The government plan scenario is produced due to the necessity of the community to build an integrated region in line with the ideal concept of spatial usage. In addition, sustain spatial planning and the welfare of the community are important goals to be achieved. These backgrounds appear due to limited natural space for living. Hence, the optimal usage of spatial is important to be implemented to provide a sustainable, productive, safe and comfortable environment.

The government plan scenario is also known as the spatial plan map, which is made based on the decisions of regulation of West Java Province Number 22, 2010 regarding the spatial plan map of West Java Province 2009-2029. This map considers the conservation aspect and was obtained from the Planning Board of West Java (Figure 19). In this study, the map of the government plan scenario was generated by incorporating a recent LULC map (LULC 2014) with a spatial plan map of West Java Province 2009-2029. Thus, the recent map was modified and incorporated by several LULC types from spatial and territorial plan map such as conservation forest, production forest, limited forest production, protected forest and suitable areas for conservation forest, geology protection area, prone to mountain eruption, prone to soil movement and water absorption area. The recent LULC map that coincides with the LULC spatial plan map was replaced by spatial plan map LULC. Meanwhile, the rest of LULC from the recent map that did not coincide with the spatial plan remains with the previous existed LULC.
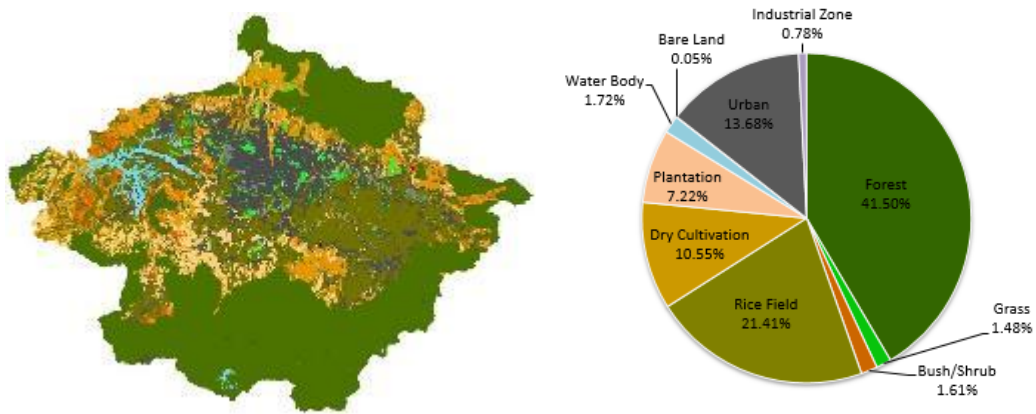
Figure 19. LULC of government plan scenario

The northern and southern parts of the study area experienced significant LULC changes compared to the recent LULC (2014). Meanwhile, the western, eastern and central areas did not experience many changes. The urban area in this scenario possesses a lower percentage. This occurs due to the replacement of all LULC in the northern and southern part of the study area by forest. The replacement of old LULC by the new LULC in the northern and southern part of the study area play an important role in the conservation point of view. By assigning the LULC forest in that location, the location is expected to play a role as the water absorber area during the heavy rains, especially in the rainy season. Infiltration is expected to increase and reduces the velocity and quantity of overland flow.

2.8.3   Natural vegetation scenario

The natural vegetation map represents the natural state of vegetation in the far-off period (centuries before the present time). Based on The Asian Bureau for Conservation and the World Conservation Monitoring Centre, West Java is included in Semi-Evergreen Rainforest (Jepson and Whittaker, 2002). The same theory has been mentioned by Whittaker (1970), which stated that the study area with an annual rainfall average of 250-450 mm month^{-1} and an average annual temperature 20-30 °C is included in the category of tropical rainforest.

In the past, the diversity of LULC due to the anthropogenic effect did not exist in the study area. LULC was occupied only by natural vegetation resulted from a natural process. Hence, LULC of the past was fully occupied by forest. The higher land of the area is also occupied by forest as commonly found in the wet tropical area. High precipitation amount supported by fertile Andisols results a vast and dense forest area in the higher land. The illegal logging was not occurred in the higher land in the former time, hence, those areas are well preserved from the human disturbance. The most accurate information related to this was issued by Lubis (2000) who stated that LULC of the study area in 1809 was filled by forest. The information is also supported by the regulation of the Municipality of Bandung Number 35, 1998 regarding the Anniversary of Bandung which clearly stated the same information. Natural vegetation map has been generated based on that information.

Producing a map of natural vegetation is simply done by replacing all the LULC in the study area with forest, except waterbody. The percentage of forest in the natural vegetation map is noted 98.43%. Meanwhile, the rest area is occupied by a waterbody with a percentage of 1.57%. Forest area increases significantly compared with the forest in LULC 2014 with 11.50% of the total area. The map of natural vegetation was incorporated with TETIS to find out the water and sediment cycle to analyze water balance, flood and sediment cycle in the past. The natural vegetation scenario of the Upper Citarum Catchment is presented in Figure 20
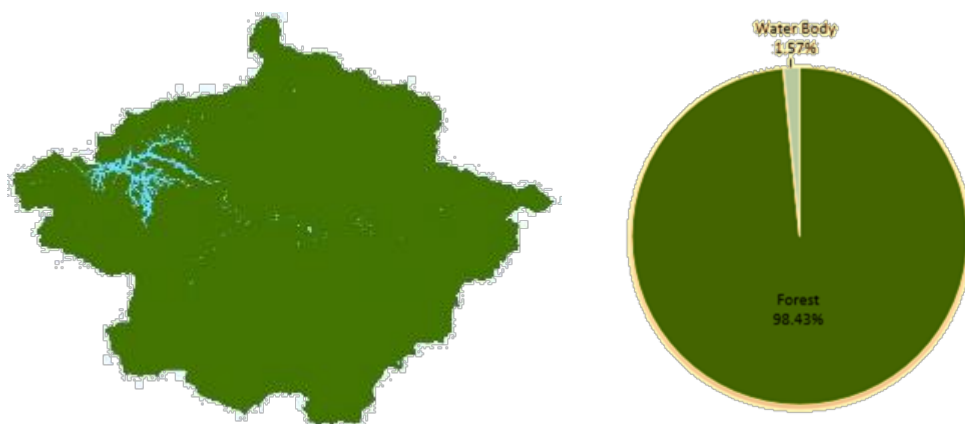
Figure 20. LULC of natural vegetation scenario

2.8.4 Future scenario generated by LCM

Future LULC was obtained by utilizing the Land Change Modeler (LCM), developed by Clark Labs (Eastman, 2016). The selection of the year 2029 for the future LULC scenario was based on the two decades of government projection plans, which were previously made in 2009. The general description of the methodology can be found in Figure 21.
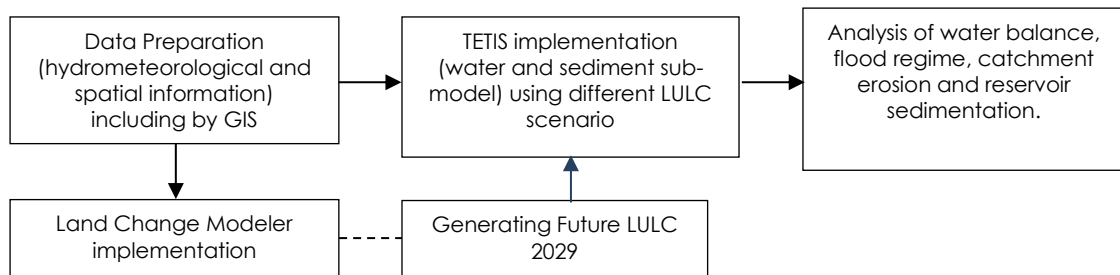
Figure 21. General scheme of implemented LCM in the study

Basic spatial inputs for LCM parameterization are comprised of topography, road and city map (Table 6). All map manipulations were done using ArcGIS with a final spatial resolution of 90 m. The required map for LCM such as topographic map was extracted directly from DEM. Meanwhile, the driver maps of distance from road and city were generated based on the road and city map from the Planning Board of West Java, Indonesia.

Table 6. Spatial information for the input of LCM

Data Type	Scale (resolution)	Source	Input, driver or parameter
Topographic map	2 arc-second (90m)	Digital Elevation Model USGS	- Slope - Elevation
Road & city map	1: 100,000	Planning Board of West Java, Indonesia	- Distance from road - Distance from city

The process to develop future LULC is presented in Figure 22. Initially, the gains, losses, persistence and transition trends between LULC 1994 and 2009 were assessed. Subsequently, the LULC categories (sub-models) of transition potential were estimated. In this study, the transitions smaller than 500 hectares were

eliminated to be more focused on significant transitions. Incorrect transitions such as from urban or industrial areas to vegetation land cover were eliminated because such transitions are hardly found in real conditions. Driver variables such as elevation, slope, distance from road and distance from the city were used in the training and testing step. This step was carried out based on the accuracy rate estimation index as the performance evaluator (Eastman, 2016). In this study, a minimum accuracy rate of 65% was the result of the training and testing process of all LULC category transitions.

The result of the future scenario resulted from LCM is presented in Figure 23. Under LULC 2029, the predicted main types of LULC will be urban areas, rice fields, dry cultivations and plantations (23.3%, 22.9%, 16.1% and 16.1% of the catchment, respectively). Compared to 2014, forests and rice fields under LULC 2029 will decrease by 3.13% (8.33 km^2) and 15.0% (93.5 km^2), respectively (Table 7). Deforestation occurs at a slower pace from 2014 to 2029 and this is presumably due to the decrease of available forested areas for other human-related use (forest makes up only 11.50% in LULC 2014). Moreover, the remaining forests are located in hillier areas, hence making them unsuitable for cultivation.
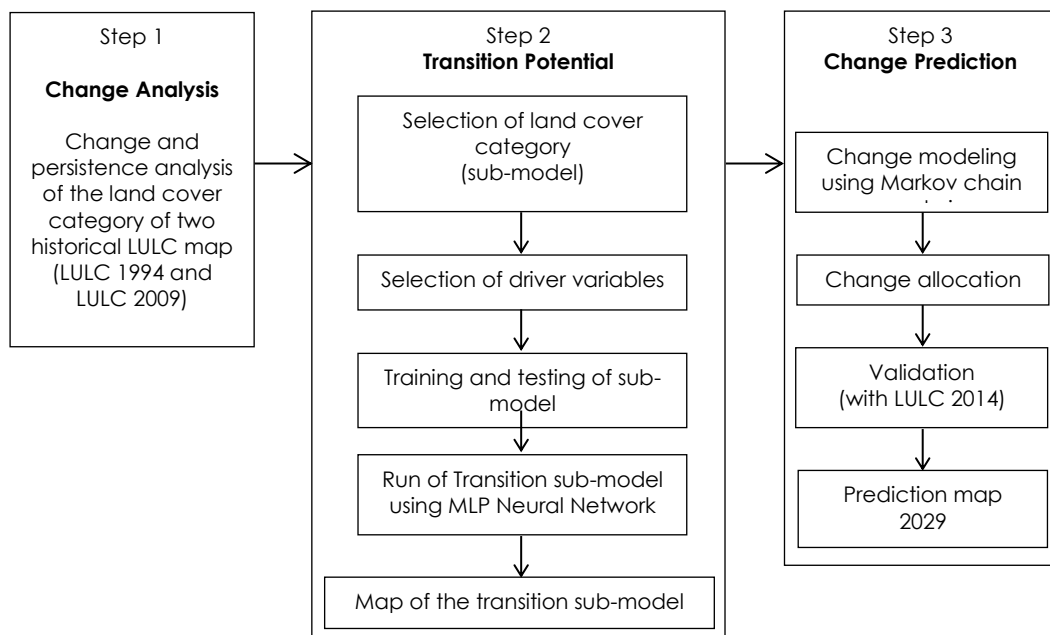
Figure 22. General description of Land Change Modeler (LCM)

58
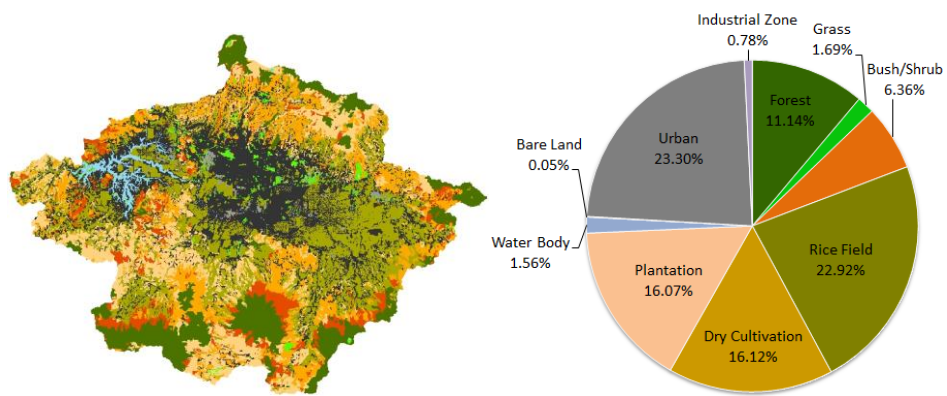
Figure 23. The future scenario of LULC generated by LCM

Beyond all the validated results of the LCM model, the representation of the real conditions in the transition of LULC categories cannot be expressed perfectly due to uncertainties. The complex relationship between driver variables and transition potential, or the representation of complex human behaviours in the transition trends may affect the quality of LCM results.

Table 7. Area and percentage of future scenario (LULC 2029)

LULC Type	Future Scenario (LULC 2029)	
	km^2	%
Land cover	258.1	11.1
Forest	39.4	1.7
Grass	146.8	6.3
Bush/Shrub	530.8	22.9
Rice Field	373.4	16.1
Dry Cultivation	372.2	16.1
Plantation	36.1	1.6
Waterbody	1.1	0.0
Bare Land	539.6	23.3
Urban	18.4	0.8

CHAPTER 3. IMPLEMENTATION RESULTS

Chapter Overview

The present chapter exemplifies the analysis of LULC change, the application of LCM and TETIS, and the preparation of climate change data. The spatial extent of historical LULC from 1994 to 2014 and future LULC changes in 2029 has been analyzed. LCM models used the change of two historical LULC to predict a future LULC. Meanwhile, TETIS model used two historical LULC in the calibration phase and the most recent LULC for the validation. Preparation of climate change data was done by involving statistical analysis (Mean and Coefficient of Variance) and comparison between historical periods of climate models with the control period. This preparation is implemented on five climate change models under two trajectories (RCP 4.5 and 8.5), four climatological elements (precipitation, maximum temperature, mean temperature and minimum temperature) and two seasons (rainy and dry). Afterward, bias correction was implemented on precipitation and temperature a selected climate model using linear scaling method. To check the robustness of bias correction, the discharges comparison resulted from TETIS implementation using climatological data prior and after bias correction was implemented.

3.1 Analysis of historical LULC changes

LULC maps for years 1994, 2009 and 2014 in the Upper Citarum Catchment are displayed in Figure 24. In 1994, the main LULC types were rice fields, forests and plantations (32.3, 23.7 and 19.0% of the catchment, respectively). Spatially, the increase of urban and the reduction of rice field areas can be clearly observed in the centre of the catchment. Meanwhile, deforestation can be detected in the southern part of the study area (Figure 24a).
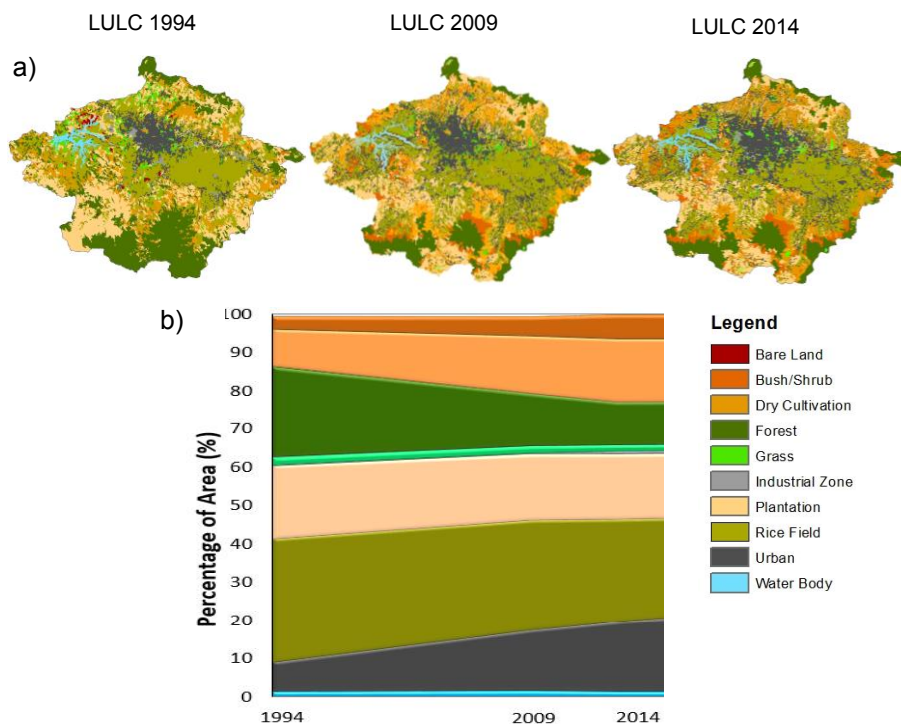
Figure 24. LULC analysis: a) LULC maps in three historical periods (1994, 2009 and 2014); b) percentage of LULC areas from 1994 to 2014

Forest and rice fields are the larger areas that have changed into another LULC during the period 1994-2009 (Figure 24b): there were 40.9% (225 km^2) and 10.9% (81 km^2) reduction of forests and rice fields, respectively. Deforestation in the southern part of the study area was presumably caused by land conversion from dry cultivation area for about 53.5% (121 km^2). This conversion is caused by its fertile soil condition and the lack of supervision by the government. Meanwhile, the increment of urban area for about 113% (197 km^2) was due to rice fields area

conversion in the centre of the study area. This change was caused by urban necessity due to a high increase in population. The increment of population in Bandung is noted 330.000 inhabitants from 1994 to 2009 (BPS, 2017). These trends of conversion were continued until 2014. From a more detailed LULC analysis of the LCM results from 1994 to 2014, it can be concluded that large forested areas have been removed; these areas now consist of predominantly bush/shrub, urban areas, dry cultivation, plantations and rice fields, with plantations holding the biggest portion (Figure 25a). The conversion of the forest into cultivation areas (dry cultivations, plantations and rice fields) was caused by the rise of food requirements due to the population growth as reflected in the increase of urban areas (Figure 25b).
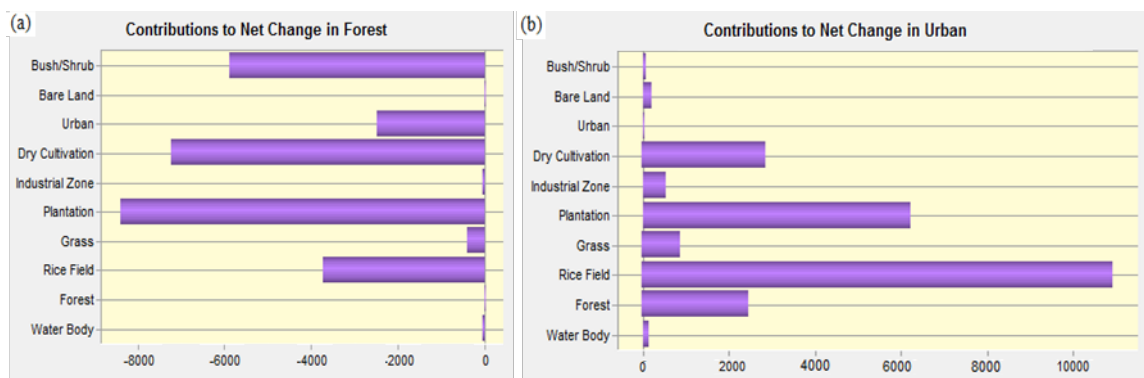
Figure 25. Contribution of different LULC to the net change between 1994 and 2014. a) forest; b) urban area

A similar situation also occurs in the Netravati watershed in India (Sinha and Eldho, 2018) and the Samin watershed in East Java, Indonesia (Marhaento *et al.*, 2018). The settlement area (urban) in the Upper Citarum Catchment increased from 7.4% to 18.1% between 1994 and 2014, mainly due to the conversion of cultivation areas (Table 8). This result aligns with those obtained by Tarigan and Tukayo (2013). They concluded the settlement area in Upper Citarum Catchment has increased by more than double during the period 2000 to 2009. Meanwhile, in 2029, the settlement area will be three times that of the settlement area in 1994. A similar trend was also predicted in the Netravati watershed (Sinha and Eldho, 2018).

Table 8. Area and percentage of three historical LULC

LULC Type	LULC 1994		LULC 2009		LULC 2014	
	km²	%	km²	%	km²	%
Forest	549.0	23.7	324.3	14.0	266.4	11.5
Grass	47.7	2.1	40.6	1.8	39.1	1.7
Bush/Shrub	75.5	3.3	115.8	5.0	147.3	6.4
Rice Field	747.4	32.3	666.0	28.8	624.3	27.0
Dry Cultivation	226.3	9.8	347.4	15.0	377.8	16.3
Plantation	440.7	19.0	395.0	17.1	386.6	16.7
Waterbody	36.1	1.6	36.5	1.6	36.1	1.6
Bare Land	13.5	0.6	1.2	0.1	1.2	0.1
Urban	173.9	7.5	370.6	16.0	419.0	18.1
Industrial Zone	5.8	0.3	7.4	0.3	18.1	0.8

3.2 LCM implementation

In the calibration process, a minimum accuracy rate of 65% was obtained from the training and testing process of all LULC category transitions. All driver variables resulted significantly. Validation was then performed by comparing the actual and predicted map of 2014 (Figure 26). The year 2014 was selected for validation, because in this study, it is more important to test the "predictive" ability of the model (going from 2009 to 2014), than its "descriptive" ability (interpolating 2009 using previous and posterior information), as (Cunnane, 1987) referred to in a similar context. The validation showed that 68.4% (184,671 pixels) were hits, 19.8% (53,542 pixels) were false alarms and 11.7% (184,671 pixels) were missed. After completing the validation process, the future prediction of 2029 was generated. The prediction for the year 2029 was based on the transitional potential between LULC 1994 to 2009 which is reflected in the implemented model.

Actual LULC 2014

Predicted LULC 2014

Validation map

Legend of validation map

- **Hit (**68.4%)
- **False (**19.8%)
- **Miss (**11.7%)
- **No potential change**
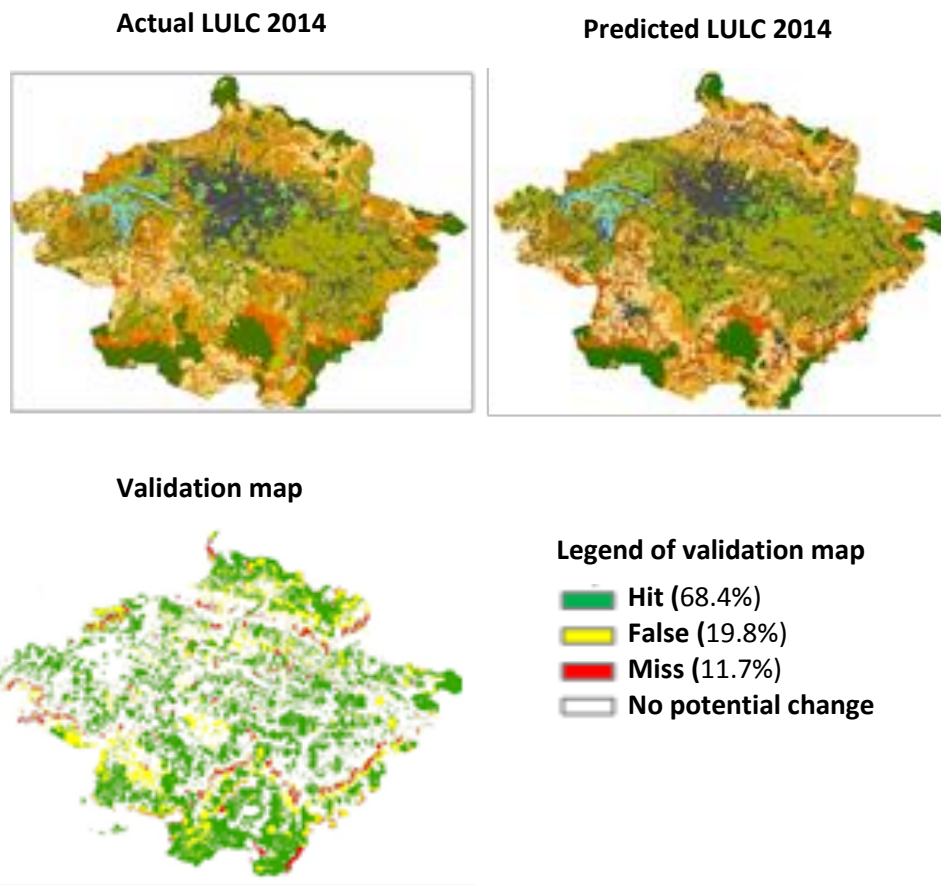
Figure 26. Comparison of actual and predicted map in the validation process

3.3 TETIS implementation

3.3.1 Water sub-model

The most influential parameters for this sub-model and case study were maximum static storage, evapotranspiration, infiltration, percolation and channel flow velocity. Therefore, the corresponding CFs were particularly considered in the calibration process. The simulated and observed discharges during the calibration and validation are presented in Figure 27a and b, respectively. In general, the observed discharge has been successfully simulated by the model, except for high flows at the beginning of the calibration period and in certain flood events. For example, the calibration result is overestimated in February 2007 and underestimated in April 2007. The reason can be attributed to the low water content in the soil in February 2007. As low rainfall existed in

January 2017, the soil was not saturated, hence soil absorbed water rapidly in February 2017 when the heavy rain started to occur. Meanwhile, the soil is already saturated by the water in April 2007 due to previous heavy rainfall. Hence, the rainfall was converted into discharge rapidly. Another reason could be due to the quality of the precipitation data, especially regarding the spatial distribution of rain gauges. Hence, some data lose their accuracy.
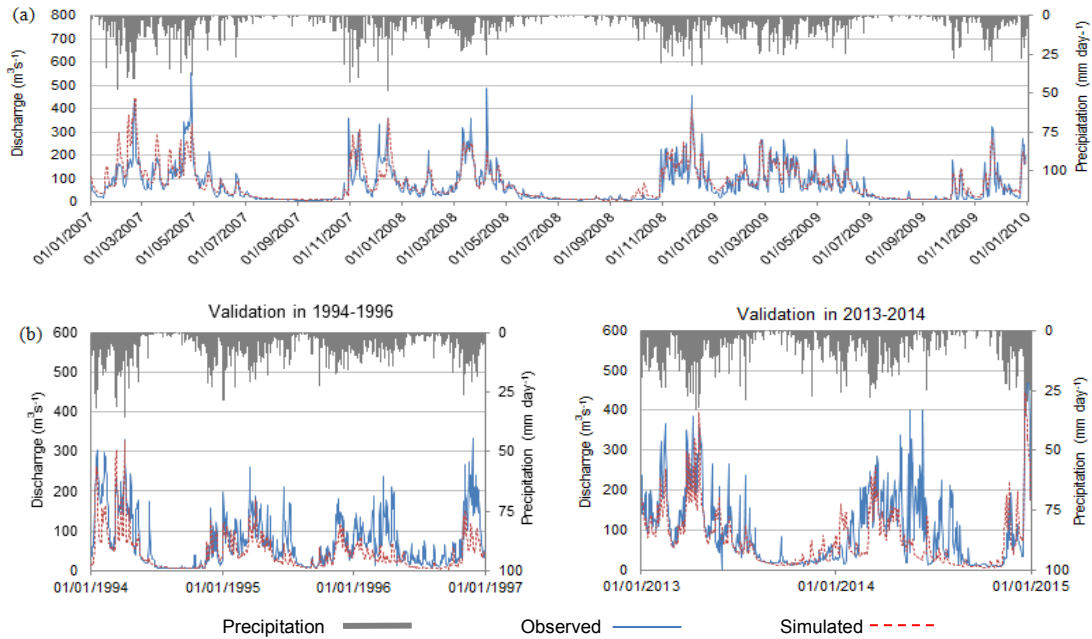
Figure 27. Implementation of the TETIS hydrological sub-model in Nanjung flow gauge station: a) calibration in the period 2007-2009; b) validation in two different periods.

The results of water sub-model calibration and validation are presented in Table 9. The model performance in the calibration can be classified as "good". Meanwhile, both validations can be classified as "satisfactory". Based on the performance index category and the difficulties of the type of validation (Differential Split-Sample), the TETIS model can be used with confidence to describe the hydrology of the Upper Citarum Catchment. The result of the calibration showed a final NSE 0.71 with volume error -9.13%. The prediction result is considered to be good based on the general performance category suggested by Moriasi *et al.* (2007).

Table 9. Model performance category based on Moriasi *et al*. (2007).

Indicator	Calibration		Validation 1994-1996		Validation 2013-2014	
	Value	Category	Value	Category	Value	Category
NSE	0.7	good	0.54	satisfactory	0.52	satisfactory
RSR	0.54	good	0.58	good	0.59	good
VE	-9.2%	-	-30%	-	-34%	-

3.3.2 Sediment sub-model

The deposited sediment of the Saguling reservoir during 2009 was recorded 4.14 Mton yr^{-1}. After it was corrected by trap efficiency and compaction, the deposited sediment increased to 4.43 Mton yr^{-1}. This amount was further compared with the sediment volume from the TETIS simulation result in the calibration phase. In the validation phase, the deposited volumes of the reservoir in 2008-2012 and TETIS simulation were compared. The result of observed sediment volume from the reservoir and TETIS simulation was recorded 21.49 Mton and 22.04 Mton, respectively. Hence, based on a comparison between both volumes, the error volume was noted only 2.5% (Figure 28). This number is considered to be an excellent outcome. The most sensitive CFs in this case study was the hill slope transport capacity. Hence, this CF plays an important role in the calibration process.
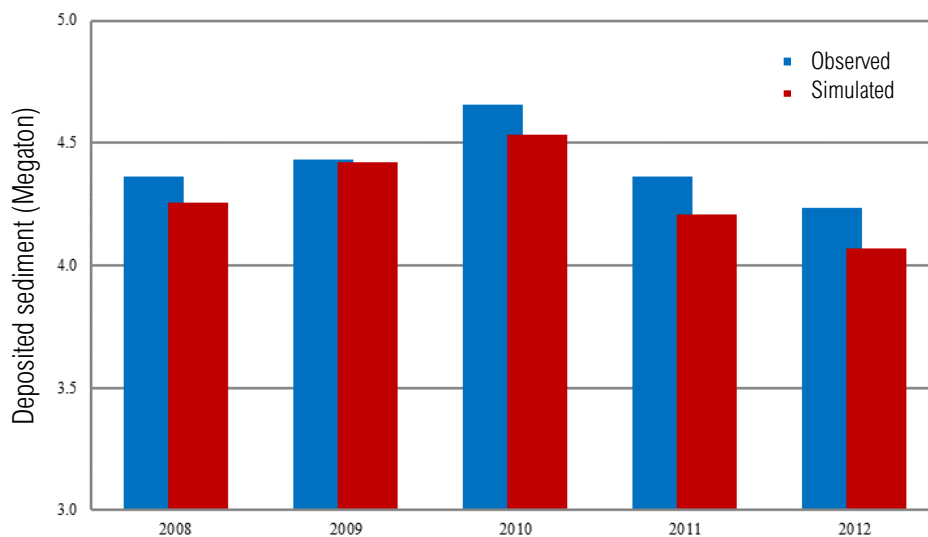
Figure 28. Comparison of observed and simulated of deposited sediment in the calibration and validation process

3.4 Preparation of climate change data

Statistical analysis of precipitation and temperature for all models is presented in Table 10. From the statistical analysis, the average precipitation of all trajectories ranged from 4.67 to 17.31 mm day^{-1}. The range of coefficient of variance (CV) of precipitation is noted 130% to 182.13%. Those values are considered as high considering that precipitation possesses a large distribution due to spatially natural variation. The smallest CV is noted under the HadGEM-3RA model by 116.82 mm day^{-1}. It refers to small (homogeneous) data distribution of the HadGEM-3RA model compared to data in other trajectories. Therefore, the HadGEM-3RA is considered as a suitable model for further precipitation analysis.

Mean of maximum temperature, average temperature and maximum temperature for all models ranged from 21.64 $^{\circ}$C to 26.37 $^{\circ}$C, 20.77 $^{\circ}$C to 23.22 $^{\circ}$C and 18.92 $^{\circ}$C to 21.74 $^{\circ}$C, respectively. Meanwhile, CV of maximum temperature, average temperature and maximum temperature for all models ranged from 3.95% to 36.82%, 3.22% to 36.67% and 3.94% to 65.60%, respectively. The CV of maximum temperature, average temperature and maximum temperature are divided into two groups. The first group is consisted of a model with high CV value, while the other group consists of a significantly lower CV value. The higher CV value of maximum temperature consists of YSU-RSM and RegCM4 with 34.07% and 36.82%, respectively. Meanwhile, the lower CV value was found under SNU MM5, SNU-WRF and HadGEM-3RA model with values 6.01, 3.95 and 5.26, respectively. The higher CV value of mean temperature consists of YSU-RSM and RegCM4 with 34.32% and 36.67%, respectively. Meanwhile, the smaller CV value was found under SNU MM5, SNU-WRF and HadGEM-3RA model with values 3.22, 3.95 and 4.09, respectively. The higher CV value of minimum temperature consists of SNU MM5, YSU-RSM and RegCM4 with 65.60%, 34.69% and 36.57%, respectively. Meanwhile, the smaller CV value was found under SNU-WRF and HadGEM-3RA model with values 3.94 and 6.36, respectively. A smaller CV value refers to a small data distribution (homogeneous) to the mean value. Therefore, the use of a model belongs to a group with a smaller CV is the best choice for further analysis.

Table 10. Statistical analysis of precipitation and temperature for all trajectories

Statistical Analysis	SNU MM5	SNU-WRF	YSU-RSM	RegCM4	HadGEM-3RA
Precipitation					
Mean	10.21	17.31	11.70	6.42	4.67
CV	182.13	176.60	130.09	143.70	116.82
Maximum Temperature					
Mean	26.37	21.98	23.59	21.64	26.11
CV	6.01	3.95	34.07	36.82	5.26
Mean Temperature					
Mean	23.22	21.98	22.64	20.77	22.14
CV	3.22	3.95	34.32	36.67	4.09
Minimum Temperature					
Mean	20.26	20.68	21.74	19.90	18.92
CV	65.60	3.94	34.69	36.57	6.36

3.4.1 Comparison between historical periods of climate models with the control period

3.4.1.1 Precipitation

Future climate change model usually contains systematic deviation that necessarily be corrected through statistical correction (Hempel *et al.*, 2013). The correction of bias will increase the accuracy of the climate change model. Due to this fact, a correction of the bias is constructed on a daily basis by comparing observed daily precipitation with five models of precipitation from CORDEX East Asia in the form of quantile (*q-q*) plots (Figure 29). Eventhough, bias correction is generally implemented on monthly means (Déqué, 2007), the correction on a daily basis was chosen in this study, because the daily scale temporal data is available for the study area. this bias correction is extremely important to identify a more accurate model to be used in the study.

Almost all of the RCMs are not able to capture the precipitation in the control period. SNU MM 5, SNU-WRF and HadGEM-3RA model commonly underestimates the observed historical precipitation (Figure 29-upper).

Meanwhile, historical precipitation of RegCM4 and YSU-RSM models commonly overestimate the observed historical precipitation. Based on the q-q plot analysis, the data distribution of HadGEM-3RA model is the closest to the 1: 1 line. Beyond that, YSU-RSM model a series of data that is also close to the 1: 1 line, but unfortunately it contains a deviation for the higher observed precipitation. Moreover, the monthly precipitation of YSU-RSM shows a bigger gap compared to the gap of HadGEM-3RA (Figure 29-upper).

HadGEM-3RA has the lowest gap with observed data compared to other climate models. The only big gap occurs in January and December with 142 mm month^{-1} and 74 mm month^{-1}, respectively. On the contrary to other models such as SNU MM5, a bigger gap was found from January to May and from September to December. For example, the gap was noted 233 mm month^{-1} in July and 206 mm month^{-1} in December. Another example is SNU-WRF with 228 mm month^{-1} and 144 mm month^{-1} for January and December, respectively.

The gap between the HadGEM-3RA model and observed historical precipitation is distributed evenly compared with another precipitation model. This assumption is shown by the same magnitude of precipitation gap in each month. The bigger difference exists only at the beginning and the end of the period (January and December). This condition differs from other precipitation models which contain a bigger gap. For example, the gap between SNU MM5 and observed historical precipitation. From that comparison, a lower gap was found in January, February, September, October, November and December. Meanwhile, the rest of the months deviate with a bigger magnitude.

In this case, the precipitation of the HadGEM-3RA model is the most accurate model compared with another model in terms of representing the historical precipitation amount in the study area. Therefore, HadGEM-3RA is assumed as the best model to predict future precipitation in the study area.
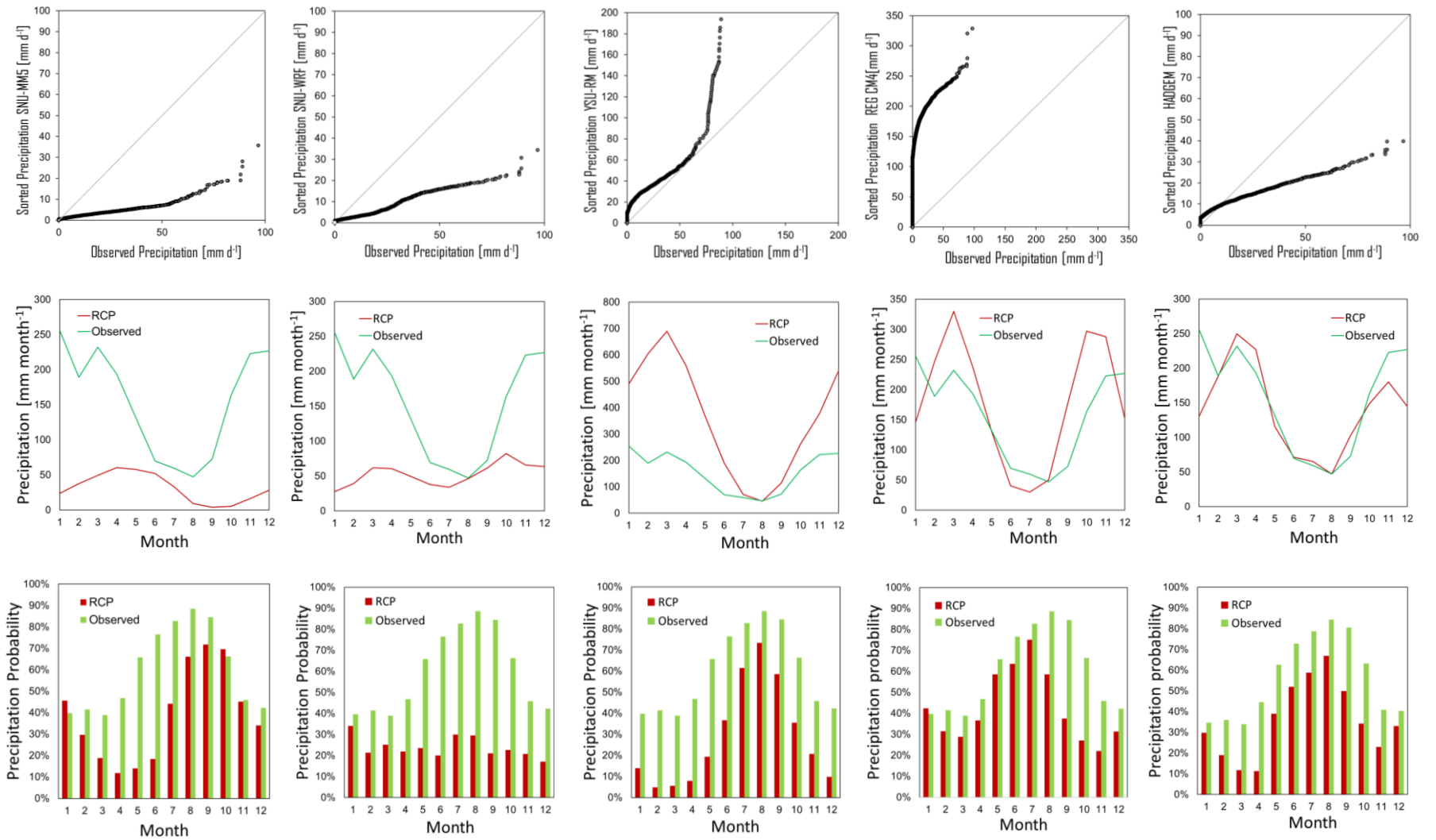
Figure 29. Comparison of historical precipitation under five climate change models

3.4.1.2 Maximum temperature

In the comparison of maximum temperature, the HadGEM-3RA model shows to be the most accurate model than the other. This fact is pointed out by the comparison of the model and observed historical maximum temperature presented in the q-q plot in Figure 30. The distribution of historical maximum temperature from the HadGEM-3RA model is closer to the 1: 1 line. A smaller gap was found in the monthly temperature data comparison between the HadGEM-3RA model and the observation compared with other models. In that comparison, the averaged gap is detected by approximately 2ºC. Meanwhile, the comparison from other models shows a bigger gap. For example, the higher averaged gap was found on SNU MM5, SNU-WRF, YSU-RSM and RegCM4 model by approximately 25ºC, 26ºC, 4ºC and 7ºC, respectively. These facts lead to the conclusion that HadGEM-3RA is the best model to describe maximum temperature in the future and deserves to be used for further analysis.
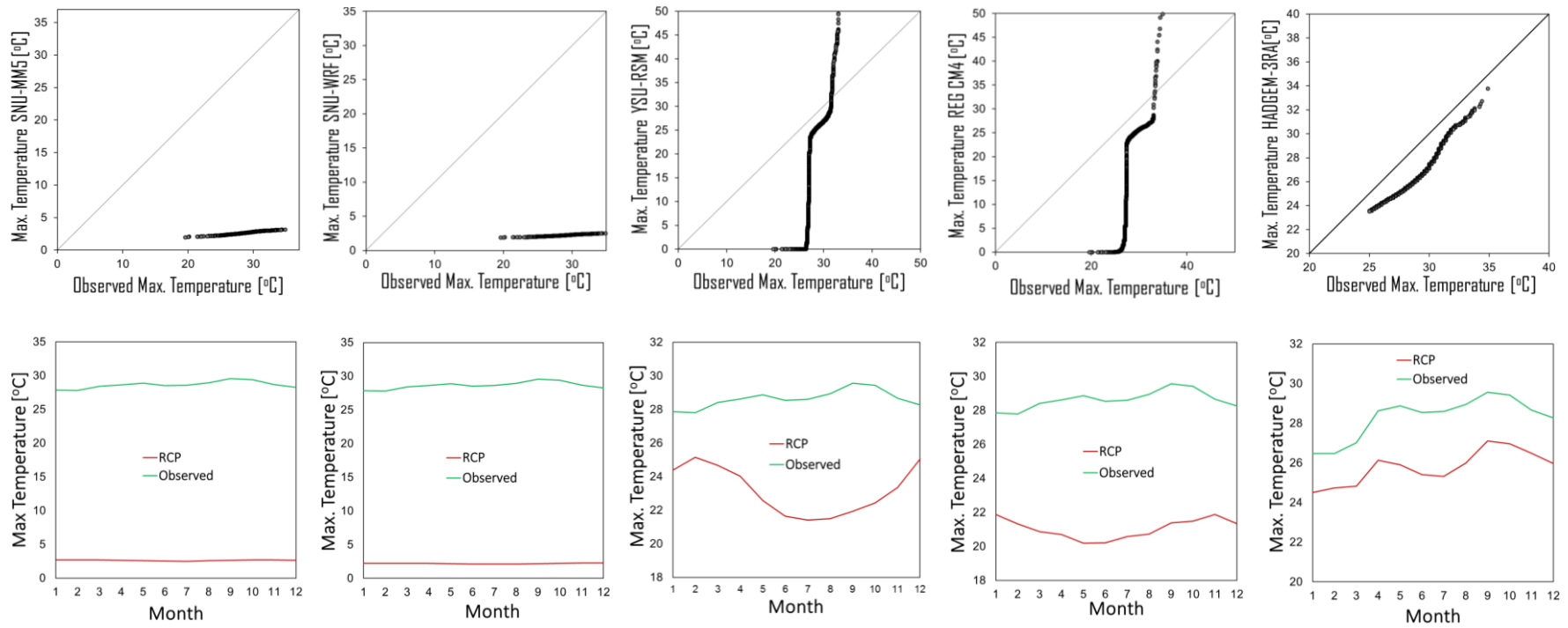
Figure 30. Comparison of the historical maximum temperature under five climate change models.

3.4.1.3 Mean temperature

Regarding the comparison of the historical mean temperature, the q-q plot shows that the SNU MM5 and SNU-WRF overestimate the observation data. Meanwhile, the YSU-RSM model overestimates the observation mean temperature lower than 25°C and underestimates the temperature higher than 25°C. RegCM4 model overestimates the observation data for the temperature lower than 13°C and underestimates the temperature higher than 13°C. Meanwhile, HadGEM-3RA are totally underestimate the observation data. The average temperature of SNU MM5 and SNU-WRF shows a high gap compared with the observation data by approximately 21 °C (Figure 31). Meanwhile, a slightly better mean temperature was found in the YSU-RSM model with 1 °C from January to April and 1-4 °C from June to November. Meanwhile, the gap of the mean temperature between RegCM4 and observations is ranged from 2-4 °C for the entire months. Compared with observation data, the HadGEM-3RA model has the lowest gap among all models, with a gap of approximately 1-1.5 °C for the entire month, based on q-q plot data and monthly mean temperature difference, HadGEM-3RA is concluded as the best model to predict the mean temperature in the future.
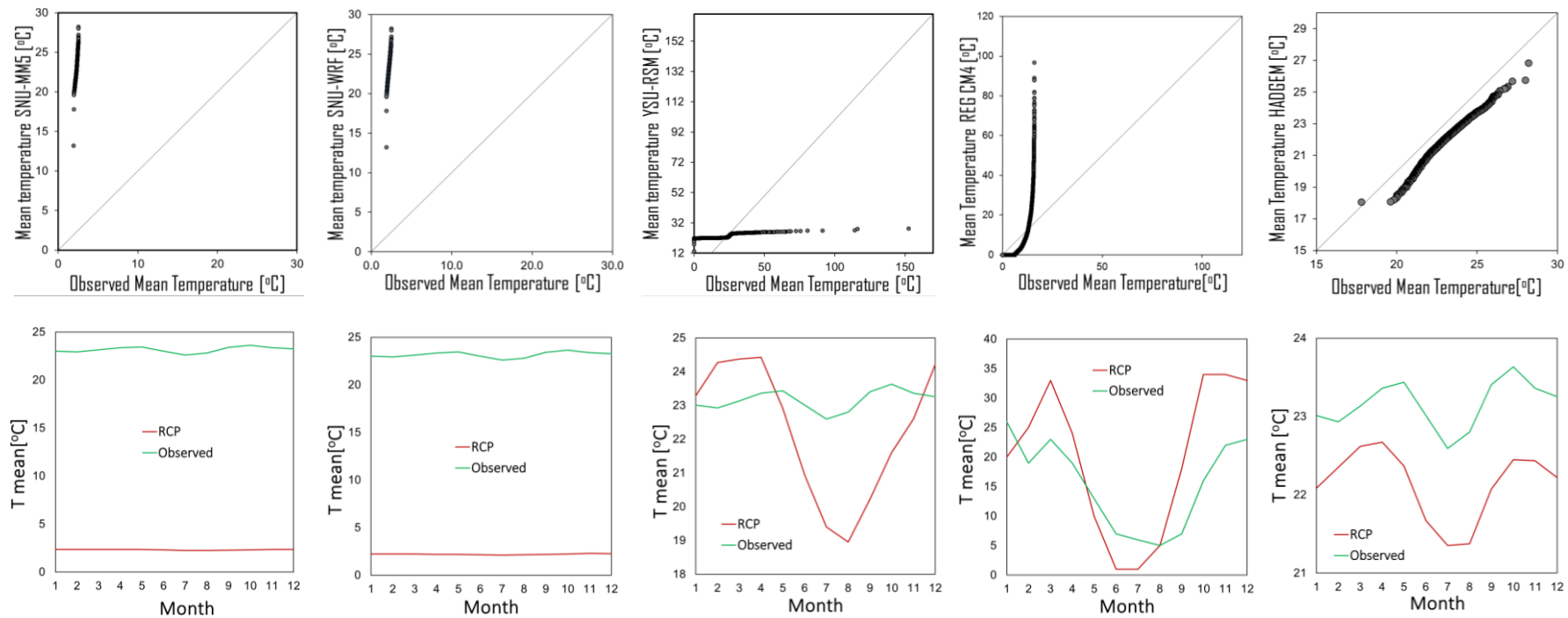
Figure 31. Comparison of the historical mean temperature under five climate change models

3.4.1.4 Minimum temperature

In the q-q plot between the historical minimum temperature of the model and observed historical minimum temperature (Figure 32), SNU MM5 and SNU-WRF overestimate the observation of minimum temperature. Meanwhile, YSU-RSM and RegCM4 are the worst projection when it is compared with observation data. The data distribution is concentrated only in the range of temperature 10-24°C and 10-25°C of observation data for YSU-RSM and RegCM4, respectively. Beyond that, HadGEM-3RA fit perfectly the observation data with the only underestimation of the temperature in the range 16-18°C. All models have a low gap for the entire month which is below 2°C, except for the YSU-RSM model with the gap by 4.5°C. The lowest difference is possessed by HadGEM-3RA with 0.75 °C. Hence, HadGEM-3RA is assumed as the best model to describe the minimum temperature in the future.
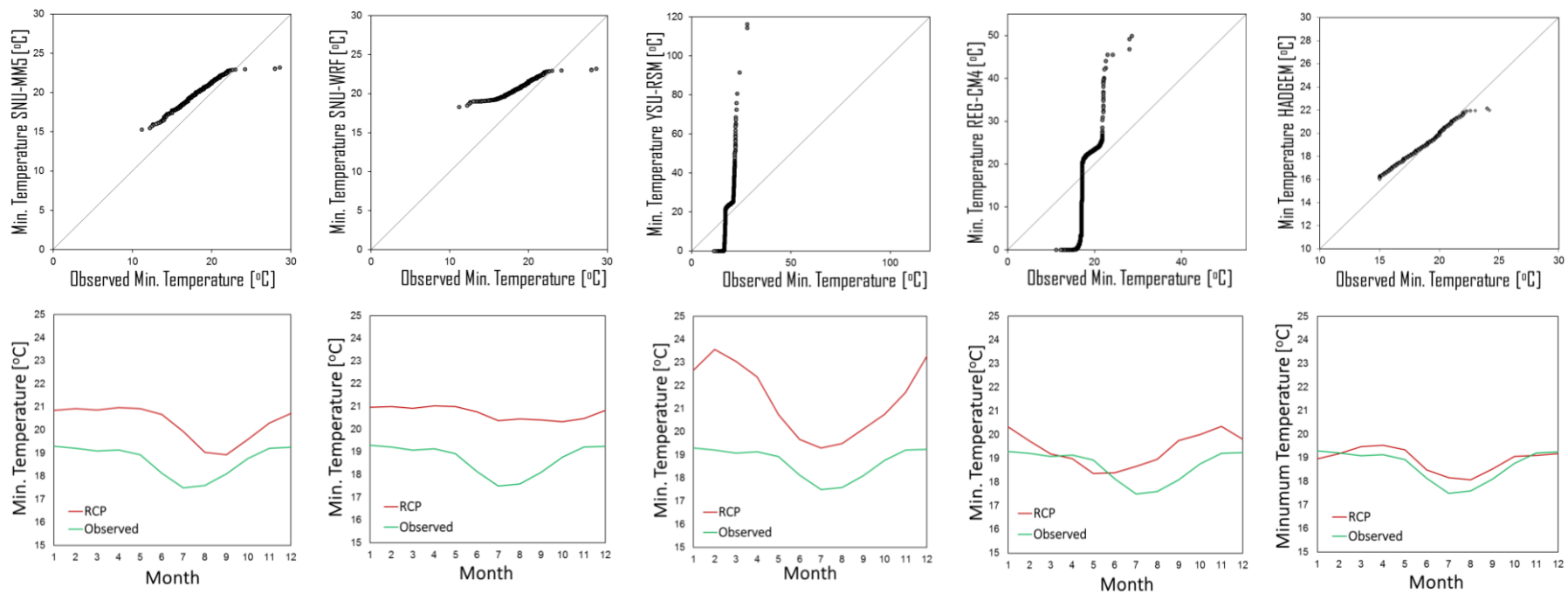
Figure 32. Comparison of the historical minimum temperature under five climate change models

3.4.2 Bias correction of climate model

3.4.2.1 Precipitation

3.4.2.1.1 Analysis of rainy and dry season

The q-q plot of precipitation in the dry and rainy season related to its observation data is presented in Figure 33 (a)-left and (b)-left, respectively. Prior to the correction, a large deviation from 1:1 line was found for the observed precipitation higher than 15 mm d^{-1} and 20 mm d^{-1} (inset) for the dry and rainy season, respectively. Meanwhile, the rest of the distribution slightly deviates from the 1:1 line. After precipitation data were corrected, the small unfitting distribution (underestimation) on 1:1 line exists in the observed precipitation higher than 39°C and 32°C for the dry and rainy season, respectively. moreover, very small unfitting (overestimation) distribution exists in the observed precipitation lower than 20°C and 22°C, respectively.

The equation which was used to correct precipitation bias in the dry season is as follows:

$$P_{corr}=2.88P\text{-}12.56 \tag{13}$$

The equation which was used to correct precipitation bias in the rainy season is as follows:

$$P_{corr}=2.1P\text{-}6.18 \tag{14}$$

The fitting probability between uncorrected precipitation of the model, corrected precipitation of the model and observed precipitation for the dry and rainy season are presented in Figure 33-right. The uncorrected distribution of precipitation was not fit with the distribution of observation data and deviate largely. This finding can be identified from Figure 33 a)-right, except in the middle of the distribution (around 7.6 and 7 mm day^{-1} of precipitation for the dry and rainy season). After the correction of the bias, the distribution of precipitation data from the model has significantly improved. Eventough, the distribution is not fit perfectly and still contains a deviation on 1:1 line. But, at least the corrected distribution of precipitation is now much closer to 1:1 line compared to the uncorrected distribution.
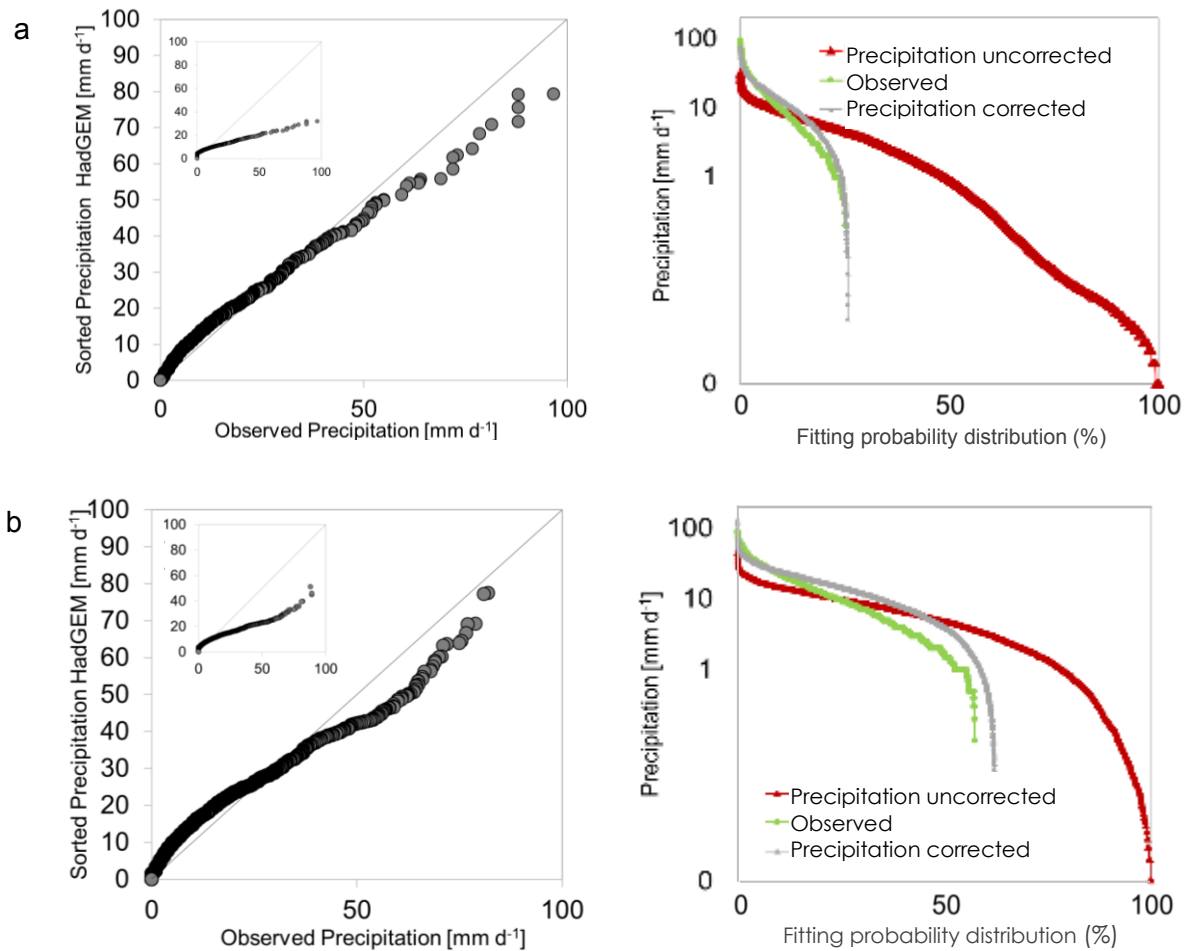
Figure 33. Bias correction of precipitation. (a) in the dry season and (b) in the rainy season. Left: q-q plot before and after correction. Right: Fitting probability distribution comparison between the uncorrected, corrected and observed precipitation.

3.4.2.1.2 Analysis in the whole period (rainy and dry season)

Dry and rainy season were considered in the process of correction. In other words, the correction is a combination of two corrections in a different season. The bias can be identified from the comparison between precipitation distribution of the model and the observation data of the whole period as indicated clearly in Figure 34. Figure 34-left (inset) shows the q-q plot of the uncorrected precipitation of the model. Meanwhile, Figure 34-left shows the q-q plot of corrected precipitation. The results of bias corrections show a better distribution of data, which is proofed by the absence of a large gap. The fitting probability between uncorrected precipitation of the model, corrected

precipitation of the model and observed precipitation are presented in Figure 34-right. The distribution of precipitation data prior to bias correction was not fit the distribution of observation data. It is noticed clearly that more than 50% of the distribution data from models (precipitation amounts lower than 7.6°C) were not fit with the observation data. After the correction of the bias, the distribution of precipitation of the model has significantly improved. It is shown by a better fitting distribution line with the observation. Large deviations between distribution data from models (corrected) and observation data were no longer exist.
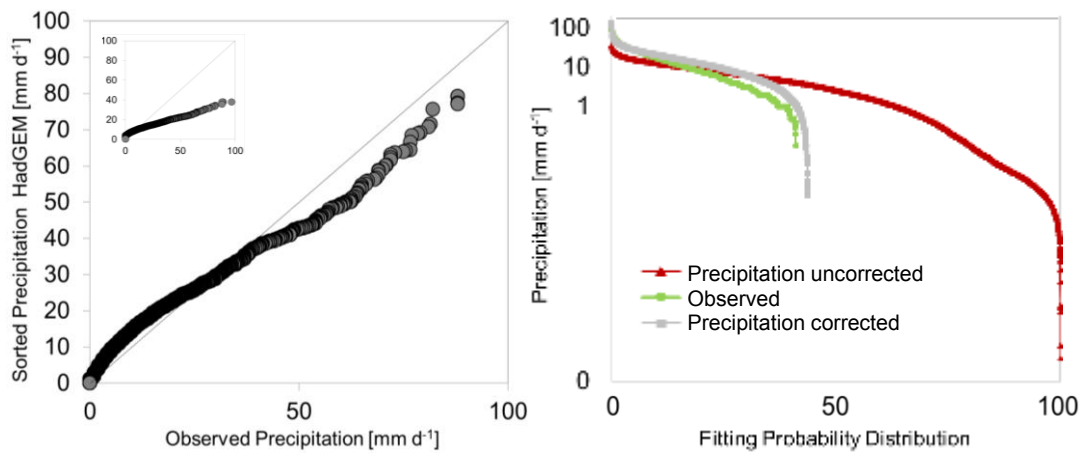
Figure 34. Bias correction of precipitation. Left: q-q plot of the prior and after correction. Right: Fitting probability distribution comparison between the uncorrected, corrected and observed precipitation.

3.4.2.2 Maximum Temperature

The deviation of the temperature maximum of the model on the observation can be identified from the inset of the q-q plot Figure 35-left. The distribution data of maximum temperature from the model are totally underestimate the distribution of observation data as clearly shown in the inset. Dry and rainy season were considered in the process of correction. In other words, the correction is a combination of two corrections in a different season. The equation which was used to correct maximum temperature bias in the dry season is as follow:

$$T_{max\,corr} = 0.99 T_{max} - 3.11 \qquad\qquad [15]$$

Meanwhile, the equation which was used to correct maximum temperature bias in the rainy season is as follows:

$$T_{max\ corr}=1.08 T_{max}$$ [16]

The distribution data of maximum temperature resulted from bias correction show the improvement (Figure 35-left). Prior to the correction, the distribution of maximum temperature of the model underestimates the observation data. After the correction of bias, there were no more severe underestimation conditions. Eventhough, the distribution of the model commonly overestimates the observation data, the distribution is now much better because they are closer to the 1:1 line. The distributions that experienced overestimation exist in the range $29.8^{o}C$ and $36.4^{o}C$.
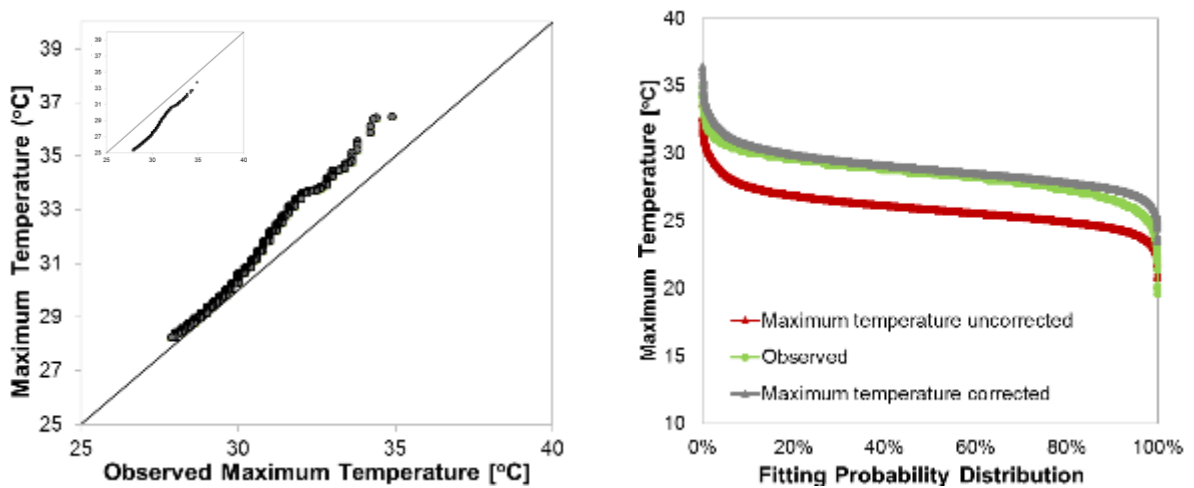
Figure 35. Bias correction of maximum temperature. Left: q-q plot of the prior and after correction. Right: Fitting probability distribution comparison between uncorrected, corrected and observed maximum temperature.

The fitting probability between the uncorrected maximum temperature of the model, the corrected maximum temperature of the model and observed maximum temperature are presented in Figure 35-right. The distribution of maximum temperature of the model prior to bias correction completely underestimate the distribution of observation data. It can be noticed from a lower line of uncorrected maximum temperature (red line). In this case, almost all uncorrected distribution of maximum temperature of the model

81

underestimates the distribution of observation data, only a few data fit with the distribution of observation data such as the higher and the lower distribution. After the correction of the bias, the distribution data of maximum temperature has significantly improved. It is shown by a better fitting distribution line between corrected maximum temperature and observation data. Large deviations between distribution data from models (corrected) and observation data were not found anymore.

3.4.2.3 Mean temperature

The q-q plot of mean temperature related to its observation data is presented in Figure 36-left. Prior to the correction, the data distribution of mean temperature underestimates the distribution of observation data. After mean temperature data were corrected, the underestimation state is no longer exist. Finally, the data distributions fit with 1: 1 line, only a minor part of distribution data deviates from 1: 1 line. The equation which was used to correct mean temperature bias in the dry season is as follow:

$$T_{mean}=0.983T_{mean}-1.682 \qquad\qquad [17]$$

Meanwhile, the equation which was used to correct mean temperature bias in the rainy season is as follows:

$$T_{mean}=1.23T_{mean}-4.38 \qquad\qquad [18]$$

The fitting probability between the uncorrected mean temperature of the model, corrected mean temperature of the model and observed mean temperature are presented in Figure 36-right. The distribution of maximum temperature of the model prior to bias correction completely underestimate the distribution of observation data. It can be noticed from the lower line of uncorrected maximum temperature (red line). Uncorrected maximum temperatures of the model are commonly underestimated, only a few data of the lowest distribution of the uncorrected distribution fit with the distribution of observation data. After the correction of the bias, the distribution of precipitation

data from the model has significantly improved. It is shown by a perfectly fitting distribution between the corrected mean temperature and the observation data. This perfectly fitting probability distribution can be identified from the grey and green lines colour.
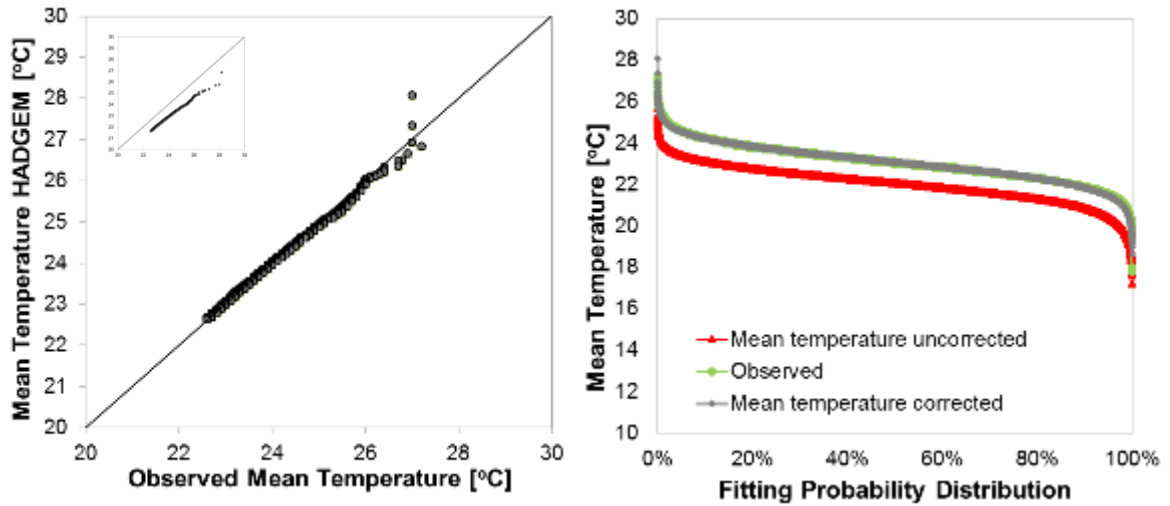
Figure 36. Bias correction of mean temperature. Left: q-q plot of the prior and after correction. Right: Fitting probability distribution comparison between uncorrected, corrected and observed mean temperature.

3.4.2.4 Minimum temperature

The q-q plot of minimum temperature related to its observation data is presented in Figure 37-left. Prior to the correction, only a few data of minimum temperature distribution did not fit 1:1 line, exactly for the minimum temperature lower than 19°C and higher than 21°C. Meanwhile, the rest of the distribution mostly fits with 1:1 line. After the correction of bias, the distribution of minimum temperature did not fit the 1:1 line only in the minimum temperature higher than 22°C.

The equation which was used to correct minimum temperature bias in the dry season is as follow:

$$T_{min}=1.27T_{min}-5.42 \qquad\qquad [19]$$

Meanwhile, the equation which was used to correct minimum temperature bias in the rainy season is as follows:

$$T_{min} = 1.11 T_m 2.193 \qquad\qquad [20]$$
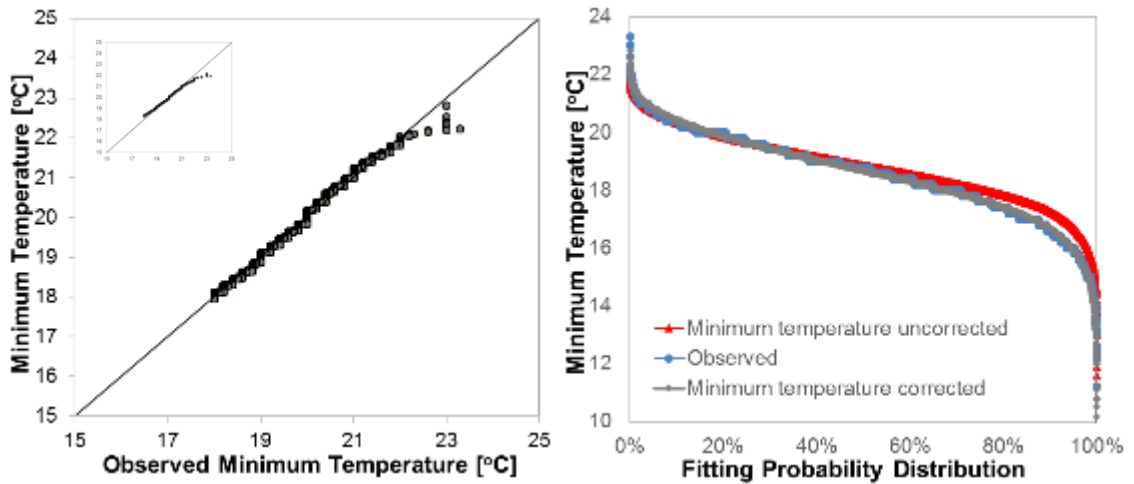
Figure 37. Bias correction of minimum temperature. Left: q-q plot of the prior and after correction. Right: Fitting probability distribution comparison between uncorrected, corrected and observed minimum temperature.

The fitting probability between the uncorrected minimum temperature of the model, corrected minimum temperature of the model and observed minimum temperature presented in Figure -37-right. The distribution of maximum temperature data prior to bias correction overestimates the distribution of observation data on some spots, but only a small gap. It can be noticed by the upper line of uncorrected maximum temperature (red line) in the range 15°C-19°C. After the correction of the bias, the distribution of precipitation data from the model has significantly improved. This is shown by a perfect fitting distribution line with the observation data, as it is represented by the grey and green lines. The overestimation of uncorrected distribution in the range 15°C -19°C is no longer exist.

3.4.2.5 Analysis of discharge

The comparison between discharges from simulation and observation, prior and after bias correction to its observation discharge can be used as a hint to determine whether the correction is correctly implemented or not. The comparison between observed discharge and discharge using climatological data from RCP 8.5 is presented in Figure 38. Figure 38-upper shows the comparison of discharges before correction with observed data from 1976 to 2005. Meanwhile, the lower one shows the comparison between discharges after correction and observed data from 1976 to 2005. From those figures, we can observe that the simulation of uncorrected discharge underestimates the discharge of observation, especially in the discharge peak. After the bias were corrected, the magnitude of discharge from the simulation increases significantly. Hence, it lowers the gap between discharge resulted from corrected and observed input.

The comparison of discharge resulted from TETIS using input data with and without bias correction is presented in Figure 39. We identify that the discharge resulted from simulation using uncorrected input underestimate the simulated discharge using corrected input. The reason for this occurrence is due to the increment of rainfall amount as explained in the previous chapter. Moreover, the increasing climatological aspect such as precipitation, maximum temperature, mean temperature and minimum temperature in the correction process, change the water balance which finally changes the discharge. In addition, temperature as part of the input of the simulation is also changed. Thus, these changes ultimately change the amount of discharge of simulation.
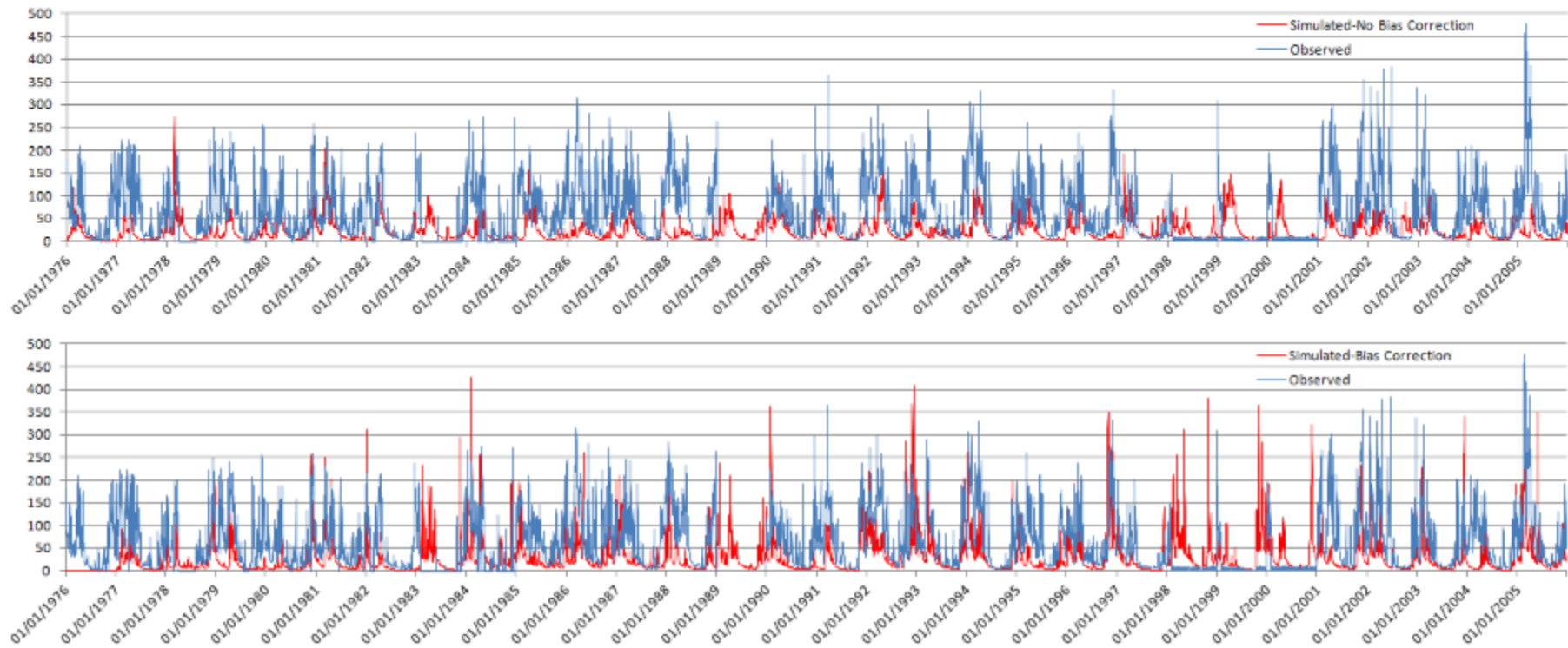
Figure 38. The comparison between observed and simulated discharge using climatological data from RCP 8.5.
upper: observed discharge vs simulation prior to bias correction. lower: observed discharge vs simulation after bias correction
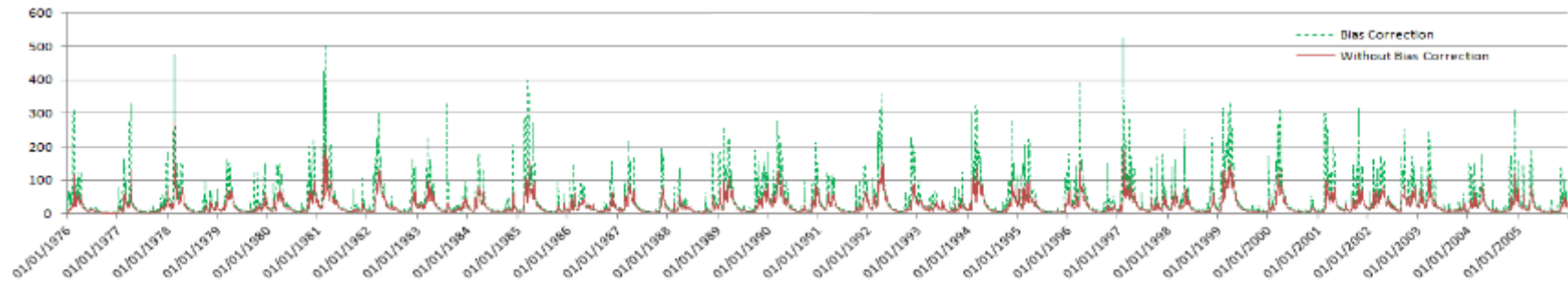
Figure 39. The comparison between discharges simulated with and without bias correction (RCP 8.5) of climatological input

Figure 40 shows the transformation of the q-q plot based on the simulated discharge of different input through bias correction. Figure 40a shows the q-q plot between observed discharge and the simulated discharge from the model without bias correction. It clearly shows that observed discharge overestimates the discharge of the simulation with input without bias correction. After the correction of bias, the distribution of discharge is much closer to the 1:1 line (Figure 40b), although it is not perfectly fit the 1:1 line. Generally, the distribution of discharge after bias correction is much better than the distribution without correction. Meanwhile, Figure 40c illustrates the discharges comparison between the observed discharge and simulated discharge using actual input. The figure shows that the simulated discharge using actual input underestimates the simulated discharge using corrected precipitation and temperature. Figure 38d shows that the discharge simulated by TETIS using historical climatic data (HadGEM) without correction underestimates the discharge simulated by TETIS using the observed climatic data. The distribution of data has significantly improved after the bias correction. The distribution of data is much closer to 1: 1 line, eventhough it did not perfectly fit the 1: 1 line as presented in Figure 40e. Bias correction results in the decline of the gap between both discharges distribution as identified in the figure. The improvement of the data distribution shows that the correction has been implemented properly.
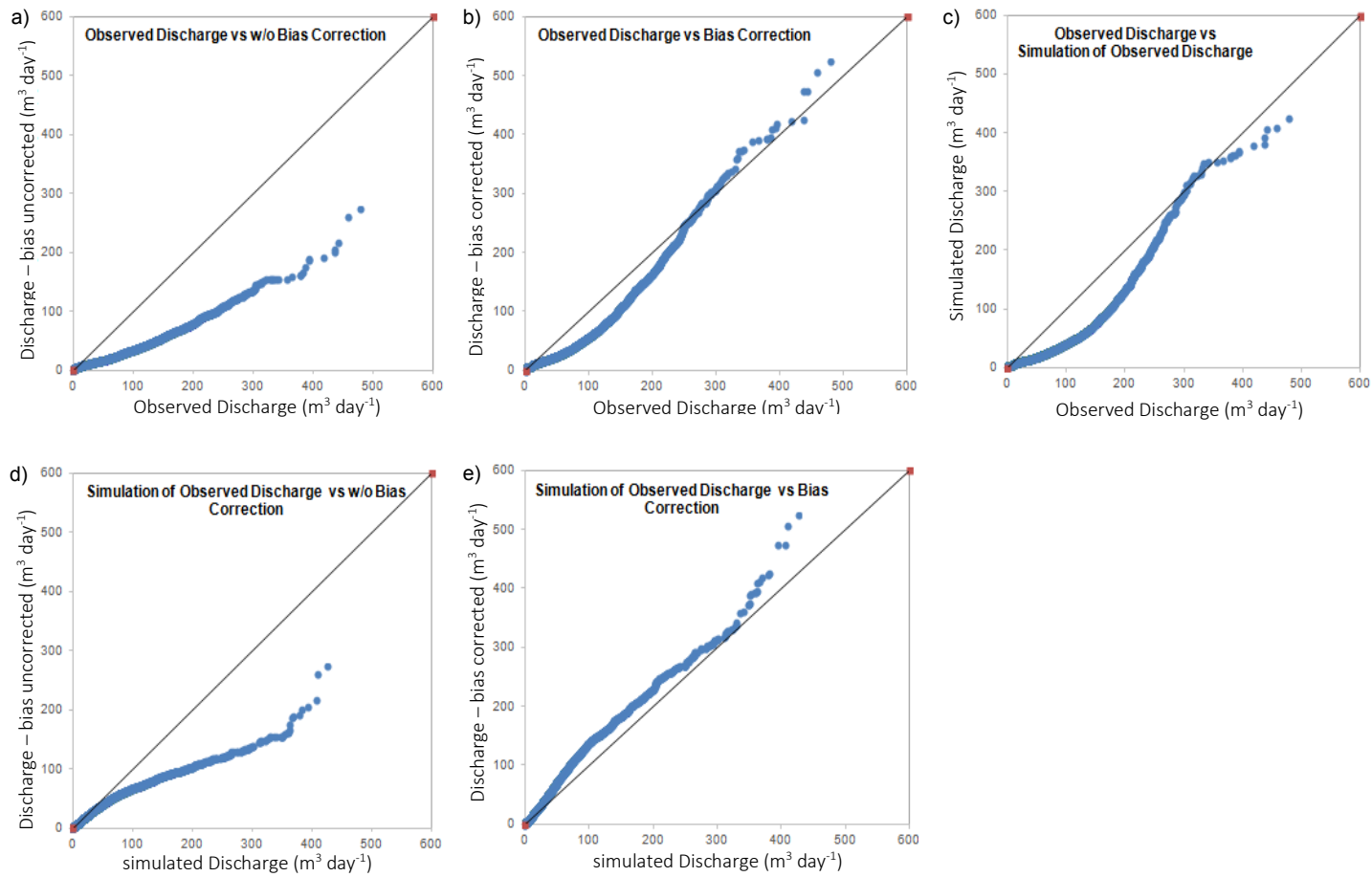
Figure 40. Comparison of discharge simulated with different climatological input. a) between observed and uncorrected input of control period; b) between observed and corrected input of control period; c) between observed and simulated using actual input; d) between simulated discharge and uncorrected input of control period; e) between simulated discharge and corrected input of control period

CHAPTER 4. IMPACT OF LAND COVER CHANGE IN HYDROLOGICAL AND SEDIMENT REGIME WITH METEOROLOGICAL OBSERVATION

Chapter Overview

This chapter explains the impact of LULC changes (from 1994 to 2014) on water balance, flood, erosion, sedimentation including the lifetime of Saguling reservoir. Deforestation, vegetation loss and increased settlement clearly affect the flows of water balance. LULC scenarios (conservation, government plan, natural vegetation, future LULC 2029) result the same impact as historical LULC. But, LULC scenarios give the opposite impact due to the addition of vegetation cover, except for the future LULC 2029. LULC 2029 and natural vegetation scenarios give a significant impact on water balance, flood, erosion, sedimentation including the lifetime of Saguling reservoir. The impact of deforestation, vegetation loss and increased settlement on changes in hydrological elements is the central discussion of this chapter.

4.1 Water balance

The effects of the assumed LULC of historical and scenarios on the proportions of hydrological cycle elements are illustrated in Figure 41. The simulated evapotranspiration for LULC 1994, 2009 and 2014 scenarios are noted 997, 915 and 875 mm yr^{-1}, respectively. The strong decline of evapotranspiration is clearly induced by the loss of natural vegetation cover, especially the densely forested areas. Forested areas play an important role in balancing the evapotranspiration within the watershed. A forest maintains a relatively constant evapotranspiration rate over time (Zhang *et al.*, 2001) and any alteration in this flux subsequently changes other elements of the water cycle such as overland flow, infiltration, interflow, percolation, baseflow and water yield. The direct consequence of a reduction of actual evapotranspiration (for the same precipitation) is the increment of water yield; in fact, the water yield increased by 15% from LULC 1994 to 2014. In this case study, this is due to the increase of all components of the water yield (overland flow, interflow and baseflow). As stated by many authors such as Zhang *et al*. (2001) and Costa (2005), water yield increases with the decrease in forest cover. Furthermore, the change from forested areas to cultivated areas will also alter the flow paths, flow velocities and water storage capacity (Rogger *et al*., 2017). The decline of vegetation generates less canopy interception, increasing the rainfall reaching the soil surface (also referred to as direct rainfall) and, therefore, increasing the possibility of infiltration and overland flow.

The infiltration capacity of the soil reduces in areas where deforestation has occurred, areas of increased settlement (such as urban and industrial areas), as well as in plantations and dry cultivations. The total infiltration is reduced in settlement areas, but due to the significant increase of direct rainfall in the rest of LULCs, watershed infiltration increased by 6% from LULC 1994 to 2014. With more infiltration, soil moisture increases and consequently interflow, percolation and baseflow also intensify.
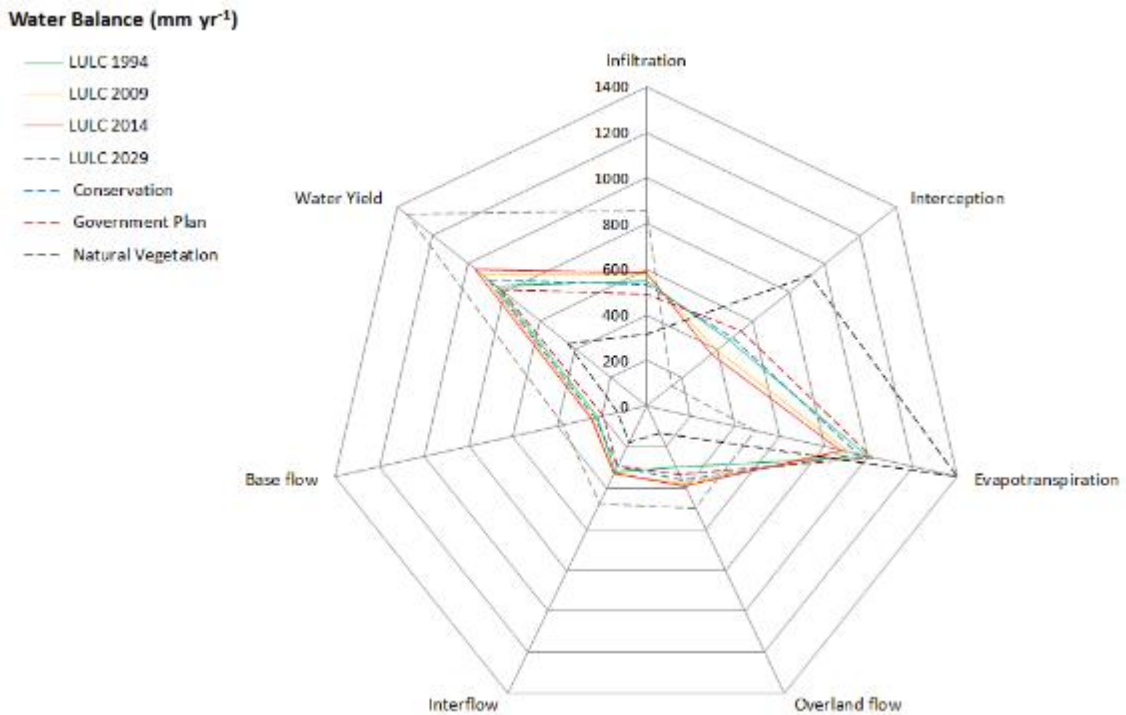
Figure 41. Water balance of three historical LULC and four scenarios simulated by TETIS using meteorological data from 1985 to 2014 (precipitation equals to 1845 mm yr^{-1})

Even though the infiltration amount has increased, the amount of water on the soil surface is still excessive, hence it emerges a high amount of overland flow. Overland flow increased by 30% increment in the period 1994 to 2014. In this case, deforestation plays an important role in this increment by triggering overland flow events due to the omission of water detained ability of the canopy. As it is well known that forest canopy has the ability to hold water, therefore water is not able to drop into the soil directly and is not converted into an overland flow. Another forest characteristic that able to combat overland flow is the proper soil physical and biological characteristics. The soil of forest is water-stable, has a low bulk density and high porosity and is formed by pores covering the full range of very small intra-aggregate pores to large interaggregate pores, many of which are continuous in depth (Gijsman, 1992). In terms of biological aspect, as stated by Emerson (1991), due to micro and macro biological activity, organic matter is profoundly mixed through the soil, leading to a stable soil structure, which is close to ideal to maintain water balance.

The expansion of settlement areas together with increased agricultural activity produces greater areas of impervious surfaces and soil compaction, which possibly escalates the overland flow (Rogger *et al.*, 2017). With regards to our case study, an increment of 30% overland flow was observed when comparing the changes from the LULC scenario in 1994 to the LULC scenario in 2014.

Moreover, rice field, plantation and dry cultivation normally maintain the rainfall to remain on its site, hence water in that area is not converted into the overland flow. But since those areas have been replaced by the settlement area, now water is converted into overland flow rapidly. As stated by Sinha & Eldho (2018), LULC changes by urban areas induce more overland flow. Moreover, the diminishing of porosity in the settlement area, makes water unable to infiltrate the soil.

The subsequent impact of the higher overland flow is the increase in water yield. Water yield increased by 15% in the period 1994 to 2014. This increment leads to a bigger possibility of flood events. The higher overland flow events decrease the amount of water for daily activity usage, because instead of stored in the aquifer, water is converted in the overland flow.

It can be concluded that the decline of vegetation cover especially forest induces an increasing overland flow and further increasing the water yield. As stated by Zhang *et al.* (2001), the reduction of forest generates more water yield. Furthermore, Drigo (2005) explains that the water yield is increasing linearly with the decreasing of forest cover percentage, the maximum increment of water yield will occur if the forest is cleared.

Regarding the LULC scenario, when compared to the most recent LULC (2014), the increment of evapotranspiration and interception rate was found in conservation, government plan and natural vegetation scenario. Under LULC 2014, 875 mm yr^{-1} of evapotranspiration and 364 mm yr^{-1} of interception were noted. Moreover, natural vegetation experienced a very significant increment in evapotranspiration and interception of 1400 and 921 mm yr^{-1}, respectively.

Meanwhile, the conservation scenario has 955 mm yr^{-1} evapotranspiration and 485 mm yr^{-1} interception. The government plan scenario has 1.018 mm yr^{-1} evapotranspiration and 533 mm yr^{-1} interception. The increase in evapotranspiration and interception is predicted due to the increment of land cover in the form of natural vegetation (forests). Forest existed in LULC conservation, government plan and natural vegetation occupy 30.16%, 41.50% and 98.43% of the total area, respectively. It is a significant increment compared to the forest area under LULC 2014 which has only 11.50% of the total area. This shows the influence of the forest vegetation on altering the hydrological cycle. If forest vegetation increased, evapotranspiration and/or interception will also increase (Zhang *et al.*, 2001). This situation changes the amount of water that accumulates in the outlet (water yield). Water yield for conservation, government plan and natural vegetation scenarios recorded at 898 mm, 834 and 442 mm yr^{-1}, respectively. These values are lower than the water yield from simulation using LULC 2014 (967 mm yr^{-1}). These lower water yields are caused by a large amount of evaporation through the evapotranspiration process.

Meanwhile, the simulation using the LCM 2029 scenario has a contradictory result. The scenario is expected to have a very significant loss in evapotranspiration and interception by 489 and 141 mm yr^{-1}, respectively. These losses are presumably due to the low forest area under the LCM 2029 scenario (11.14% of the total area). This percentage of forest area is slightly different from the forest area under LULC 2014, however, the total area of vegetation cover (forest, grass, bush/shrub, rice field, dry cultivation and plantation) reduced to 74.30% from 79.51% under LULC 2014. This concludes that a reduction in vegetation will reduce evapotranspiration and interception (Chang and Franczyk, 2008). The amount of water yield from a simulation under the LULC 2029 scenario is noted 1345 mm yr^{-1} which is higher than the water yield under LULC 2014 (967 mm yr^{-1}). This 40% increment of water yield is caused by low interception and evapotranspiration due to the reduction of vegetation cover in the study area.

Table 11 shows the percentage of each flows compared to precipitation. It is clear from Table 11, the changes in the land use-cover influence flows of the water balance. The highest magnitude of infiltration, overland flow, interflow, base flow and water yield, can be found under LULC 2029 by 46.54%, 26.92%, 25.73%, 20.40% and 72.99%, respectively. Meanwhile, the lowest magnitude of infiltration, overland flow, interflow, base flow and water yield was found under natural vegetation by 16.94%, 7%, 9.76%, 6.94%, and 23.70%, respectively. The lowest interception and evapotranspiration are possessed by LULC 2029 by 7.64% and 26.50% respectively. Meanwhile, the highest interception and evapotranspiration are possessed by natural vegetation by 49.93% and 75.87%, respectively. Those data show that the LULC condition under LULC 2029 scenario greatly influences the flows of water balance. High infiltration capacity is caused by the abundant water on the surface as the impact of the low evapotranspiration rate. Moreover, low evapotranspiration rate is caused by the low vegetation cover under LULC 2029. LULC 2029 has only 74% of vegetation cover (acquired from forest, grass, bush/shrub, rice field and plantation). This percentage is much smaller compared to the previous LULC, for example, LULC 1994 with total vegetation cover of 90%.

Table 11. Flow percentage (precipitation baseline) of historical LULC and scenarios

Flow	LULC 1994 (%)	LULC 2009 (%)	LULC 2014 (%)	LULC 2029 (%)	Conservation (%)	Government Plan (%)	Natural Veg (%)
Infiltration	29.72	30.95	31.52	46.54	28.74	26.58	16.94
Interception	25.02	21.35	19.71	7.64	26.13	28.87	49.93
ET	54.06	49.59	47.42	26.50	51.74	55.17	75.87
Overland flow	16.17	20.48	21.03	26.92	19.47	18.17	7.00
Interflow	17.44	18.15	17.78	25.73	15.92	15.71	9.76
Base flow	11.95	13.01	13.42	20.40	12.52	10.56	6.94
Water Yield	45.56	50.08	52.22	72.99	47.91	44.44	23.70

Eventhough infiltration occurs in large amounts, a remain abundant amounts of water on the surface eventually lead to an increase of overland flow which in turn increases water yield. Moreover, increased infiltration triggers the increment of interflow, baseflow and water yield. In addition, infiltrated water is the same cause of the increment of water yield. The increasing trend of infiltration, overland flow, interflow, base flow and water yield is clearly visible

from 1994, 2009, 2014 and 2029. It indicates the effect of land use change on flows of water balance. As discussed earlier, land vegetation cover area has declined, historically. It is a clue for the fall over the trend in evapotranspiration and an increment trend of water at the surface. The shift of low evapotranspiration LULC to high evapotranspiration LULC leads to the decline of surface discharge (Prasena dan Shrestha, 2013 in Yusuf *et al.*, 2018).

In general, conservation scenarios, government plans and natural vegetation have a bigger percentage of interception and evapotranspiration compared to other LULCs. It leads to a lower infiltration, overland flow, interflow, base flow and water yield. A high percentage of interception and evapotranspiration from the three scenarios is caused by the increment of vegetation cover. The percentage of vegetation cover (forest, grass, bush/shrub, rice field and plantation) are noted 80%, 84% and 98% for conservation, government plans and natural vegetation scenarios, respectively. Moreover, the forest has a big portion of those scenarios. Thus, it supports the increment of interception and evapotranspiration. Interception and evapotranspiration from the natural vegetation scenario are recorded as the highest magnitude. It is caused by massive forest vegetation almost in all area of the natural vegetation scenario.

4.2   Flood regime

Figure 42 represents the empirical and the fitted Gumbel distribution function for the three historical LULC and four scenarios. Gumbel function shows high ability in analyzing flood frequency. It is reflected by the proper fitting line between the function and observation data. The calculated quantiles for specific return periods can be found in Table 12. The evolution of LULC in time increases flood quantiles, it increases both interflow and overland flow, which are the two components of the surface erosion. To summarize, it is accurate to predict that there will be an increase in both the frequency and magnitude of floods in the region. The increase in frequency and magnitude of floods will occur for all return periods as indicated in Figure 42 and Table 12.
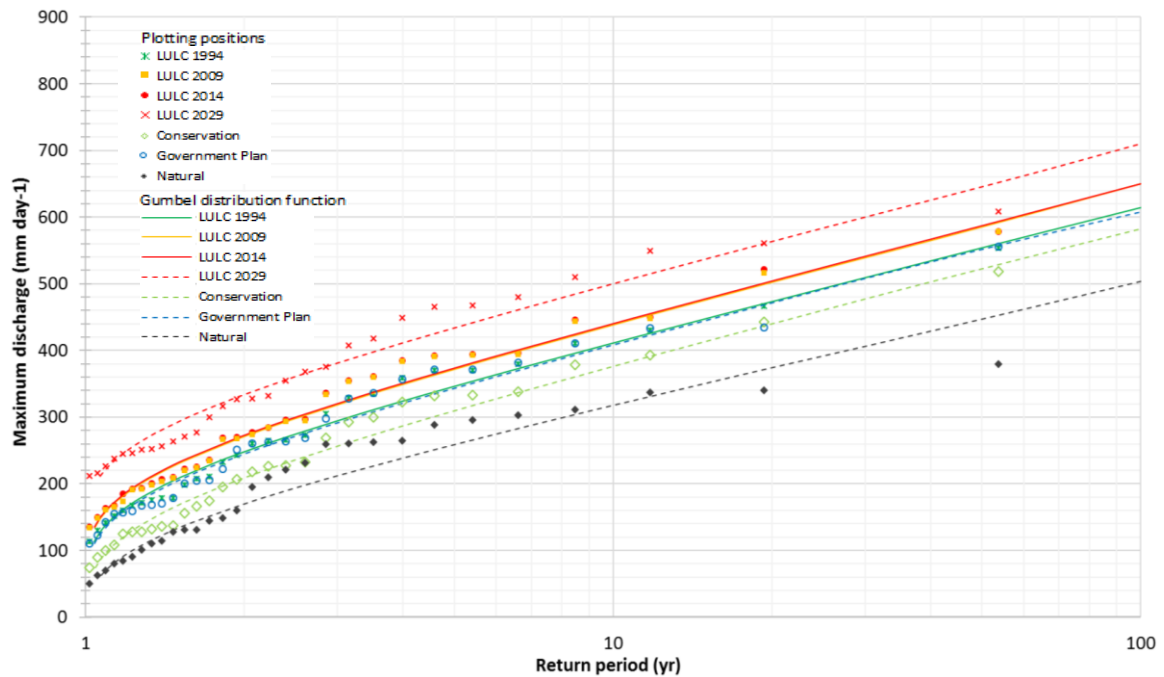
Figure 42. Comparison of flood regimes for historical LULC (1994, 2009, 2014) and scenarios (LULC 2029, conservation, government plan, natural vegetation) representing the corresponding plotting positions (dots) and the fitted (lines) Gumbel distribution function (simulation period 1985-2014).

Table 12. Flood quantiles of Gumbel and percentages between five to one hundred years return period for historical and scenarios of LULC.

Return period (yr)	Max discharge (m³s⁻¹) ¦ Percentage (%) compared with LULC 2014						
	1994	2009	2014	2029	Conservation	Government Plan	Natural Vegetation
5	346 ¦ -7.32	372 ¦ -0.49	374	434 ¦ 16.14	360 ¦ -3.76	343 ¦ -8.13	259 ¦ -30.71
10	411 ¦ -6.62	438 ¦ -0.42	440	500 ¦ 13.58	426 ¦ -3.22	408 ¦ -7.27	318 ¦ -27.83
25	493 ¦ -5.99	523 ¦ -0.36	524	584 ¦ 11.27	510 ¦ -2.73	490 ¦ -6.50	392 ¦ -25.24
50	554 ¦ -5.63	585 ¦ -0.33	587	646 ¦ 9.99	573 ¦ -2.46	551 ¦ -6.07	447 ¦ -23.80
100	614 ¦ -5.53	647 ¦ -0.30	649	707 ¦ 8.96	635 ¦ -2.24	612 ¦ -5.72	502 ¦ -22.64

For example, LULC changes from 1994 to 2014 has increased from 346 to 374 m³s⁻¹ (equal to 7.90% increment) in the 5-yr return period but only a 5.65% (from 614 to 649 m³s⁻¹) in the 100-yr return period. Moreover, the maximum discharge for a high probability return period (5 years), has increased 16.14% for the period 2014-2029, respectively. This behaviour is assumed as the relative effect of the LULC changes. This significant increment is the sign that the change in LULC affects maximum discharge significantly. As explained in the previous

section, the replacement of vegetation cover especially forest will alter the water balance and finally alter the water yield. Moreover, the additional overland flow by 30% and 60% in the period 1994-2014 and 2014-2029, respectively, emerge a higher maximum discharge and also flood events.

However, this change is not homogeneous, being larger in percentage for lower return periods than for the higher ones. For example, LULC changes from 2014 to 2029 increases the flood quantile by 16.14% for the 5-year return period, but only increases by half (8.96%) for the 100-years return period quantile. Also, it can be highlighted that the change in the future will be larger than it was in the past. One of the main reasons behind these increments is the decrease in forested areas, as the forest has the ability to intercept rainfall, decrease soil humidity, increase transpiration and increase soil permeability (Rogger *et al.*, 2017).

The comparison of flood regime between scenarios and LULC 2014 (most recent LULC) might give information about the impact of scenarios on water balance. The flood regime of conservation scenario, government plan and natural is expected to decrease with conservation scenario as the lowest increment of flood regime. For example, the maximum discharge of the highest probability return period (5 years) was noted 374 m^3s^{-1} in 2014. Meanwhile, the conservation, government plan and natural scenario were noted 360, 343 and 259 m^3s^{-1}, respectively. Those are equal to 3.76%, 8.13% and 30.71% of reduction, respectively. This reduction occurs due to the additional forests in those scenarios. The canopy of the forest is able to increase interception and evapotranspiration as explained in the previous chapter. As discussed in the previous chapter, the additional forest in the scenarios increase interception by 24.6%, 31.7% and 84.7% for the conservation scenario, government plan and natural vegetation, respectively. Meanwhile, it increases evapotranspiration by 8.4%, 14.1% and 65.1% for conservation scenarios, government plans and natural vegetation, respectively.

Upper Citarum Catchment has suffered severe damage. It is signed by the high gap between the average minimum and maximum discharge of historical LULC. For example, in the simulation under LULC 1994 and 2014 (Table 13), the gap is recorded 261.99 and 286.32 m^3s^{-1}, respectively. By this condition, the possibility of the flood occurrence in 2014 in the heavy rain is higher. This is the reason floods have been happening during the rainy season almost all year in Upper Citarum Catchment.

Table 13. The gap between the minimum and maximum discharge of historical LULC

LULC scenario	Minimum (m^3s^{-1})	Maximum (m^3s^{-1})	Gap (m^3s^{-1})
1994	5.99	267.98	261.99
2009	6.85	291.32	284.47
2014	6.73	293.05	286.32

4.3 Soil erosion at catchment scale

The areas within the Upper Citarum Catchment that are susceptible to soil erosion for historical and scenarios LULC are illustrated in Figure 43 and summarized numerically in Table 14. Both Figure 43 and Table 14 follow the Hammer (1981) classification for erosion rates, plus a tolerable erosion threshold of 13.5 ton ha^{-1} yr^{-1} as specifically proposed for Indonesia by Arsyad (2000). In general, in LULC 1994, 2009, 2014 and 2029, the low erosion class (< 1 ton ha^{-1} yr^{-1}) affected the flat areas, whereas the hilly areas possessed higher erosion rates due to higher overland flow velocities for erosion and transportation. The lower rate of erosion in flat areas in this case study is caused by two factors. Firstly, the flat area does not suffer high erosion rates due to low overland flow velocities associated with small slopes. Secondly, the majority of the flat areas are occupied by either urban zones, industrial zones or rice fields. The soil in the urban and industrial areas is mostly covered by buildings, pavements and/or miscellaneous structures. Hence, the soil does not receive the necessary exposure needed for erosion to occur. Meanwhile, the rice fields are designed to be practically horizontal. Throughout the evolution of erosion of historical LULC (1994, 2009, 2014 and 2029), it seems in a first approach there are no significant

changes. However, from a more detailed analysis, it is possible to detect two main changes. The first change noted is the clear increase in erosion due to deforestation in the northern and southern parts of the watershed. The same increment of erosion due to deforestation in the historical LULC was also found in the Samin catchment, East Java (Marhaento *et al.*, 2018). As explained in the previous sections, deforestation induces more overland flow and consequently, this results in higher erosion and sediment transport capacities. Also, the removal of the canopy increases the probability of rainfall detaching soil aggregate in large quantities, due to the direct impact of rainfall on the bare soil. Experts such as (Mohammad and Adam, 2010) have always seen forests as the optimum type of vegetation to reduce overland flow and erosion. The reduction of rice field areas could be another factor contributing to the increment of erosion. Rice fields are normally cultivated in a terraced landscape that permits them to collect water, thus lowering the overland flow and erosion (Rogger *et al.*, 2017). A significant change in erosion rates can be identified in the conservation, government plan and natural vegetation scenario. Low erosion class is evenly distributed in almost all locations, not only in the flat location. This condition is completely different from erosion map using LULC 1994, 2009, 2014 and 2029.

Table 14. Aggregated erosion (simulated by TETIS) for different historical and scenarios of LULC

Erosion class (ton ha^{-1} yr^{-1})	Area (% of basin ¦ km^2)						
	1994	2009	2014	2029	Conservation	Government Plan	Natural Vegetation
<1 (low)	67.0 ¦1552	64.9 ¦1503	65.8 ¦1524	63 ¦1459	83.0 ¦1923	41.9¦969	98.0 ¦2270
1-4 (moderate)	8.2 ¦ 189	8.6 ¦200	8.1 ¦188	8.2 ¦189	9.3 ¦214	41.6 ¦ 964	1.9 ¦ 44
4-10 (high)	5.0 ¦ 115	5.8 ¦135	5.0 ¦ 115	5.1 ¦117	5.8 ¦134	3.9 ¦ 90	0.1 ¦ 2
>10 (severe)	19.9 ¦ 460	20.6 ¦ 477	21.1¦ 489	23.8 ¦551	1.9 ¦ 44	12.6 ¦292	0.0 ¦ 0
Exceed *Tsl*	17.8 ¦ 412	18.4 ¦426	18.6 ¦ 431	21.5 ¦ 499	0.3 ¦6	11.3 ¦263	0.0 ¦ 0

The percentage of erosion with respect to the total area based on Hammer's (1981) classification is compared in Table 14. The erosion magnitude ranged from 0 to more than 13.5 ton ha^{-1} yr^{-1}. Since 1994, a stagnant erosion rate area has occurred in moderate and high class for the historical LULC. Hence, only low and severe classes experience alteration. Between 1994 and 2014, the severe class has increased by 6.3% (19 km^2) and the low class has decreased by about the same percentage. Meanwhile, A magnitude of severe erosion class is

expected to be 23.8% (551 km^2) under LULC 2029. It is a bigger magnitude compared with under LULC 2014 which has 21.1% (489 km^2). On the contrary, other LULC scenarios have a smaller percentage of severe erosion compared to LULC 2014 which has only 1.9%, 12.6% and 0.01% under conservation scenarios, government plans and natural vegetation, respectively. It shows, the addition of forest vegetation has a significant effect on reducing erosion.
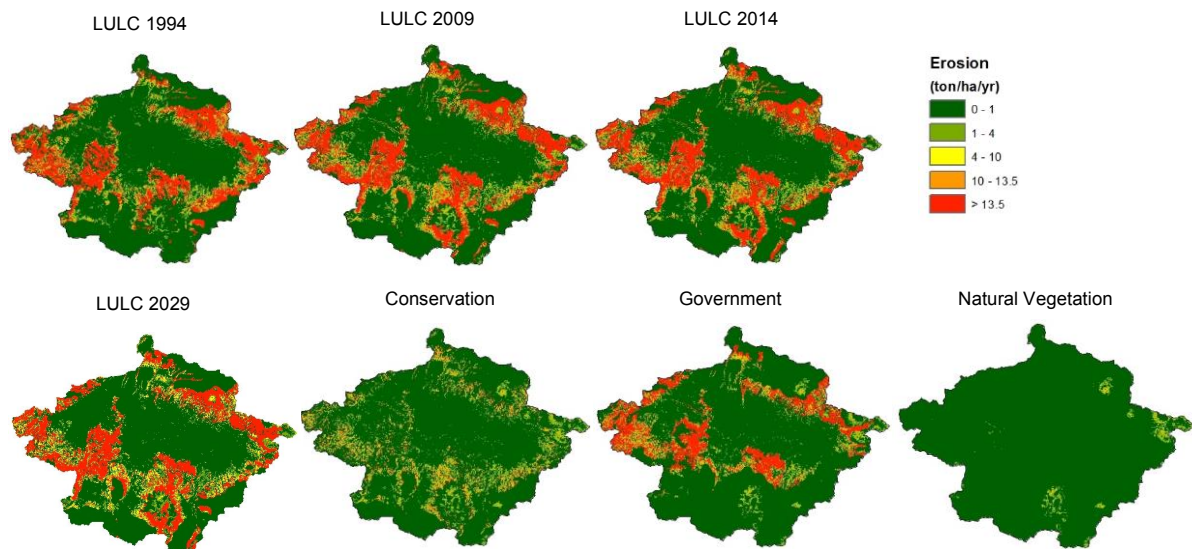
Figure 43. Spatial distribution of erosion rates simulated by TETIS under different trajectories for a different period.

The second main change refers to the evolution of areas exceeding *Tsl*, which is the major part of the severe erosion rate class. The percentage of historical severe erosion was noted 17.8 (412 km^2), 18.4 (426 km^2) and 18.6 (431 km^2) under LULC 1994, 2009 and 2014, respectively. Comparing the historical LULC, the areas exceeding *Tsl* increases by 0.6% (14 km^2) and 0.2% (5 km^2) from 1994 to 2009 and from 2009 to 2014, respectively. Those areas mostly in the hillier parts of the watershed. The possibility of the hillier area to have potential exceeding tolerance is higher due to the higher overland flow and the ease of particle to be transported. The increasing area in the hillier parts is compensated in space by a similar decrease in the low erosion rate class, located predominantly in the West, due to the conversion into urban areas. However, regarding the future, the area exceeds Tsl was noted 21.5% (499 km^2). The

difference in the area exceeds Tsl erosion between LULC 2014 and 2029 was noted 67.86 km^2 representing an increment of 15.7%. Areas exceeding tolerable erosion was noted 0.3% (6 km^2), 11.3 (263 km^2) and 0.01% (0.23 km^2) for conservation, government plan dan natural vegetation scenario, respectively.

The increment of erosion is caused by the decline of vegetation cover as a consequence of urban development. The areal of severe class and area exceeding the *Tsl* under conservation scenarios, government plans and natural vegetation are located in the steep slope area. Moreover, a drastic appearance can be identified for a natural vegetation scenario that possesses no area exceed the *Tsl*. Exceeding *Tsl* area is noted 0.3% (6 km^2), 11.3 (263 km^2) and 0% (0 km^2) under conservation, government plans and natural vegetation scenarios, respectively. Compared with the result using LULC 2014, those are a drastic reduction which is caused by the addition of forest in the steep slope. The change of LULC in the scenarios clearly minimizes erosion in the steep slope. These are caused by the effectiveness of forest vegetation in preventing erosion. As it is widely known, forests have a maximum canopy and optimal microenvironment to prevent erosion.

4.4   Reservoir sedimentation

The gross sediment input that enters the Saguling reservoir is equal to its watershed sediment yield. The sediment yield increased from 13.6 ton ha^{-1} yr^{-1} in LULC 1994 scenario to 5.9 ton ha^{-1} yr^{-1} in 2009 to 17.7 ton ha^{-1} yr^{-1} in 2014 and 28.8 ton ha^{-1} yr^{-1} in 2029 (Table 15). Sinha and Eldho (2018) found a similar increase in sediment yield, studying the past and future of the Netravati watershed in India.

Meanwhile, the sediment yields under the conservation scenario, government plans and natural vegetation were noted 0.27 tons ha^{-1} yr^{-1}, 0.27 tons ha^{-1} yr^{-1} and 0.45 tons ha^{-1} yr^{-1}, respectively. These amounts are much lower than the sediment yield resulted from the simulation under historical LULC (LULC 1994, 2009 and 2014). It shows the effectiveness of the forest on decreasing the sediment amount through the reduction of erosion.

Table 15. Comparison of sediment yield, the reservoir and hydropower lifetimes for the different historical and scenarios of LULC

.		1994	2009	2014	2029	Conservation	Government	Natural
Sediment yield	Mton yr^{-1}	3.1	3.7	4.1	6.7	0.062	0.062	0.1
	ton ha^{-1} yr^{-1}	13.6	15.9	17.7	28.8	0.27	0.27	0.45
Lifetime alteration caused by sedimentation in the reservoir								
Reservoir lifetime (yr)		239	191	182	113	long time	long time	long time
Hydropower lifetime (yr)		21	16	15	8	long time	long time	long time

As discussed in the previous section, the increasing overland flow will be followed by an increase in catchment erosion and reservoir sedimentation. These increments are caused by the increment of sediment yield in the historical period due to the decline of vegetative cover. Sediment yield increment occurs under LULC 1994, 1999, 2009 and 2029 as the result of overland flow increment. The transport capacity of water on the eroded material is increasing simultaneously with the increase of overland flow. As stated by (Yu, Zhang and Fu, 2015), the transport capacity of overland flow will determine the amount of material in the flow. Furthermore, Orchiston *et al*. (2013) stated that by reducing overland flow, the yield of sediment was reduced considerably. The reduction of sediment yield under the scenarios (conservation, government plans and natural vegetation) is an example of the impact of overland flow reduction on sediment yield. These findings lead us to the conclusion that lower the overland flow, lower the sediment. Vice versa, the higher the overland flow, the higher the sediment.

The increment of the sediment yield can be explained not only by the increase in erosion rates, but also by the increase of river channel transport capacity, mainly during flood events. Flood events have increased as it has described in the previous chapter. These events can be identified from the maximum discharge which continued to increase over time (Figure 42). Maximum discharge can be related to transport capacity since maximum discharge contains the amount of water as the carrier in the transport capacity. Moreover, the maximum discharge will also be depending on overland flow since the overland flow amount will be accumulated in the river network as maximum discharge. The transport capacity of water on the eroded material increases simultaneously with the increase in watershed overland flow (Yu *et al*., 2015) and also affects the remobilization of previously deposited materials

(Bussi *et al.*, 2014).

A direct consequence of a greater quantity of sediment draining into the reservoir is the reduction of its lifetime (Figure 44). This study define threshold by 50 Hm^3 as minimum operational volume of the reservoir. Climatological data from 1985 to 2014 has been selected. With this hypothesis, the reservoir lifetime is noted 239, 191, 182 and 113 years for LULC scenarios 1994, 2009, 2014 and 2029, respectively. These numbers show the impact of LULC on degrading the lifetime of the reservoir due to the increment of sediment amount into the reservoir. These results are more pessimistic than the half lifetime of 189 years obtained by the Ministry of Public Works of Indonesia using a simpler methodology under LULC 2009 (Ministry of Public Works, 2011). This difference could be attributed to different LULC maps for the model and limit of full storage. This study used LULC 2014 for recent analysis. Meanwhile, the ministry used LULC 2009 for their study. Five years of different LULC is enough to make a significant difference since LULC change during that period was highly occur. Moreover, the Ministry of Public Works of Indonesia found that the sediment has accelerated from 1989 to 1999. Another reason is the different full storage limit. This study used 50 hm3 as a full storage limit Meanwhile, the study of the ministry used 7 hm^3. It makes a much greater lifetime for the study from the Ministry of Public Works of Indonesia.
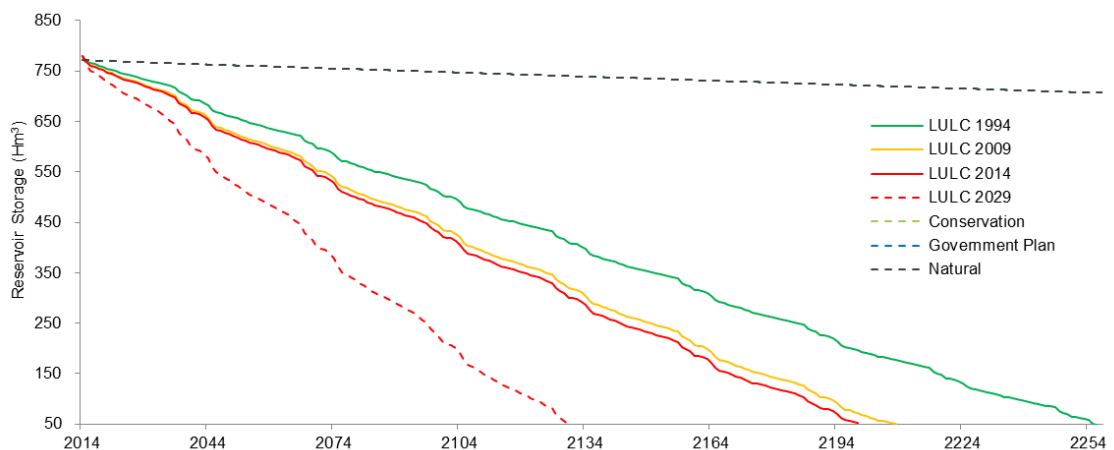
Figure 44. Comparison of reservoir storage evolution for historical LULC (1994, 2009, 2014) and scenarios (2029, conservation, government plan, natural)

Regarding the hydropower lifetime, the decrease in hydropower lifetime occurs from 20 to 15 to 16 and 8 years from LULC 1994 to LULC 2014, from LULC 2014 to LULC 2009 and from LULC 2009 to LULC 2029, respectively (Figure 45). Those indicate that the increment of sedimentation induces the reduction of reservoir and hydropower lifetime.
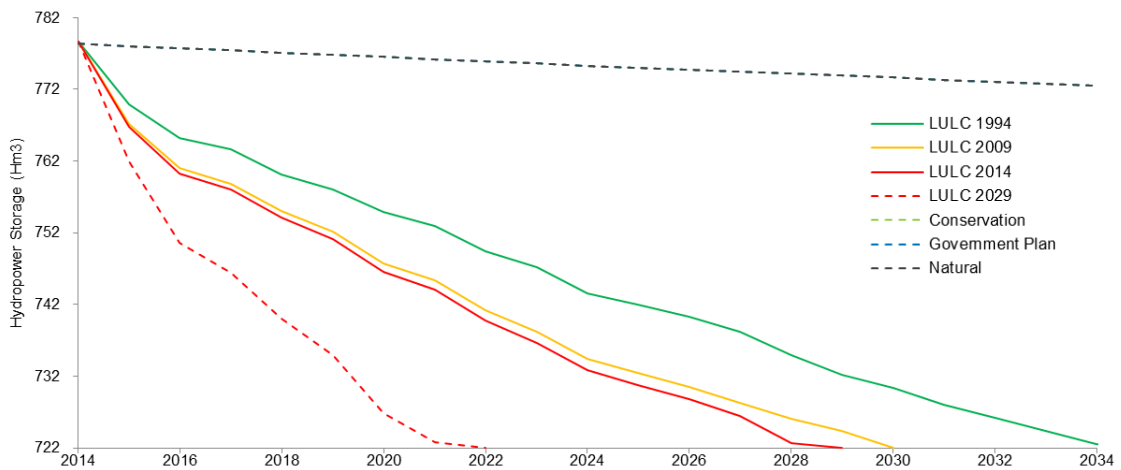
Figure 45. Comparison of hydropower storage evolution for historical LULC (1994, 2009, 2014) and scenarios (2029, conservation, government plan, natural).

The severity of this situation is further emphasized when considering the problem of hydroelectric power production: hydropower water intake corresponds to a storage capacity of 722 Hm^3, which means that there will be serious hydropower production problems within the next twenty years if no immediate action is taken. The reduction of hydropower lifetime is a big disadvantage for the community since electricity is considered as a basic necessity.

Meanwhile, the lifetime of the reservoir and hydropower for conservation, government plans and natural vegetation scenarios are noticed very long. These are caused by very small quantities of stored sediment yield in the reservoir. The amount of sediment yield for conservation, government plans and natural vegetation are recorded 0.27 tons ha^{-1} yr^{-1}, 0.27 tons ha^{-1} yr^{-1} and 0.45 tons ha^{-1} yr^{-1}, respectively. These nearly the same small amounts result the same line position in the figure. Hence, it is hard to distinguish the line of conservation, government plans and natural vegetation scenarios. The small amount of those

106

sediment yield is caused by the small amount of erosion and the small transport capacity. The addition of forested areas in the scenarios prevents erosion effectively. Meanwhile, another consequence of additional forest in the scenarios is the increment of evapotranspiration and infiltration which results in a lower overland flow and sediment yield.

CHAPTER 5. IMPACT OF CLIMATE CHANGE IN HYDROLOGICAL AND SEDIMENT REGIME

Chapter Overview

This chapter explains the impact of bias correction on trajectories data (RCP 4.5 and 8.5) in three different periods (2011-2040, 2041-2070 and 2071-2100). The corrected precipitation, minimum temperature, mean temperature and maximum temperature of RCP 4.5 and 8.5 were compared to see the impact of different trajectories on those parameters. This comparison was also applied between precipitation under trajectories and control periods. Compared to the control period, precipitation and temperature of the trajectory (RCP 8.5) have a bigger variation than the RCP 4.5. The impact of bias correction on RCP 4.5 and 8.5 regarding its hydrological aspect is analyzed in this chapter. Comparisons between trajectories and control periods in terms of the hydrological aspect were also analyzed. The impact of climate change (RCP 4.5 and 8.5) in 30-year time frame up to 2100 is also analyzed. Water balance, flood regime, erosion and reservoir sedimentation, including the lifetime of Saguling reservoir is impacted by the shift of climate change under different trajectories.

5.1 Comparison between corrected RCP 4.5 and corrected RCP 8.5

5.1.1 Precipitation

A comparison of precipitation under trajectories is examined using a quintile-quintile (q-q) plot from 2011-2100 (Figure 46-left). In general, the distribution of precipitation less than 55 mm day-1 under RCP 8.5 is nearly the same as the distribution of precipitation under RCP 4.5. Meanwhile, RCP 4.5 produces a lower precipitation amount compared to the RCP 8.5 for the precipitation higher than 55 mm day^{-1}. Monthly precipitation of the original RCP 4.5 and RCP 8.5 and the precipitation resulted from bias corrections are explained in Figure 46-left. A distinct seasonal cycle can be seen in precipitation in the study area. The lowest precipitation amount of observed, corrected and uncorrected trajectories are almost the same (about 50 mm day^{-1}). Meanwhile, the highest monthly precipitation for observed, corrected and uncorrected trajectories are different. In the beginning of the year, the corrected and uncorrected trajectories produce higher precipitation than the observed precipitation Meanwhile, in the end of the year, precipitation amount of the observation is bigger than the uncorrected trajectories and lower than the corrected trajectories. Moreover, from month 4 to 10, the observation line is located closer to the corrected and uncorrected line. In this regard, the variability of the precipitation in the rainy season (at the beginning and the end of the year) gives a clear effect on the precipitation amount under trajectories.

After applying the correction of bias, calculated monthly mean precipitation in uncorrected RCM data is significantly reduced. The mean monthly precipitation of corrected precipitation is decreased compared with the uncorrected one. These declines mainly occurred in the heavier precipitation from February to May and from October to December. Meanwhile, only a slight increment occurs from June to September. The peak of rainfall, such as in March, April, November and December reach 350-400 mm month^{-1}. This value has increased compared to the original rainfall amount (170-280 mm month^{-1}).
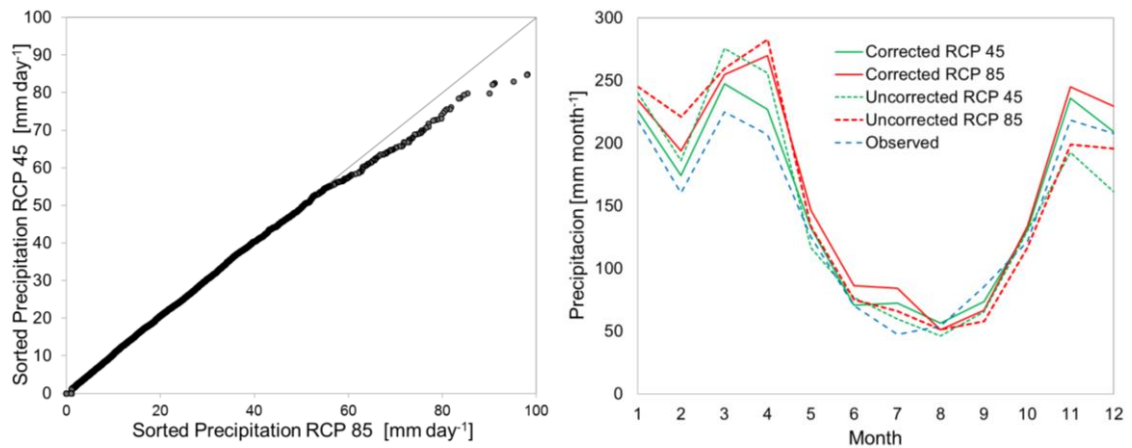
Figure 46. Comparison of precipitation from different trajectories. Left: q-q plot between precipitation of RCP 4.5 and RCP 8.5. Right: monthly precipitation of RCP 4.5, RCP 8.5, corrected RCP 4.5, corrected RCP 8.5 and observed.

In addition, Figure 47 shows the increment of monthly precipitation under RCP 4.5 and RCP 8.5 compared to the control period. The graph indicates that the increment of precipitation will occur in the future due to climate change. For example, the peak of the precipitation in March is noted 446, 460 and 338 mm month^{-1} for RCP 4.5, RCP 8.5 and control period, respectively. The trend of this magnitude can be found again for the second peak which occurs in November by 266, 272 and 188 mm month^{-1} for RCP 4.5, RCP 8.5 and control period, respectively.

After the correction of bias, calculated monthly mean precipitation in uncorrected RCM data are significantly reduced. The mean monthly precipitation of corrected precipitation is decreased compared with the uncorrected one.
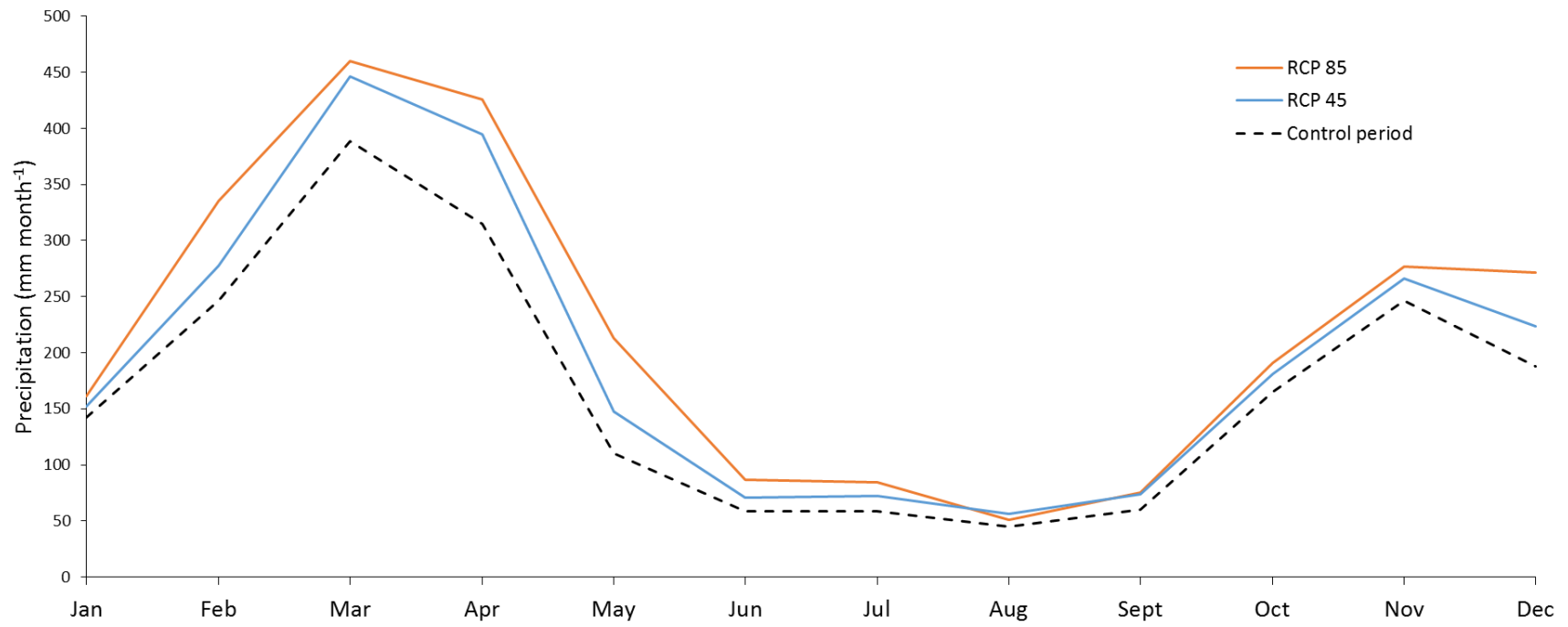
Figure 47. The monthly scale of precipitation amount in the period 1975-2005 of RCP 4.5, RCP 8.5 and the control period.

5.1.2 Maximum, Mean and Minimum Temperature

Q-q plot analysis of maximum, mean and minimum temperature under RCP 4.5 and RCP 8.5 is presented in Figure 48-left. The mean, maximum and minimum temperature under RCP 4.5 are totally underestimated (compared to RCP 8.5). It signifies that the mean, maximum and minimum temperature under RCP 8.5 has a higher magnitude than under RCP 4.5. This finding is also supported by the analysis of monthly temperature presented in Figure 48-right. Monthly maximum temperature under RCP 8.5 is noted higher than the monthly maximum temperature under RCP 4.5 with the difference between 0.8 and 1.4°C and temperatures peak existed from September to October. Meanwhile, the mean and minimum temperatures experienced the same pattern with the difference in the range 2.0-2.2 °C and 2.0-2.5 °C, respectively. The peak of the mean temperature is noticed in April and November. Meanwhile, the peak of minimum temperature is noticed in April and May. These indicate a temperature increment of different trajectories (RCP). Regarding RCP 8.5, this trajectory is widely known to predict the temperature increment without any climate mitigation efforts. Hence the temperature continues to rise beyond the 21st century (IPCC, 2014).

Table 16 shows the changes in the mean state variable values of the trajectories compared to the control period. All mean state variables in trajectories are generally expected to increase. The amount of precipitation is expected to increase by 6.6% and 14.6% under RCP 4.5 and RCP 8.5, respectively. The extreme precipitation values are expected to increase, despite the global rainfall decrease. This phenomenon has already been documented in various papers (e.g. (Alpert *et al.*, 2002). They stated that the extreme precipitation is expected to increase more under the B2 scenario than under the A2 scenario. This aspect is likely further to affect soil erosion and sediment yield.
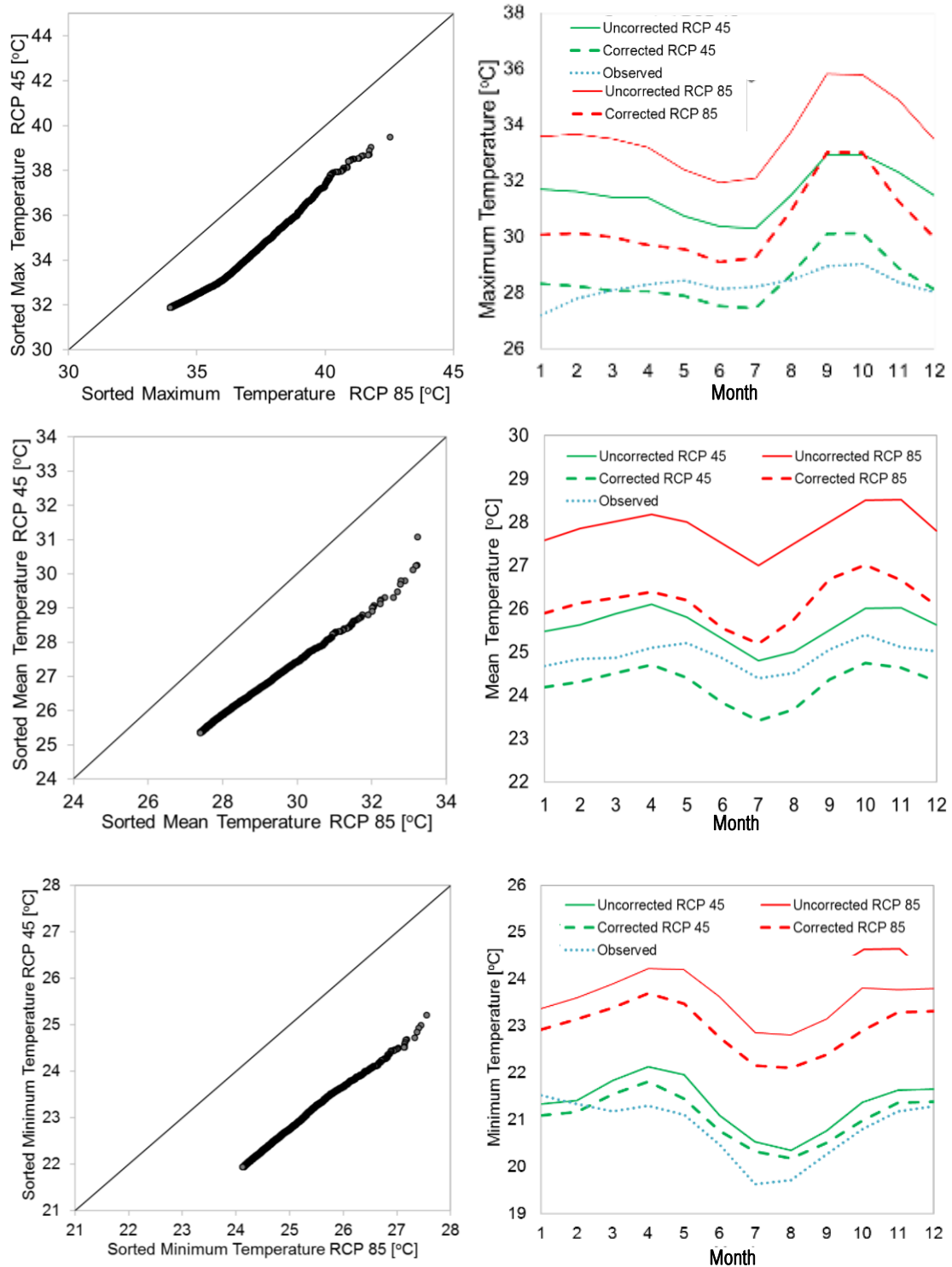
Figure 48. Comparison of maximum, mean and minimum temperature from different trajectories. Left: q-q plot comparison between the temperature of RCP 4.5 and RCP 8.5. Right: monthly temperature of RCP 4.5, RCP 8.5, corrected RCP 4.5, corrected RCP 8.5 and observed.

The amount of maximum, mean and minimum temperature under RCP 4.5 is expected to increase by 3.3°C, 0.7°C and 0.53°C, respectively. Meanwhile, under RCP 8.5 is expected to increase by, 5.4°C, 3.0°C and 2.78°C, respectively. These data indicate that temperature under RCP 8.5 is expected to have a greater increment compared with the increment experienced under RCP 4.5. This increment is due to the continuous increment of radiative forcing in RCP 8.5, even beyond 2100. This finding is in line with the result from several studies. For example, the study conducted by Wang *et al*. (2018) found a higher temperature increment by 3.5°C and 5.6 °C under RCP 4.5 and RCP 8.5, respectively.

Table 16. Comparison of precipitation and temperature between the control period and trajectories

Mean state variable	Control	RCP 4.5 scenario	RCP 8.5 scenario	RCP 4.5 Variation	RCP 8.5 Variation
Precipitation (mm yr^{-1})	1741	1856	1996	115 (6.6%)	255 (14.6%)
Maximum temperature (°C)	28	32	34	3.3	5.4
Mean Temperature (°C)	25	26	28	0.7	3.0
Minimum temperature (°C)	21	21	24	0.53	2.78

5.2   Water balance

The effects of the different trajectory (RCP 4.5 and RCP 8.5) with (w/) bias correction in three periods (2011-2040, 2041-2070 and 2071-2100) using the recent LULC (2014) on water balance are illustrated in Figure 49. The simulated water balance for both RCP 4.5 and RCP 8.5 shows the same trend. In general, the elements of water balance have increased from 2011-2040 to 2041-2070 and 2071-2100. For example, the evapotranspiration under RCP 4.5 from the period 2011-2040 to 2041-2070 and 2071-2100 are expected to have 755 to 768 and 854 mm yr^{-1}, respectively. Meanwhile, RCP 8.5 is expected to have 764, 792 and 895 mm yr^{-1} of evapotranspiration for the period 2011-2040, 2041-2070 and 2071-2100, respectively. Other water cycle elements such as interception are expected to increase along with the increment in precipitation occurred in all trajectories. An interception under RCP 4.5 is expected to have 278, 282 and 298 mm yr^{-1} for the

period 2011-2040, 2041-2070 and 2071-2100, respectively. Meanwhile, interception under RCP 8.5 is expected to have 276, 294 and 307 mm yr^{-1} for the period 2011-2040, 2041-2070 and 2071-2100, respectively.
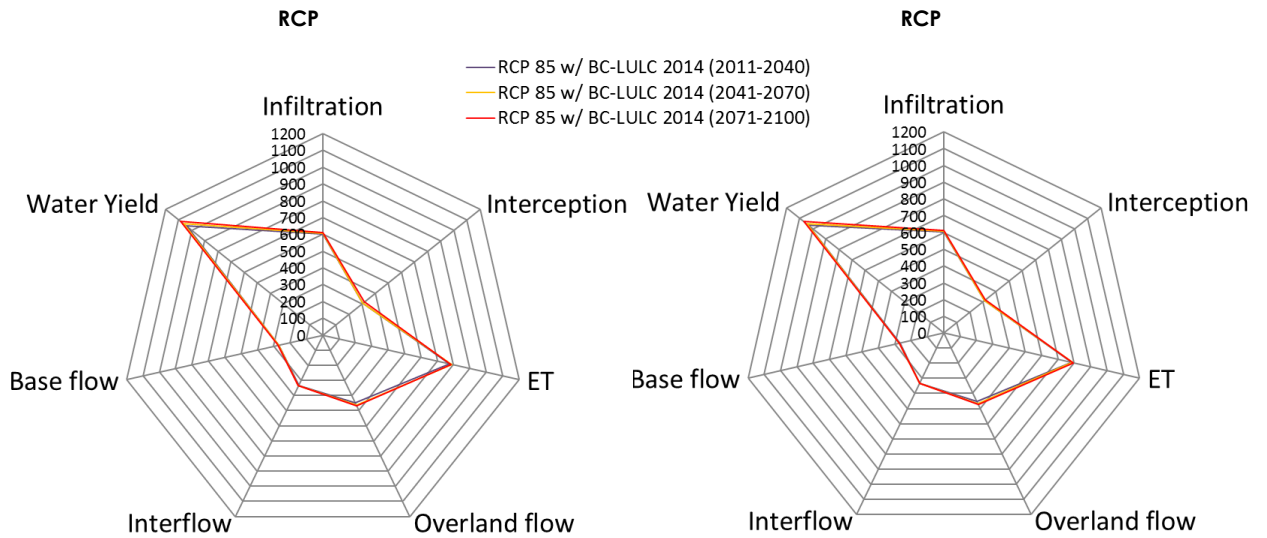
Figure 49. Water balance simulated by TETIS for three different periods (2011-2040, 2041-2070 and 2071-2100) of RCP 4.5 and RCP 8.5 using LULC 2014

Climate change alter evaporation due to the increment of radiative forcing, which eventually alters the whole system of the water cycle. In the storm-impacted area as a result of higher evaporation, precipitation will have a tendency to increase (IPCC, 2014). Another water cycle element that considered to be crucial in this study is the increment of overland flow and water yield. Overland flow under RCP 4.5 is expected to have 269, 285 and 294 mm yr^{-1} for the period 2011-2040, 2041-2070 and 2071-2100, respectively. Meanwhile, RCP 8.5 is expected to have 263, 275 and 299 mm yr^{-1} of overland flow for the period 2011-2040, 2041-2070 and 2071-2100, respectively. The increment of overland flow due to different RCP projection is in line with the result of the study conducted by Nilawar and Waikar (2019). The result of the study in the Purna river basin, India found that overland flow under RCP 8.5 is increased about four times compared to overland flow under RCP 4.5.

116

The increment of overland flow will impact floods, erosion and sedimentation since it is directly connected with flood, erosion and sedimentation. As explained previously, the transport capacity of overland flow will determine the amount of material resulted from erosion (Yu, Zhang and Fu, 2015). Furthermore, Orchiston *et al.* (2013) stated that by reducing overland flow, the yield of sediment was reduced considerably. As stated by Ribolzi *et al.* (2017), the amount of overland flow contributes to the magnitude of streamflow during the flood.

Regarding water yield, RCP 4.5 is expected to have 888, 924 and 956 mm yr^{-1} for the period 2011-2040 to 2041-2070 and 2071-2100, respectively. Meanwhile, the RCP 8.5 is expected to have 875, 897 and 932 mm yr^{-1} of overland flow for the period 2011-2040, 2041-2070 and 2071-2100, respectively. The shift of water yield affects floods by changing the frequency and magnitude of flows. Those alterations are the sign of the trajectories (RCPs) impact on hydrological balance. As stated by Asokan & Dutta (2008) and Rees & Collins (2006), climate change would alter hydrological elements and change the behaviour of the hydrological cycle.

Table 17 shows the percentage of each flows under different climate change periods compared to precipitation. The increment trend of flows in three period for both RCP 4.5 and RCP 8.5 are indicated in Table 17. The increment of flows can be identified under RCP 4.5 and RCP 8.5 from the period 2011-2040 to 2041-2070 and also during the period 2041-2070 to 2071-2100.

Table 17. Flow percentage (precipitation baseline) of two trajectories in three periods

Flow	RCP 4.5 2011-2040 (%)	RCP 4.5 2041-2070 (%)	RCP 4.5 2071-2100 (%)	RCP 8.5 2011-2040 (%)	RCP 8.5 2041-2070 (%)	RCP 8.5 2071-2100 (%)
Infiltration	42.45	43.73	45.89	45.46	45.98	46.55
Interception	15.23	16.93	16.35	15.67	16.75	16.74
Evapotranspiration	38.77	39.47	43.97	46.49	47.18	48.39
Overland flow	17.55	18.02	20.64	18.22	18.80	18.96
Interflow	26.96	27.00	27.29	27.71	27.03	28.00
Base flow	22.47	22.57	23.03	22.76	23.77	24.65
Water Yield	66.06	66.41	67.41	66.42	67.19	68.78

The increment of infiltration, overland flow, interflow, base flow dan water yield under trajectories are caused by the increment of precipitation. RCP 8.5 gives a bigger magnitude of increment compared to RCP 4.5. This presumably caused by the bigger increment of precipitation under RCP 8.5. As discussed in the previous chapter, the delta changes between RCP 4.5 and RCP 8.5 compared to the control period are noted 115 and 225 mm yr^{-1}, respectively.

5.3 Flood regime

The empirical and the fitted Gumbel distribution function for the three LULC scenarios under RCP 4.5 and 8.5 are presented in Figure 50. As described earlier, the increment of overland flow and water yield will affect the flood regime. Thus, affecting the return period. Return periods of RCP 4.5 dan RCP 8.5 are expected to increase for the three periods (2011-2040 to 2041-2070 and 2071-2100). The calculated quantiles for specific return periods can be found in Table 18. The time period (nearest to the farthest) of both RCP increases in both the frequency and magnitude of floods for each return period.

Table 18. Flood quantiles of Gumbel and percentages between five to one hundred years return period for different future climate change trajectories in three periods.

Return period (yr)	Max discharge (m³s⁻¹) ¦ Percentage (%) compared with LULC 2014 ¦ Percentage (%) compared with the previous period					
	Baseline (2014)	RCP 4.5 (2011-2040)	RCP 4.5 (2041-2070)	RCP 4.5 (2071-2100)	RCP 8.5 (2011-2040)	RCP 8.5 (2041-2070)	RCP 8.5 (2071-2100)
5	374	399 ¦ 6.8 ¦ 0	400 ¦ 7.1 ¦ 0.28	402 ¦ 7.5 ¦ 0.37	400 ¦ 7.0 ¦ 0	401 ¦ 7.3 ¦ 0.28	405 ¦ 7.7 ¦ 0.37
10	440	456 ¦ 3.6 ¦ 0	469 ¦ 6.5 ¦ 2.82	482 ¦ 9.5 ¦ 2.81	451 ¦ 2.5 ¦ 0	457 ¦ 3.8 ¦ 1.33	458 ¦ 4.0 ¦ 0.22
25	524	553 ¦ 5.5 ¦ 0	558 ¦ 6.3 ¦ 0.76	561 ¦ 7.0 ¦ 0.67	555 ¦ 5.8 ¦ 0	558 ¦ 6.3 ¦ 0.47	559 ¦ 6.5 ¦ 0.19
50	587	618 ¦ 5.3 ¦ 0	623 ¦ 6.1 ¦ 0.76	627 ¦ 6.8 ¦ 0.66	616 ¦ 4.9 ¦ 0	622 ¦ 5.9 ¦ 0.95	624 ¦ 6.3 ¦ 0.38
100	649	638 ¦ 0.1 ¦ 0	662 ¦ 2.0 ¦ 1.85	689 ¦ 6.2 ¦ 4.12	678 ¦ 4.5 ¦ 0	695 ¦ 7.1 ¦ 2.47	716 ¦ 10.3 ¦ 3.02

Generally, compared to the baseline (2014), the maximum discharge for each return period is expected to decrease. For example, the percentage of increment in maximum discharge for the highest return period (5 yr) in 2011-2040 period under RCP 4.5 is noted at 6.8%. Meanwhile, the lower return period (10 yr) increased by only 3.6%. As mentioned by Mal, Singh, & Huggel (2018), higher discharge is related to a higher probability. Meanwhile, the lower discharge is related to the lower probability. Beyond that, the biggest percentage increment

for the maximum return period is possessed under RCP 8.5 in the period 2071-2100 ranged 3.4-10.3%.
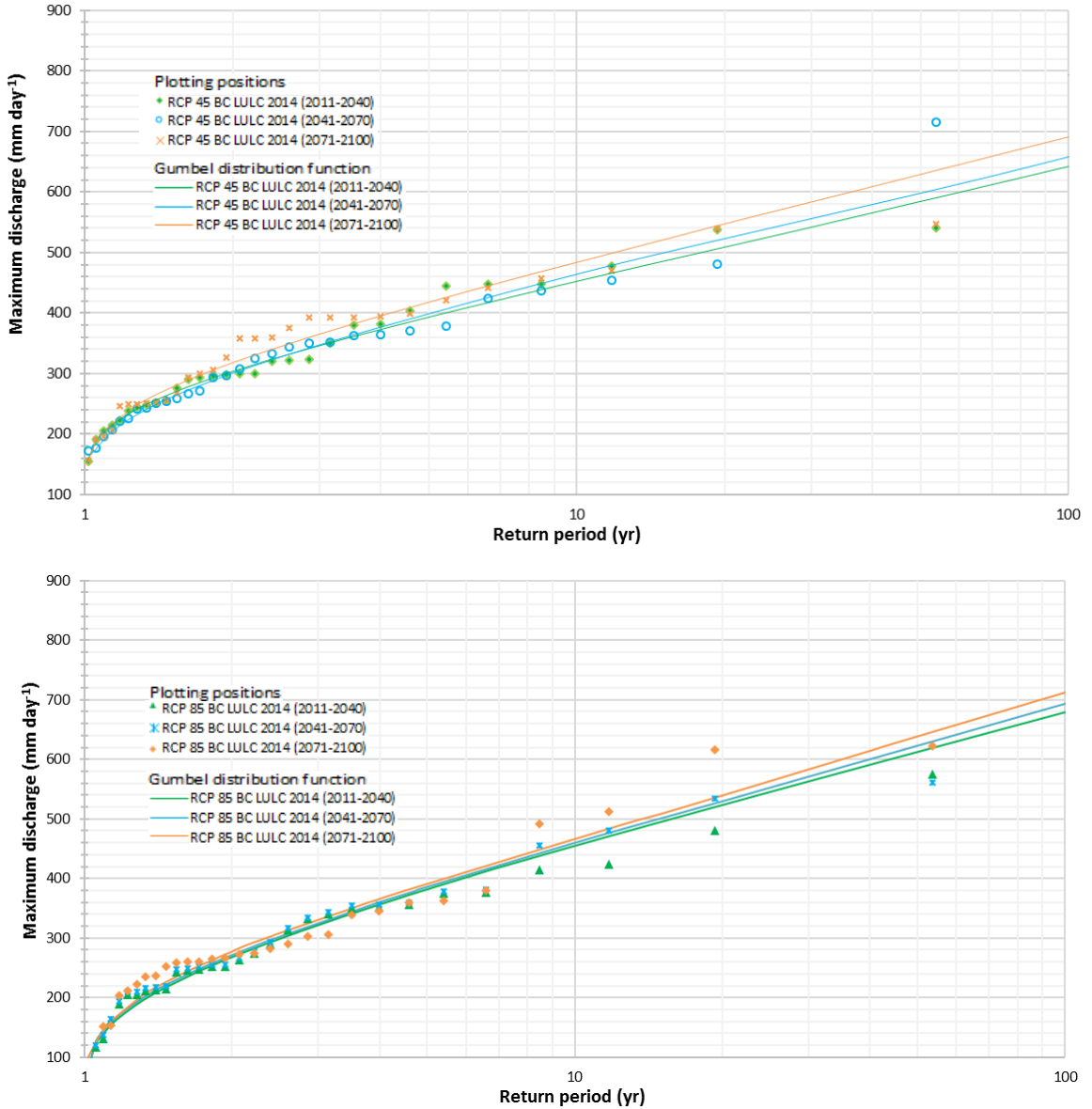
Figure 50. Comparison of flood regimes using LULC 2014 under different trajectories for period 2011-2040, 2041-2070 and 2071-2100, representing the corresponding plotting positions (dots) and the fitted (lines) Gumbel distribution function.
Upper: simulated using trajectory RCP 4.5. Lower: simulated using trajectory RCP 8.5

The return periods of 5 to 100 years for both RCP were noted 399 to 697 m^3s^{-1}, respectively. The farthest period of RCP in higher return periods generates

more flood possibility. For example, the period 2011-2040 of RCP 4.5 is expected to have 456 m^3 s^{-1} in the 10-yr maximum discharge. Meanwhile, the period 2071-2100 is expected to have 472 m^3 s^{-1} for the same trajectory and return period. The discharge under RCP 4.5 in the period 2011-2040 to 2041-2070 for the whole return period is expected to increase by 0.28%, 2.82%, 0.76%, 0.76%, and 1.85 % for 5, 10, 25, 50 and 100 years of the return period, respectively. Meanwhile, the return period from the 2041-2070 to 2071-2100 is expected to increase by 0.37%, 0.65%, 0.67%, 0.66% and 4.12% for 5, 10, 25, 50 and 100 years of return period, respectively. The same trend was found under RCP 8.5, but comes with different magnitude. The return period under RCP 8.5 in period 2011-2040 to 2041-2070 is expected to increase by 0.28%, 1.33%, 0.47%, 0.95% and 2.47% for the 5, 10, 25, 50 and 100 years, respectively. Meanwhile, for the period 2071-2100 under RCP 8.5, the return period is expected to increase by 0.37%, 0.22%, 0.19%, 0.38% and 0.29% for the year 5, 10, 25, 50 and 100 year, respectively.

5.4   Soil erosion at catchment scale

Erosion rates resulted from TETIS simulation under RCP 4.5 and RCP 8.5 trajectories, with and without (w/o) bias correction are shown in Figure 51. The erosion magnitude ranged from less than 1 to more than 13.5 ton ha^{-1} yr^{-1}. The rate of erosion shifts dramatically when both RCPs (with and without bias correction) were simulated and compared. For example, erosion rate exceeds *Tsl* (in red color) resulted from simulation using both RCPs (RCP 4.5 and RCP 8.5) in the period 2011-2040, experienced a significant increment compared to erosion rate under the same period and the same RCP without correction. The erosion rate exceeds *Tsl* (under the corrected RCP) in the north, centre and southern part of the study area is expected to increase significantly compared to the erosion rate resulted under RCP without correction. These increments occur in the hilly area due to the maximum impact of hydrometeorological alteration. The reason is accounted for the precipitation correction which results in a higher precipitation amount. Thus, the erosivity impact of the rainfall is greater due to a bigger soil detachment. Moreover, as explained in the previous

chapter, a high rainfall amount increases the overland flow which ultimately increases erosion.

The spatial distribution of erosion rates simulated by TETIS under different trajectories for a different period is presented in Figure 51. The effect of climate change on the erosion rate in different periods cannot be identified clearly. Small increment area of severe class erosion for a different period of RCP 4.5 and RCP 8.5 can be detected only in the southern part of the study area. The hilly area is the most impacted area caused by climate change.
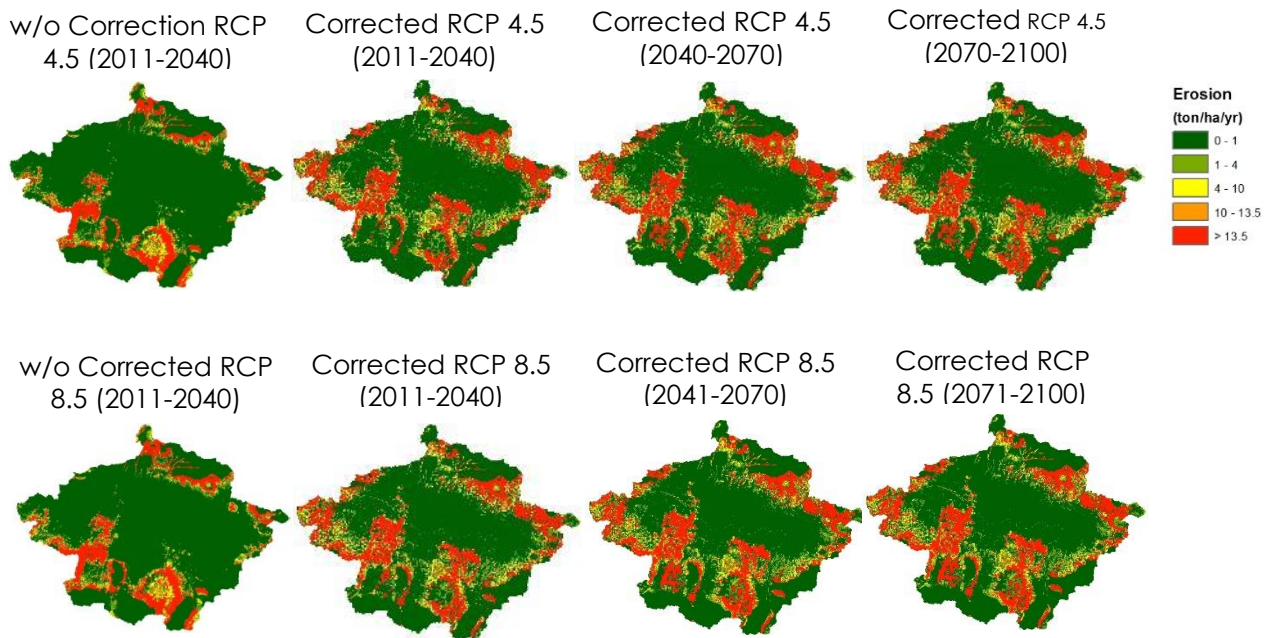
Figure 51. Spatial distribution of erosion rates simulated by TETIS under different trajectories for a different period.

The second main change refers to the evolution of areas that exceed the *Tsl*, which is the major part of the severe erosion rate class. The percentage of erosion with respect to the total area based on Hammer (1981) classification is compared in Table 19. A low fluctuation of erosion rate area has occurred in the moderate and high class for all RCP and all periods. The lower percentage area of erosion rate is possessed by the moderate and high class. Meanwhile, the highest percentage area of erosion rate is possessed by the low class. As can be

identified clearly in the figure, the flat area dominantly occupies the study area. Hence, low class becomes a dominant class of erosion rate. The fluctuation in the moderate and high class is noted in the range 8.2% to 8.5% and 64.8% to 65.8% under RCP 4.5 and RCP 8.5 within all periods, respectively.

The low and severe classes experience a bigger change. Under RCP 4.5, the low class is expected to decrease by 10 km^2 (0.5%) and increase 6 km^2 (0.2%) for the period (2011-2040) to (2041-2070) and (2041-2070) to (2071-2100), respectively. Meanwhile, the severe class is expected to increase by 4 km^2 0.8(%) and 2 km^2 (0.1%) for the same period. Moreover, the area exceeds Tsl erosion is expected to increase by 3 km^2 (0.1%) and 5 km^2 (0.2%) for the same period. Meanwhile, under RCP 8.5, the low class is expected to decrease by 14 km^2 (0.6%) and 9 km^2 (0.4%) from the period (2011-2040) to (2041-2070) and from (2041-2070) to (2071-2100), respectively. The severe class is expected to increase by 4 km^2 (0.2%) and 2 km^2 (0.1%) in the same period. Meanwhile, the area exceeds Tsl erosion is expected to increase by 4 km^2 (0.2%) and 1 km^2 (0.1%) in the same period.

The percentages of severe erosion under RCP 4.5 for the three consecutive periods are recorded at 21.9%, 22.1% and 22.2%, respectively. Meanwhile under RCP 8.5 is recorded 22.0%, 22.2% and 22.2%, respectively. Low magnitude of delta change between each period in both RCP 4.5 and RCP 8.5 can be identified. These slight changes are in line with the description of the erosion rate in Figure 51. The increment of erosion rate in different periods in Figure 51 is hard to be identified, and this low delta change could be the reason for that. The low magnitude of increment is also happened for the class of erosion class exceed *Tsl*. The erosion rate exceeds the *Tsl* is noted 19.0%, 19.1% and 19.3% under RCP 4.5 and 19.1%, 19.3% and 19.4% under RCP 8.5, respectively.

Erosion increments that occurred under RCP 4.5 and RCP 8.5 are caused by the increment of precipitation in the future. As discussed previously, future precipitation in the study area is expected to increase due to climate change. Precipitation is the main trigger of erosion (through erosivity process). Thus, the

erosion rate is produced. In addition, precipitation increment enhances the amount of overland flow which finally will elevate erosion (Yu, Zhang and Fu, 2015).

Table 19. Aggregated erosion simulated by TETIS for two trajectories for three different periods

Erosion class (ton ha^{-1} yr^{-1})	Area (% of basin ¦ km^2)					
	RCP 4.5 (2011-2040)	RCP 4.5 (2041-2070)	RCP 4.5 (2071-2100)	RCP 8.5 (2011-2040)	RCP 8.5 (2041-2070)	RCP 8.5 (2071-2100)
<1 (low)	64.8 ¦ 1500	64.3 ¦ 1490	64.1 ¦ 1484	64.6 ¦ 1496	64.0 ¦ 1482	63.6 ¦ 1473
1-4 (moderate)	8.2 ¦ 190	8.3 ¦ 192	8.4 ¦ 195	8.2 ¦ 191	8.4 ¦ 194	8.5 ¦ 197
4-10 (high)	5.1 ¦ 118	5.3 ¦ 122	5.3 ¦ 123	5.2 ¦ 120	5.3 ¦ 123	5.4 ¦ 125
>10 (severe)	21.9 ¦ 508	22.1 ¦ 512	22.2 ¦ 514	22.0 ¦ 509	22.2 ¦ 513	22.2 ¦ 515
Exceed *Tsl*	19.0 ¦ 440	19.1 ¦ 443	19.3 ¦ 448	19.1 ¦ 442	19.3 ¦ 446	19.4 ¦ 449

5.5   Reservoir sedimentation

The sediment yield amount under RCP 8.5 is noted greater than the sediment yield amount under RCP 4.5 (Table 20). Sediment yield amount under RCP 4.5 is 13.3 Mton yr^{-1} or 57.7 tons ha^{-1} yr^{-1}. This amount is slightly lower than the sediment yield resulted from the simulation under RCP 8.5 by 13.8 Mton yr^{-1} or 59.5 tons ha^{-1} yr^{-1}. These number indicates the increment of erosion over the watershed which triggered by the change in the climate element especially precipitation. The increment of erosion due to different RCP projection is in line with the result of the study conducted by Nilawar and Waikar (2019). They found that the sediment supply in the Purna river basin, India under RCP 8.5 is increased by about 5% compared to sediment supply under RCP 4.5.

Table 20. Sediment yield and the lifetime of the reservoir for different trajectories

.		RCP 4.5	RCP 8.5	Uncorrected RCP 4.5	Uncorrected RCP 8.5
Sediment yield	Mton yr^{-1}	13.3	13.8	1.4	1.5
	ton ha^{-1} yr^{-1}	57.7	59.5	6.03	6.46
Lifetime alteration caused by sedimentation in the reservoir					
Reservoir lifetime (yr)		153	148	long time	long time
Hydropower lifetime (yr)		9	8	101	107

A direct consequence of a greater quantity of sediment draining into the reservoir is the reduction of its lifetime. Based on the minimum operational volume of 50 Hm^3 as has been determined previously, the reservoir lifetime is noted 153 and 148 years under RCP 4.5 and RCP 8.5, respectively. Those are equal to the year 2165 and 2169, respectively (Figure 52). The reservoir lifetime of this scenario shows the impact of climate change on degrading the lifetime of the reservoir due to the increment of sediment amount into the reservoir.
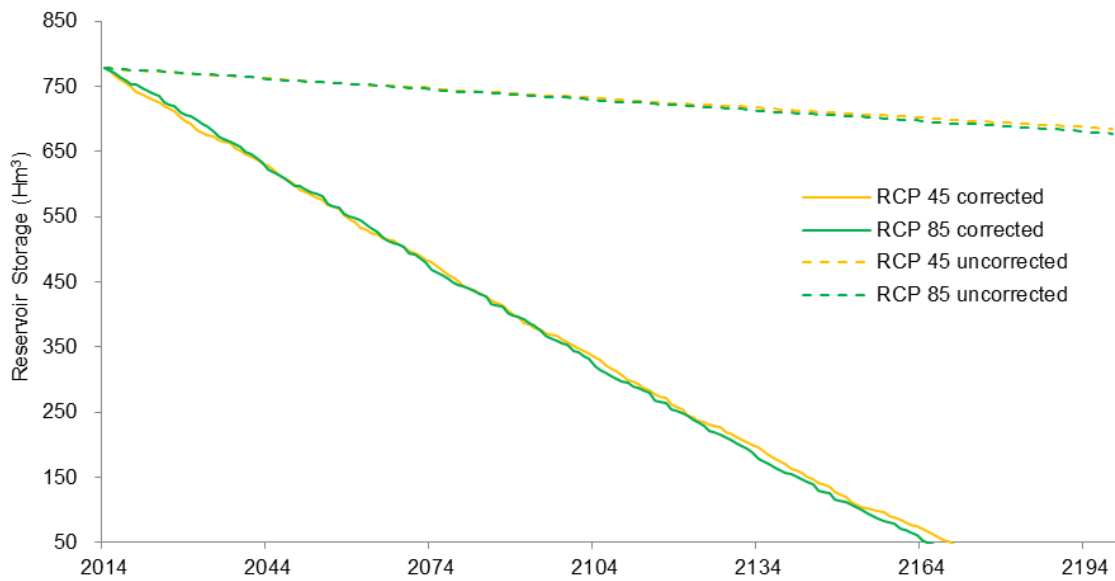
Figure 52. Comparison of reservoir storage evolution under RCP 4.5 and RCP 8.5 for corrected and uncorrected input data

The uncorrected trajectories result in very low sediment yield and longer reservoir and hydropower lifetime compared to corrected trajectories. The sediment yields under uncorrected RCP 4.5 and RCP 8.5 are noted 10 and 9 times lower than under corrected RCP 4.5 and RCP 8.5, respectively. Thus, this condition extends the reservoirs and hydropower lifetime of the uncorrected RCP 4.5 and RCP 8.5. The reservoir lifetime of corrected RCP 4.5 and 8.5 are noted 153 and 148 years, respectively. Meanwhile, a "long time" reservoir lifetime for both uncorrected RCP would occur. Moreover, an increment of hydropower lifetime from corrected RCP 4.5 to uncorrected RCP 4.5 is almost 11 times. Meanwhile, an increment of hydropower lifetime from corrected RCP 8.5 to uncorrected RCP 8.5 is almost 13 times.

124

These increments are caused by the changes in climate elements, especially the increasing precipitation amount as discussed in the previous chapter. The increment of precipitation due to bias correction was noted by 30%. Thus, it will certainly increase the amount of erosion. The description of erosion rates increment due to bias correction can be found clearly in Figure 52. The difference in erosion rates between uncorrected and corrected RCP is the reason for the different sediment amount that flows into the reservoir. Increment of erosion under the corrected RCP increases the amount of sediment in the reservoir. There will be serious hydropower problems if climate change scenarios occur in the future, as it only gives 8-9 years of hydropower lifetime from the recent time.

CHAPTER 6. COMPARISON AND COMBINATION OF CLIMATE CHANGE AND LULC CHANGE IMPACT ON THE CYCLE OF HYDROLOGY AND SEDIMENT

Chapter Overview

This chapter explains the comparison of TETIS simulation results under historical LULC (from 1994 to 2014) and climate change (in three different periods) and 2 trajectories (RCP 4.5 and 8.5)) using the most recent LULC (2014) as the baseline. Individually, the impact of LULC change is generally bigger than the impact of climate change. Meanwhile, the combination of LULC 2014 and climate change results in a bigger magnitude on water balance, flood regime, erosion, reservoir sedimentation, including the lifetime of the Saguling reservoir. In particular, the RCP 8.5 results in a bigger magnitude compared to the RCP 4.5.

6.1   Water balance

Alteration   of   historical   LULC   shifts   the magnitude of water balance elements   such   as the   increment   of infiltration,   evapotranspiration, overland flow, water yield, etc. Meanwhile, the decline of the water balance element was also detected such as interception flow. Beyond that, the alteration of water balance elements due to climate change also occurred. These changes can be identified in Figure 53. For example, infiltration, overland flow and water yield under RCP 4.5 (2011-2040) are expected to increase by 21 mm yr^{-1}, 61 mm yr^{-1} and 70 mm yr^{-1}, respectively. Meanwhile, under RCP 8.5 (2040-2100) are expected to increase by 31 mm yr^{-1}, 86 mm yr^{-1} and 120 mm yr^{-1}, respectively. When these numbers are compared with the magnitude of the same element of water balance resulted from LULC change, we can find that these numbers are lower than the water balance resulted from the impact of LULC change. Delta change of water balance under LULC 1994 to LULC 2014 increased by 34 mm yr^{-1}, 90 mm yr^{-1} and 123 mm yr^{-1}, for infiltration, overland flow and water yield, respectively. by comparing those number, it is clear that LULC change produces a greater impact than climate change

These differences of magnitude between the impact of LULC and climate change is in line with the study conducted by Ma *et al.*, (2009) and Ma, Xu, & van Noordwijk (2010) which stated that the magnitude of the change caused by LULC change will be greater than the impact of climate change. These percentage analyzes should take into account the different amounts of precipitation under historical LULC (1994-2014) and climate change (2011-2100). The average amount of precipitation is noted by 1741 mm yr^{-1} in the period 1994-2014. Meanwhile, it is expected to have 1829 and 1832 mm yr^{-1} under RCP 4.5 and RCP 8.5, respectively. Thus, the impact of LULC is considered bigger than the impact of climate change.

The combination of future LULC (LULC 2029) and climate change (RCP 4.5 and 8.5) give a significant effect on the flow of water (Figure 53). compared to the simulation under LULC 2014, the increment of infiltration, land flow, interflow,

base flow and water yield was noted. The increment of flow is caused by an increment in rainfall amount due to climate change in the future. In addition, future LULC changes followed by lower vegetation cover and higher urbanization escalate the overland flow and water yield. Meanwhile, the decline of flow magnitude was occurred in evapotranspiration due to a decline of vegetation cover that occurred under LULC 2029. Generally, the pattern of changes in water balance under RCP 4.5 also typically occurs under RCP 8.5.
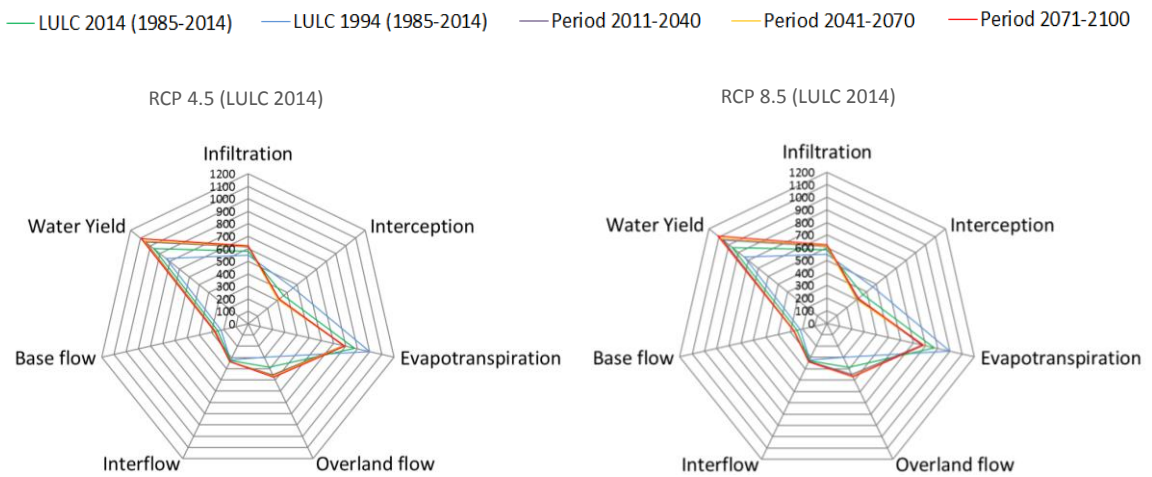
Figure 53. Water balance of different temporal simulation under RCP 4.5 and RCP 8.5 and LULC 2014 for periods 2011-2040, 2041-2070 and 2071-2100.

The comparison of the percentage between flows and precipitation due to the influence of LULC change and climate change (LULC 2014 as baseline) is presented in Table 21. LULC 1994 is the oldest historical LULC. Hence, it is chosen as a representative LULC for the comparison due to its larger LULC impact. Interception, evapotranspiration and water yield under LULC 1994 is greater compared to the other flows. The reason behind this fact is the bigger portion of vegetation cover of LULC 1994 compared to the LULC which is used for climate change implementation (LULC 2014).

129

Table 21. Delta change of flow percentage of historical LULC and two trajectories (using LULC 2014 with present climate as the baseline for % of change)

Flow	LULC 1994 (%)	LULC 2014 (%)	RCP 4.5 2011-2040 (%)	RCP 4.5 2041-2070 (%)	RCP 4.5 2071-2100 (%)	RCP 8.5 2011-2040 (%)	RCP 8.5 2041-2070 (%)	RCP 8.5 2071-2100 (%)
Infiltration	548¦33	582	603¦21	604¦23	611¦29	605¦24	607¦26	613¦31
Interception	462¦-98	364	307¦-57	304¦-60	318¦-46	310¦-53	309¦-55	319¦-45
Evapotranspiration	997¦-122	875	775¦-100	788¦-87	785¦-90	782¦-93	788¦-80	795¦-87
Overland flow	298¦90	388	449¦61	465¦77	470¦82	455¦67	467¦79	474¦86
Interflow	322¦6	328	333¦4	333¦5	333¦5	332¦4	333¦5	333¦5
Base flow	221¦27	248	269¦21	270¦22	272¦25	269¦21	272¦24	274¦26
Water Yield	841¦123	964	1041¦70	1064¦83	1084¦105	1033¦78	1047¦100	1069¦120

Meanwhile, a lower impact on interception, evapotranspiration and water yield is identified under climate change. The bigger effect of climate change compared to LULC change on flows of water balance can be identified from the higher value of infiltration, overland flow, interflow, base flow and water yield. The reason would be accounted for the increment of precipitation under RCP 4.5 and RCP 8.5. Abundant water on the soil surface due to higher precipitation amounts leads to a greater chance of water to be infiltrated. Furthermore, interflow and base flow will increase along with the increment of infiltration capacity. A large amount of surface flow would also increase overland flow. It occurs because water on the surface is not infiltrated completely.

Meanwhile, compared to historical LULC (2014), the shift of the flow occurs under the combined impact of LULC 2029 and climate change (RCP 4.5 & RCP 8.5). The trend of the impact is noted almost the same as the combined impact between LULC 2014 and climate change (RCP 4.5 dan RCP 8.5), but, with a bigger magnitude (Table 22 & Figure 54). The bigger impact can be identified from the higher value of infiltration, overland flow, interflow, base flow and water yield. Meanwhile, the lower impact can be identified from interception and evapotranspiration. For example, infiltration, overland flow and water yield under LULC 2029 and RCP 4.5 (2011-2040) are expected to increase by 55 mm yr^{-1}, 94 mm yr^{-1} and 157 mm yr^{-1}, respectively. Those values are bigger than values resulted under LULC 2014 and RCP 4.5 (2011-2040) with 21 mm yr^{-1}, 61 mm yr^{-1} and 70 mm yr^{-1}, respectively. another example, flows under LULC 2029 and RCP 8.5 (2071-2100) are expected to increase by 81 mm yr^{-1}, 131 mm yr^{-1} and 235 mm yr-

[1], respectively. These bigger magnitudes are caused by a massive loss of vegetation under LULC 2029. Those drastic increments in overland flow and water yield must be given a serious attention because it will produce a massive erosion and flood in the future.

Table 22. Delta change of flow percentage of historical LULC and two trajectories (using LULC 2029 with present climate as the baseline for % of change)

| Flow	LULC 1994 (%)	LULC 2014 (%)	RCP 4.5 2011-2040 (%)	RCP 4.5 2041-2070 (%)	RCP 4.5 2071-2100 (%)	RCP 8.5 2011-2040 (%)	RCP 8.5 2041-2070 (%)	RCP 8.5 2071-2100 (%)
Infiltration	548¦33	582	637¦55	649¦67	658¦77	641¦59	652¦70	663¦81
Interception	462¦-98	364	316¦-48	314¦-50	323¦-40	325¦-38	324¦-39	334¦-29
Evapotranspiration	997¦-122	875	804¦-71	815¦-60	808¦-67	822¦-53	829¦-46	822¦-52
Overland flow	298¦90	388	482¦94	494¦106	507¦119	486¦98	499¦111	519¦131
Interflow	322¦6	328	348¦20	342¦14	344¦16	342¦14	344¦16	346¦18
Base flow	221¦27	248	279¦30	281¦33	283¦36	279¦32	287¦39	289¦41
Water Yield	841¦123	964	1120¦157	1130¦167	1155¦192	1147¦183	1179¦216	1199¦235
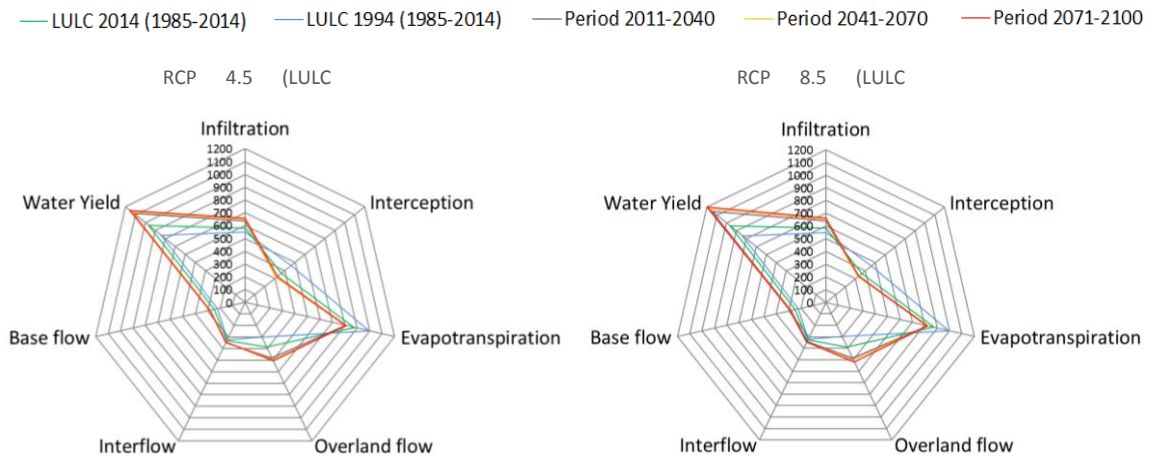
Figure 54. Water balance of different temporal simulation using RCP 4.5 and RCP 8.5 and LULC 2029 for periods 2011-2040, 2041-2070 and 2071-2100.

6.2 Flood regime

The comparison between the impact of LULC and climate changes on mean watershed discharge is presented in Table 23. The increment of maximum discharge from LULC 1994 to 2014 was recorded in the range of 5.65 to 7.90 m^3s^{-1}. Meanwhile, climate change increases the maximum discharge in the

range 0.1-7.7 m³s⁻¹ for the whole period and return period. Thus, the impact of LULC change on the mean discharge is noticed bigger than the impact of climate change. This fact is in line with a previous analysis of water balance which explains a higher impact of LULC on water balance element (overland flow and water yield). LULC is expected to increase overland flow and water yield for 16% and 9.5% higher than the increment caused by climate change. These facts lead to the conclusion that LULC has a bigger effect on the return period compared with the effect of climate change.

Table 23. Flood quantiles of Gumbel and percentages under historical LULC 2014 and future climate change trajectories.

Return period (yr)	Max discharge (m³s⁻¹) ¦ Percentage (%) compared with LULC 2014							
	LULC 1994	Baseline (2014)	RCP 4.5 (2011-2040)	RCP 4.5 (2041-2070)	RCP 4.5 (2071-2100)	RCP 8.5 (2011-2040)	RCP 8.5 (2041-2070)	RCP 8.5 (2071-2100)
5	346 ¦ -7.90	374	399 ¦ 6.8	400 ¦ 7.1	402 ¦ 7.5	400 ¦ 7.0	401 ¦ 7.3	402 ¦ 7.7
10	411 ¦ -7.09	440	456 ¦ 3.6	469 ¦ 6.5	482 ¦ 9.5	451 ¦ 2.5	457 ¦ 3.8	458 ¦ 3.4
25	493 ¦ -6.37	524	553 ¦ 5.5	558 ¦ 6.3	561 ¦ 7.0	555 ¦ 5.8	558 ¦ 6.3	559 ¦ 6.5
50	554 ¦ -5.97	587	618 ¦ 5.3	623 ¦ 6.1	627 ¦ 6.8	616 ¦ 4.9	622 ¦ 5.9	624 ¦ 6.3
100	614 ¦ -5.65	649	638 ¦ 0.1	662 ¦ 2.0	689 ¦ 6.2	678 ¦ 4.5	695 ¦ 7.1	697 ¦ 7.4

The combined impact of LULC 2029 and future climate change on the return period can be identified in Table 24 and Figure 55. A combination of LULC 2029 and future climate change results in a bigger impact on the maximum discharge of return periods compared with a historical LULC 2014 only, or even with a combination of future climate change. For example, combined LULC 2029 and future climate change under RCP 4.5 (2011-2040) for 5 years return period is expected to have maximum discharge by 456 m³s⁻¹. Meanwhile, the LULC 2014 has only 346 m³s⁻¹ for the same return period. The maximum discharge resulted from combined LULC 2014 and future climate change under RCP 4.5 (2011-2040) is expected to have 399 m³s⁻¹. Hence, the delta changes of maximum discharge between combined LULC 2029-future climate change and combined LULC 2014-future climate change under RCP 4.5 (2011-2040) is noted 57 m³s⁻¹. This magnitude shows the impact of the reduction of vegetation cover and additional settlement area under LULC 2029 on flood quantile. As explained in the previous chapter, vegetation loss under LULC 2029 for about 1.2% and

settlement area by 5.55%. Both vegetation loss and additional settlement area result in a bigger amount of water on the surface due to uninfiltrated water. Meanwhile, the delta changes of maximum discharge between combined LULC 2029-future climate change under RCP 4.5 (2011-2040) and LULC 2014 for 5 year return period are noted 82 m^3s^{-1}. In this case, the bigger delta change is caused also by the effect of climate change. As previously discussed, climate change shifts the rainfall amount and temperature. Thus, it increases the amount of maximum discharge.

Table 24. Flood quantiles of Gumbel and percentages under LULC 2029 and future climate change trajectories.

Quantile estimator	Return period (yr)	Max discharge (m^3s^{-1}) ¦ Percentage (%) compared with LULC 2014						
		LULC 1994	Baseline (2014)	RCP 4.5 (2011-2040)	RCP 4.5 (2041-2070)	RCP 4.5 (2071-2100)	RCP 8.5 (2011-2040)	RCP 8.5 (2041-2070)	RCP 8.5 (2071-2100)
	5	346¦-7.90	374	456¦22.1	462¦23.7	479¦28.2	498¦33.3	507¦35.7	513¦37.3
	10	411¦-7.09	440	517¦17.4	527¦19.7	542¦23.1	552¦25.4	563¦27.9	576¦30.8
GUMBEL	25	493¦-6.37	524	592¦12.9	608¦15.9	622¦18.6	620¦18.2	632¦20.5	647¦23.4
	50	554¦-5.97	587	655¦11.6	663¦12.9	674¦14.8	693¦18.1	672¦14.4	708¦20.6
	100	614¦-5.65	649	715¦10.2	731¦12.6	752¦15.9	728¦12.2	745¦14.8	767¦18.2
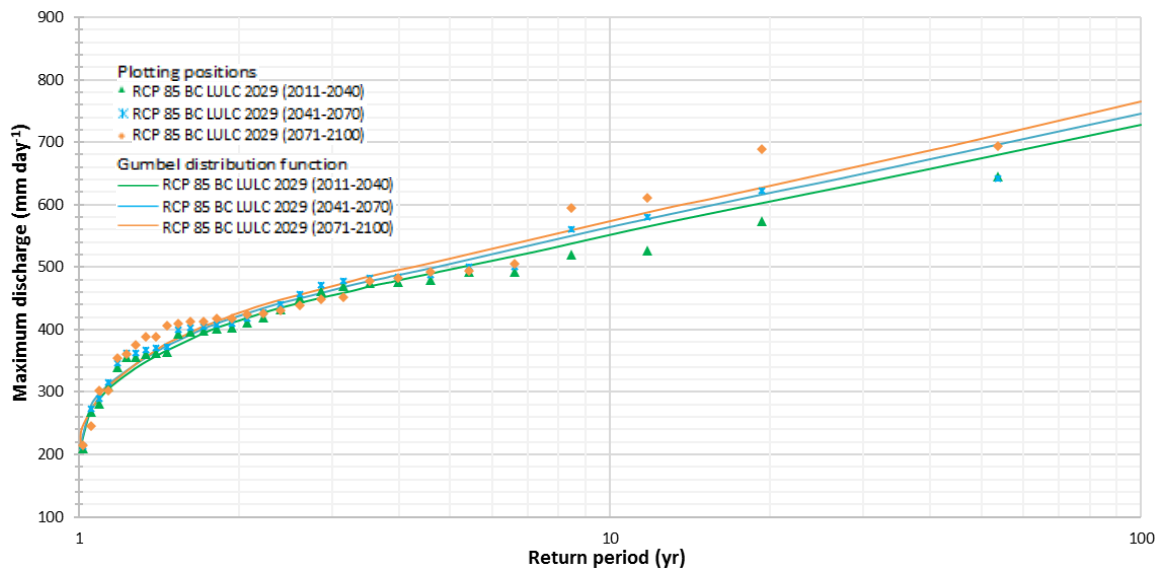
Figure 55. Comparison of flood regimes using LULC 2029 under different trajectories in the period 2011-2040, 2041-2070 and 2071-2100, representing the corresponding plotting positions (dots) and the fitted (lines) Gumbel distribution function. Upper: simulated using trajectory RCP 4.5. Lower: simulated using trajectory RCP 8.5

6.3   Soil erosion at catchment scale

The distribution of erosion under climate change is detected almost the same as the distribution under LULC change. The low erosion class (< 1ton ha^{-1} yr^{-1}) as usually affected the flat areas, whereas the hilly areas possessed higher erosion rates due to geophysical characteristics. The lower rate of erosion in the flat areas is caused by low overland flow velocities (lower slope steepness) and the occupation of those areas by urban zones, industrial zones or rice fields which has low erosivity. Meanwhile, higher erosion rates in the hilly areas are caused by higher overland flow velocity due to high slope steepness.

The change of erosion rate distribution caused by LULC changes from 1994 to 2014 can be identified in the southern part of the study area. Meanwhile, the increment of erosion due to climate change cannot be identified clearly in Figure 56. As mentioned in the previous chapter, the increment of erosion due to LULC change can only be identified in some small spots, especially in the southern part of the study area occupied by a mountainous area.

Based on the observation of erosion map dynamics, it can be concluded that the impact of LULC change on erosion is greater than the impact of climate change. This indicates that LULC change has a significant impact on erosion in the study area. The reason for this increment is associated with the increment of the overland flow rate under the LULC change. A massive alteration of LULC especially the decline of vegetation cover of the study area is clearly identified. Thus, it increases the overland flow velocity and finally increases the erosivity as the initial step of erosion (Favis-Mortlock and Guerra, 1999; Nearing, 2001).

The combined impact of future LULC (LULC 2029) and climate change (RCP 4.5 and 8.5) has a significant effect on the erosion rate (Figure 56). The area that Exceeds *Tsl* of Erosion is clearly identified in some spots in the steeper areas. The areas which previously did not contain area exceeds *Tsl* class, now it shifts into the area containing that class. This happens due to an increment of overland flow caused by the increment of urban areas and the decline of vegetation

cover. Moreover, higher rainfall under trajectories produces a higher erosivity impact and run-off.

PRESENT CLIMATE UNDER LULC 1994

PRESENT CLIMATE UNDER LULC 2014

PRESENT CLIMATE UNDER LULC 2029

Erosion (ton/ha/yr)
0 - 1
1 - 4
4 - 10
10 - 13.5
> 13.5

RCP 4.5 (2011-2040) UNDER LULC 2014

RCP 4.5 (2041-2070) UNDER LULC

RCP 4.5 (2070-2100) UNDER LULC

RCP 8.5 (2011-2040) UNDER LULC 2014

RCP 8.5 (2041-2070) UNDER LULC 2014

RCP 8.5 (2071-2100) UNDER LULC 2014

RCP 4.5 (2011-2040) UNDER LULC 2029

RCP 4.5 (2041-2070) UNDER LULC 2029

RCP 4.5 (2071-2100) UNDER LULC 2029

RCP 8.5 (2011-2040)   RCP 8.5 (2041-2070)   RCP 8.5 (2071-2100)
UNDER LULC 2029   UNDER LULC 2029   UNDER LULC 2029

Figure 56. Spatial distribution of erosion rates simulated by TETIS under different trajectories for a different period.

The impact of LULC change is greater than the impact of climate change as indicated in Table 25. This conclusion is based on the comparison of the delta change between historical LULC and the period of climate change. The main concern of this analysis is the erosion class of severe and erosion class exceeds *Tsl*. Those classes are very important because it contains a threshold of permitted erosion. From both classes, the erosion exceeds *Tsl* class should be given more attention because it has a high erosion rate. The delta changes under the historical LULC are noted at 5.9% and 4.4% for severe and erosion exceeds *Tsl* class. Meanwhile, absolut delta change under RCP 4.5 in the period (2011-2040), (2041-2070) and (2071-2100) is noted 3.9%, 4.7% and 5.1% for severe class, respectively. Meanwhile, absolut delta change under RCP 8.5 in the period (2011-2040), (2041-2070) and (2071-2100) is noted 4.1%, 4.9% and 5.3% for erosion class exceeds *Tsl*, respectively.

Table 25. Delta change of historical LULC 2014 and the period of climate change

Erosion class (ton ha^{-1} yr^{-1})	Area (percentage of change compared to 2014 | km^2)						
	LULC 1994	LULC 2014	RCP 4.5 (2011-2040)	RCP 4.5 (2041-2070)	RCP 4.5 (2071-2100)	RCP 8.5 (2011-2040)	RCP 8.5 (2041-2070)	RCP 8.5 2071-2100)
<1 (low)	1.8| 1552	1524	-1.6|1500	-2.2|1490	-2.6|1484	-1.8|1496	-2.8| 1482	-3.3|1473
1-4 (moderate)	0.5| 189	188	1.1|190	2.1| 192	3.7| 195	1.6| 191	3.2| 194	4.8|197
4-10 (high)	0.0| 115	115	2.6| 118	6.1| 122	7.0| 123	4.3| 120	7.0| 123	8.7|125
>10 (severe)	-5.9| 460	489	3.9|508	4.7| 512	5.1| 514	4.1|509	4.9| 513	5.3|515
Exceed *Tsl*	-4.4| 412	431	2.1|440	2.8| 443	3.9|448	2.6| 442	3.5| 446	4.2| 449

Delta change under historical LULC is noted higher than the delta changes under climate change. The delta change of severe class under

136

historical LULC is noted at 5.9%. Meanwhile, under climate change is noted in the range 3.9%-5.3%. Moreover, the delta changes of erosion class exceed *Tsl* under historical LULC is noted at 4.4% and under climate change is noted in the range 3.9%-4.2%. These facts lead to the conclusion that historical LULC change produces a greater impact than climate change.

The combined impact of LULC 2029 and future climate change can be identified in Table 26. A combination of LULC 2029 and future climate change results in a bigger impact on erosion rate compared with a historical LULC 2014. For example, combined LULC 2029 and future climate change under RCP 4.5 (2011-2040) for severe erosion class is recorded in the range 11.8%-17.0%. Meanwhile, the absolute delta change of severe erosion under LULC 1994 is noted only 5.9%. this comparison trend has also occurred for the erosion class exceeds *Tsl*. combined LULC 2029 and future climate change under RCP 4.5 (2011-2040) for erosion class exceeds *Tsl* is recorded in the range 7.9%-14.2%. Meanwhile, the absolute delta change of severe erosion under LULC 1994 is noted only 4.4%. A combination of LULC 2029 and future climate change results in a bigger impact on erosion rate compared with the combination of future climate change and LULC 2014. For example, the severe erosion class resulted from combined LULC 2029 and future climate change under RCP 4.5 (2071-2100) is expected to have 564 km^2. Meanwhile, the delta changes of severe erosion class with the same RCP and period under combined LULC 2014 is expected to have only 514 km^2. These magnitudes show the impact of the increment of overland flow on erosion rate. As previously discussed, the increment of overland flow is noted 33 mm yr^{-1} due to different LULC (LULC 2014 vs LULC 2029) with the same climate change projection. This increment increases the erosion rate since overland flow is a key factor for erosion.

Table 26. Delta change of historical LULC 2029 and the period of climate change

Erosion class (ton ha^{-1} yr^{-1})	Area (percentage of change compared to 2014 | km^2)						
	LULC 1994	LULC 2014	RCP 4.5 (2011-2040)	RCP 4.5 (2041-2070)	RCP 4.5 (2071-2100)	RCP 8.5 (2011-2040)	RCP 8.5 (2041-2070)	RCP 8.5 (2071-2100)
<1 (low)	1.8| 1552	1524	-4.1| 1461	-5.6|1438	-6.6 |1423	-5.0|1449	-7.1|1416	-8.5|1394
1-4 (moderate)	0.5| 189	188	2.6| 193	5.0| 197	8.3|204	4.1| 196	7.4|202	10.7|208
4-10 (high)	0.0| 115	115	0.4| 116	7.3| 123	9.0| 125	3.8| 119	9.0| 125	12.5|129
>10 (severe)	-5.9| 460	489	11.8| 547	13.9| 557	15.3|564	12.9|552	15.5| 565	17.0|572
Exceed *Tsl*	-4.4| 412	431	7.9| 465	10.2| 475	13.0|487	8.8| 469	11.6| 481	14.2|4922

6.4 Reservoir sedimentation

The rate of sediment yield and its percentage under LULC and climate change compared to the 2014 scenario are presented in Table 27. The low erosion rate under LULC 1994 compared to erosion under other scenarios shows the effectiveness of land cover on reducing erosion. Rainfall increments under RCP 4.5 and 8.5, obviously do not surpass the impact of LULC on erosion. Optimum land use with a better vegetation cover under LULC 1994 protects the soil from rainfall erosivity, overland flow impact and increases the infiltration capacity. Hence, the sedimentation as the final step of the erosion process under LULC 1994 exists in the lowest rate. Due to the importance of vegetation cover, the loss of vegetation cover in 2014 leads to the increment of sedimentation (24%), and it is recorded higher than the increment of sediment due to climate change (10% and 12%). Moreover, the combined impact of future LULC (LULC 2029) and climate change (RCP 4.5 and 8.5) produce a significant effect on the sedimentation rate. The increment of sediment is noted 24% and 32% for RCP 4.5 and RCP 8.5 under LULC 2029. Hence, it surpasses the impact of LULC on sedimentation which has only 24% (particularly compared to RCP 8.5).

Table 27. Sediment yield and lifetime of the reservoir for historical LULC and two trajectories.

| | | Rate ¦ Percentage (%) compared with baseline (LULC 2014) | | | | | |
		1994	2014 (baseline)	RCP 4.5 LULC 2014	RCP 8.5 LULC 2014	RCP 4.5 LULC 2029	RCP 8.5 LULC 2029
Sediment yield	Mton yr^{-1}	3.1 ¦ -24	4.1	4.5 ¦ 10	4.6 ¦ 12	5.1 ¦ 24	5.4 ¦ 32
	ton ha^{-1} yr^{-1}	13.6 ¦ -23	17.7	19 ¦ 9	20 ¦ 13	24 ¦ 36	26 ¦ 47
		Lifetime alteration due to sedimentation in the reservoir					
Reservoir		239 yr	182 yr	153 yr	148 yr	136 yr	131 yr
Hydropower		21 yr	15 yr	9 yr	8 yr	7 yr	6 yr

The decline of reservoir lifetime from 1994 to 2014 can be observed in Figure 57. c. As a consequence of greater sedimentation due to LULC change, the reservoir lifetime has decreased dramatically from 239 years under LULC 1994 to 182 years under LULC 2014. It is much greater than the reduction of reservoir lifetime caused by climate change which is noted only 153 and 148 years under RCP 4.5 and RCP 8.5, respectively (with baseline 2014). The combined impact of future LULC (LULC 2029) and climate change (RCP 4.5 and 8.5) produce a higher

impact on the sedimentation rate. The reservoir lifetime for RCP 4.5 and 8.5 under LULC 2029 are noted 136 and 131 years.
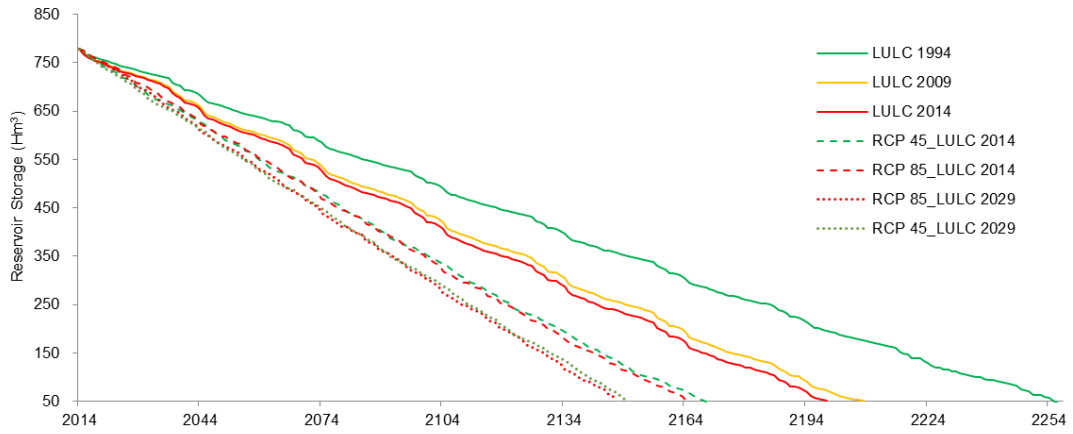
Figure 57. Comparison of reservoir storage evolution under LULC and climate change

CHAPTER 7. CONCLUSIONS

Since Indonesia became independent seventy five years ago, human activity has produced severe LULC changes within the Upper Citarum Catchment. The reproduction of historical changes of the last thirty years has required the reconstruction of the LULC maps for years 1994, 2009 and 2014. During this period, significant LULC changes have occurred, primarily due to the demands of the ever-increasing population growth in the region. There has also been significant and continuous development of urban areas and rice fields. This rise in population equates to a 141% increase in urban areas. With the expansion of these urban areas, there is a significant reduction in the quantity of land utilized by rice fields in the central part of the catchment. Also, the fact that forested areas have been sacrificed to use the land for cultivation purposes (plantations, dry cultivations and rice fields) to meet the increased demands for food that has arisen from the nation´s population growth. In addition, the conversion of forests into bush contributed to a total of 51.5% historical forest areal reduction. The net balance in 2014 for rice fields was a reduction of 16.5% from its original area in 1994.

The LCM model was utilized to forecast future LULCs, in particular in 2029. The training and validation of this model using the three historical maps were satisfactory. The transitional potential of historical LULC changes was used to forecast the future LULC map. The forecasted results show, on one hand, a continuation in the expansion of urban areas at the expense of the contiguous rice fields, but, on the other hand, a significant decrease in the future deforestation rate. This positive consequence is mainly because most of the remaining forests do not currently have the appropriate conditions for anthropogenic LULC types.

A distributed hydrological model, called TETIS, was implemented in the Upper Citarum Catchment to assess the impact of the different historical (1994, 2009 and 2014) and LULC scenarios (LULC 2029, conservation, government plan and natural vegetation) on its water and sediment cycles. The water component of the model was calibrated using the LULC 2009 and validated satisfactorily within the periods corresponding to the 1994 and 2014 LULC maps. I.e., it was a

Differential Split-Sample validation (Klemes, 1986). Regarding the sediment component, it was highly valuable to assess the bathymetric information in the Saguling reservoir for its calibration and validation, despite the understanding that there are uncertainties in the reconstruction of the observed annual sediment yields.

The results determined that deforestation and urbanization were the most influential factors for the alteration of the hydrological and sedimentological processes in the Upper Citarum Catchment. In the period 1994 to 2014, the change of LULC decreased evapotranspiration by 12% and, as a direct and expected consequence, water yield increased by 15%. Meanwhile, for the period from 2014 to 2029, evapotranspiration is expected to decrease by an additional 44%, which will increase water yield by 40%. At the catchment scale, the combined effects of deforestation and urbanization in this case study increase water yield by increasing all its components; overland flow, interflow and baseflow. In particular, the increase in overland flow results in more frequent flooding. With regards to erosion, the changes in LULC are currently producing and will produce in the future, a relatively small increment of erosion rates, increasing the area exceeds Tsl erosion from 412 km^2 in 1994 to 499 km^2 in 2029. However, in terms of sediment yield the situation is worse, because from the 3.1 Mton yr^{-1} for the LULC 1994 scenario, the Upper Citarum Catchment will have a mean sediment yield of 6.7 Mton yr^{-1} in the LULC 2029 scenario. This will be catastrophic for the hydropower operation of the Saguling Dam. Compared with LULC 2014, other scenarios such as conservation, government plan and natural vegetation scenarios are expected to have an increment in total evapotranspiration for about 8.35%, 14.05% and 65.07%, respectively. These increments are associated with the increment of forest area, which significantly increases the transpiration and the evaporation from interception. As the final result, the water yield is expected to decrease by 9.01, 17.52 and 207.97%, respectively. These alterations lead to a substantial reduction in flood regime, erosion and sedimentation in these alternative scenarios. The reduction of sedimentation leads to a massive increment of reservoir and hydropower lifetime signed by a very long period of lifetime.

142

The climate change scenario has been analyzed in this study and implemented in the TETIS model to identify the alteration of hydrology due to climate change. The expected climate change will increase the precipitation and temperature, and its impact on the water balance can be identified from the increment of flows of water balance. Those increments will finally increase flood regime and catchment erosion. Beyond that, LULC change results in a bigger impact on the water balance compared to the impact of climate change. This is indicated by the greater percentage of the change of water balance impacted by LULC than by climate change. It means the rainfall increments under RCP 4.5 and 8.5, generally do not surpass the impact of LULC on water balance. Historical LULC results higher magnitude of infiltration, overland flow and water yield increment than climate change from trajectories (all period) with a difference of at least 2%, 4% and 3%, respectively (precipitation based). Meanwhile, the combination of future LULC and future climate change results a bigger impact. It enhances the infiltration, overland flow and water yield at least 22%, 4% and 34%, respectively (precipitation based). Generally, the delta change of maximum discharge under LULC change is higher than under climate change for the whole period and year of the return period. Meanwhile, the maximum discharge resulted from combined future LULC and future climate change offset the maximum discharge from either single impact of LULC or climate change. In terms of erosion, the impact of LULC change once again offset the impact of climate change. The delta changes of severe erosion class under historical LULC and climate change are noted 5.9% and less than 5.3%, respectively. Meanwhile, the delta changes of erosion class exceed *Tsl* under historical LULC and climate change is noted 4.4% and less than 4.2%, respectively. Meanwhile, all erosion class resulted by the combination of future LULC and future climate change is expected to increase significantly. The increment in much bigger than the individual impact of either LULC or climate change. The delta change of sediment yield under historical LULC changes is noted 1 Mton yr^{-1}, meanwhile, the delta changes of sediment yield under climate change are noted 0.4 Mton yr^{-1} and 0.5 Mton yr^{-1} under RCP 4.5 and RCP 8.5, respectively. Meanwhile, the combined future LULC 2029 and future climate

change results delta changes by 2.0 Mton yr^{-1} and 2.3 Mton yr^{-1} under RCP 4.5 and RCP 8.5, respectively. Those differences lead to a different lifetime of reservoir and hydropower.

One of the biggest challenges in mathematical modeling is the model implementation with changing conditions. It is our opinion that the implementation of distributed hydrological models is essential to seamlessly alter the parameters that are represented on the LULC at pixel scale and to extrapolate the model calibration to different LULC scenarios. Also, the hydrological model should be able to consider all the potential interactions within and between the water and sediment cycles. From all these parameters, TETIS hydrological distributed model was a robust tool to estimate the effect of LULC changes on water resources, flood regime, erosion rates and sediment yield in the Upper Citarum Catchment.

Those outcomes leave many open lines of research and future developments. The most important future research lines and/or tasks that should be done in the Upper Citarum Catchment is the use of more complete detail input data for the model will produce a more robust model output. A model will analyze and illustrate the mechanism of the object with higher accuracy when supported by adequate input data. An increase of hydrometeorology, spatial and sediment data quantitatively and spatially will increase the output of the model. For example, the implementation of more years of data discharges for the water calibration sub-models process. The use of a higher spatial resolution (30 m) to get a better spatial variability of the study area. This improvement can also be applied in the climate change model. Recently, there is a new update of climate change data with higher resolutions. It will be very helpful to increase spatial climate variability.

Another future lines of research could attempt to:
1. Various sources of uncertainty normally occur in hydrological modeling, including in the output of TETIS model. The errors could be addressed to the simplification of the model, input data, structure of the model, or even the

non-related aspect of the model. Those could raise significant uncertainty which leads to weak model output. Investigating this aspect could be interesting and beneficial to improve the quality of this study.

2. The use of more complete detail input data for the model will produce a more robust model output. A model will analyze and illustrate the mechanism of the object with higher accuracy when supported by adequate input data. An increase of hydrometeorology, spatial and sediment data quantitatively and spatially will increase the output of the model. For example, the implementation of more years of data discharges for the water calibration sub-models process. The use of a higher spatial resolution (30 m) to get a better spatial variability of the study area. This improvement can also be applied in the climate change model. Recently, there is a new update of climate change data with higher resolutions. It will be very helpful to increase spatial climate variability.

3. For spatial models (LCM), the use of LULC with a longer period will increase the robustness of the model. Due to data limitations, the 15 year time period was used in the calibration process, meanwhile, for validation was only 5 years. The addition of the period (year) for the calibration and validation will be a benefit to produce a better model.

4. The implemented validation method of the TETIS water sub-model was only temporal validation. Another method called spatial validation could not be implemented due to data limitation. For further research development, spatial validation could be implemented to improve the quality of the model.

5. The use of more detailed LULC classification. For example, the use of the various classification of plantations such as tea, coffee, etc, instead of using only one classification, such as plantations classification. The use of a more detailed LULC will produce a more detail result.

6. This study uses a value one (1) for the management practice index (P) in the erosion calculation (sediment sub-model of TETIS). The use of value one (1) for the P index results in an inaccurate erosion rate. P-value will give a

significant effect on the surface runoff amount and rate. Therefore, for further research, a more complete P indices distribution needs to be established.

References

Abernethy, C. (1990). The use of river and reservoir sediment data for the study of regional soil erosion rates and trends. Paper presented at the International Symposium on Water Erosion, Sedimentation and Resource Conservation. Dehradun, India.

Agatona, M., Setiawan, Y., & Effendi, H. (2016). Land use/land cover change detection in an urban watershed: a case study of upper Citarum Watershed, West Java Province, Indonesia. The 2nd International Symposium on LAPAN-IPB Satellite for Food Security and Environmental Monitoring, 33, 654 – 660.

Agus, F., Wahyunto, Watung, R. L., Tala'ohu, S. H., & Sutono. (2004). Land use changes and their effects on environmental functions of agriculture. Proceedings of the Multifunctionality of Agriculture and Land Conservation Conference.

Alatorre, L. C., Beguería, S., & García-Ruiz, J. M. (2010). Regional scale modeling of hillslope sediment delivery: A case study in the Barasona Reservoir watershed (Spain) using WATEM/SEDEM. Journal of Hydrology, 391(1–2), 109–123.

Alpert, P., Ben-gai, T., Baharad, A., Benjamini, Y., Yekutieli, D., Colacino, M., … Manes, A. (2002). The paradoxical increase of Mediterranean extreme daily rainfall in spite of decrease in total values.

Apip, Takara, K., Yamashiki, Y., & Ibrahim, A. B. (2010). Distributed sediment budget and potential shallow landslide area for investment prioritization in sediment control of ungauged catchment: a case study on the Upper Citarum river, Indonesia. Annual of Disaster. Prev. Rest., 53, 45–59.

Arsyad, S. (2000). Konservasi tanah dan air. Bogor: IPB pers.

Asokan, S. M., & Dutta, D. (2008). Analysis of water resources in the Mahanadi River Basin, India under projected climate conditions. Hydrological Processes, 22(18), 3589–3603.

Asselman, N. E. M., Middelkoop, H., & van Dijk, P. M. (2003). The impact of changes in climate and land use on soil erosion, transport and deposition of suspended sediment in the River Rhine. Hydrological Processes, 17(16), 3225–3244.

Baker, T. J., & Miller, S. N. (2013). Using the Soil and Water Assessment Tool (SWAT) to assess land use impact on water resources in an East African watershed. Journal of Hydrology, 486, 100–111.

Bergström, S., Carlsson, B., Gardelin, M., Lindstrom, G., Petterson, A., & Rummukainen, M. (2001). Climate change impacts on runoff in Sweden - Assessments by global climate models, dynamical downscalling and hydrological modeling. Climate Research, 16(2), 101–112.

Berliana, S., Febrianti, N., Cholianawat, N., & Susanti, I. (2010). Dampak perubahan iklim terhadap daerah aliran sungai citarum berbasis satelit climate change impact on citarum river basin based on satellite data analysis.

Berti, A., Tardivo, G., Chiaudani, A., Rech, F., & Borin, M. (2013). Assessing reference evapotranspiration by the Hargreaves method in north-eastern Italy. Agric Water Manag, 140, 20–25.

Boer, R., Dasanto, B. D., Perdinan, & Marthinus, D. (2012). Hydrologic balance of Citarum Watershed under current and future climate (pp. 43–59).

Boongaling, C. G. K., Faustino-Eslava, D. V., & Lansigan, F. P. (2018). Modeling land use change impacts on hydrology and the use of landscape metrics as tools for watershed management: The case of an ungauged catchment in the Philippines. Land Use Policy, 72, 116–128.

Bosmans, J. H. C., Van Beek, L. P. H., Sutanudjaja, E. H., & Bierkens, M. F. P. (2017). Hydrological impacts of global land cover change and human water use. Earth Syst. Sci, 21, 5603–5626.

BPS. (2017). Badan Pusat Statistik.

Bruijnzeel, L. A. (2004). Hydrological functions of tropical forests: not seeing the soil for the trees? Agriculture, Ecosystems & Environment, 104(1), 185–228.

Budiyono, Y., Aerts, J. C. J. H., Tollenaar, D., & Ward, P. J. (2016). River flood risk in Jakarta under scenarios of future change. Hazards Earth Syst. Sci, 16, 757–774.

Bussi, G., Rodríguez-Lloveras, X., Francés, F., Benito, G., Sánchez-Moya, Y., & Sopeña, A. (2013). Sediment yield model implementation based on check dam infill stratigraphy in a semiarid Mediterranean catchment. Hydrology and Earth System Sciences, 17(8), 3339–3354.

Calijuri, M. L., Castro, J. de S., Costa, L. S., Assemany, P. P., & Alves, J. E. M. (2015). Impact of land use/land cover changes on water quality and hydrological behavior of an agricultural subwatershed. Environmental Earth Sciences, 74(6), 5373–5382.

Carpenter, T. M., & Gergakakos, K. P. (2006). Intercomparison of lumped versus distributed hydrologic model ensemble simulations on operational forecast scales. Journal of Hydrology, 329(1–2), 174–185.

Chaidar, A. N., Soekarno, I., Wiyono, A., & Nugroho, J. (2017). Spatial analysis of erosion and land criticality of the upstream citarum watershed. International Journal of GEOMATE, 13(37), 133–140.

Chiew, F. H. S., Whetton, P. H., McMahon, T. A., & Pittock, A. B. (1995). Simulation of the impacts of climate change on runoff and soil moisture in Australian catchments. Journal of Hydrology, 167(1–4), 121–147.

Christensen, J. H., Boberg, F., Christensen, O. B., & Lucas-Picher, P. (2008). On the need for bias correction of regional climate change projections of temperature and precipitation. Geophysical Research Letters, 35(20).

Clarke, R. T. (2002). Estimating time trends in Gumbel-distributed data by means of generalized linear models. Water Resources Research, 38(7), 16-1-16–11.

Cochran, J. K., Bokuniewicz, J. H., & Yager, L. P. (2019). Encyclopedia of Ocean Sciences (Third). Elsevier.

Costa, M. H. (2005). Forests, water and people in the humid tropics: past, present and future. In M. Bonell & L. A. Bruijnzeel (Eds.) (pp. 590–597). Cambridge: Cambridge University Press.

Cousino, L. K., Becker, R. H., & Zmijewski, K. A. (2015). Modeling the effects of climate change on water, sediment, and nutrient yields from the Maumee River watershed. Journal of Hydrology: Regional Studies, 4, 762–775.

Cunnane, C. (1987). Review of Statistical Models for Flood Frequency Estimation. In Hydrologic Frequency Modeling (pp. 49–95). Dordrecht: Springer Netherlands.

Dasanto, D. B., Boer, R., Pramudya, B., & Suharnoto, Y. (2014). Simple method for assessing spread of flood prone areas under historical and future rainfall in the Upper Citarum watershed. EnvironmentAsia, 7(1), 104–111.

De Graff, J. V. *et al.* (2012). Recognizing the importance of tropical forests in limiting rainfall-induced debris flows. Environmental Earth Sciences. Springer-Verlag, 67(4), pp. 1225–1235.

De Graff, J. V., Sidle, R. C., Ahmad, R., & Scatena, F. N. (2012). Recognizing the importance of tropical forests in limiting rainfall-induced debris flows. Environmental Earth Sciences, 67(4), 1225–1235.

Defra. (2004). Making space for water developing a new government strategy for flood and coastal erosion risk management in England. London: Department for Environment, Food and Rural Affairs.

Delang, C. O. (2002). Deforestation in northern Thailand: The result of Hmong farming practices or Thai development strategies? Society and Natural Resources, 15(6), 483–501.

Dendy, F. E. (1974). Sediment trap efficiency of small reservoirs. Journal of Soil and Water Conservation, 39(4), 278–280.

Déqué, M. (2007). Frequency of precipitation and temperature extremes over France in an anthropogenic scenario: Model results and statistical correction according to observed values. Global and Planetary Change, 57(1–2), 16–26.

Duan, Q., Sorooshian, S., & Gupta, V. K. (1994). Optimal use of the SCE-UA global optimization method for calibrating watershed models. Journal of Hydrology, 158(3–4), 265–284.

Eastman, J. R. (2016). TerrSet Tutorial. Worchester: Clark University.

Emerson, W. (1991). Structural decline of soils, assessment and prevention. Australian Journal of Soil Research, 29(6), 905–921.

Engelund, F., & Hansen, E. (1967). A monograph on sediment transport in alluvial streams. Copenhagen: Denmark Tech Univ, Hydraul Lab.

Fan, M., & Shibata, H. (2015). Simulation of watershed hydrology and stream water quality under land use and climate change scenarios in Teshio river watershed, Northern Japan. Ecological Indicators, 50, 79–89.

Favis-Mortlock, D. T., & Guerra, A. J. T. (1999). The implications of general circulation model estimates of rainfall for future erosion: A case study from Brazil. Catena, 37(3–4), 329–354.

Fenli, Z., Keli, T., Cheng-e, Z., & Xiubin, H. (2002). Vegetation destruction and restoration effects on soil erosion process on the loess plateau. In ISCO conference (pp. 208–213).

Field, C. B., Barros, V. R., Dokken, D. J., Mach, K. J., Mastrandrea, M. D., Bilir, T. E., White, L. L. (2014). Climate Change 2014 Impacts, Adaptation, and Vulnerability, Part A: Global and Sectoral Aspects. Organization & Environment, 24(3), 1–44.

Francés, F., & Benito, J. (1995). La modelación distribuida con pocos parámetros de las crecidas. Ingeniería Del Agua, 2(4), 7–24.

Francés, F., Upegui, J. V., Múnera, J. C., Medici, C., & Bussi, G. (2017). Description of the distributed conceptual hydrological model TETIS V.8. Valencia.

Francés, F., Vélez, J. I., & Vélez, J. J. (2007). Split - parameter structure for the automatic calibration of distributed hydrological models. Journal of Hydrology, 332, 226–240.

Ghaffari, G., Keesstra, S., Ghodousi, J., & Ahmadi, H. (2010). SWAT-simulated hydrological impact of land-use change in the Zanjanrood basin, Northwest Iran. Hydrological Processes, 24(7), 892–903.

Gijsman, A. J. (1992). Deforestation and land use: changes in physical and biological soil properties in relation to sustainability - tropenbos international. Wageningen: Department of Soil Science and Geology.

Goldewijk, K. K., & Ramankutty, N. (2010). Land use changes during the past 300 years. London, UK. 1.

Gupta, A. (2011). Tropical geomorphology (1st ed.). New York: Cambridge University Press.

Gyamfi, C., Ndambuki, J., & Salim, R. (2016). Hydrological responses to land use/cover changes in the Olifants basin, South Africa. Water, 8(12), 588.

Hammer, W. I. (1981). Second Soil Conservation Consultant Report.

Hannah, L. (2015). Climate Change Biology. (Elsevier, Ed.) (Second edi). Oxford.

Hansen, J., Sato, M., Ruedy, R., Lo, K., Lea, D. W., & Medina-Elizade, M. (2006). Global temperature change. Proceedings of the National Academy of Sciences of the United States of America, 103(39), 14288–14293.

Happ, M. (2014). Impacts of land-cover change and high rainfall on soil erosion among three farms in Cerro Punta, Chiriquí, Panamá. Independent Study Project (ISP) Collection. Panama: College of Wooster.

Harlan, D., Wangsadipura, M., & Munajat, C. M. (2009). Penentuan debit harian menggunakan pemodelan rainfall runoff GR4J untuk analisa unit hidrograf pada DAS Citarum Hulu. Jurnal Teknik Sipil, 16(1), 1–12.

Hempel, S., Frieler, K., Warszawski, L., Schewe, J., & Piontek, F. (2013). A trend-preserving bias correction &ndash; the ISI-MIP approach. Earth System Dynamics Discussions, 4(1), 49–92.

Hidayat, Y., Murtilaksono, K., Wahjunie, E. D., & Panuju, D. R. (2013). The characteristics of river discharge of Citarum Hulu. Jurnal Ilmu Pertanian Indonesia (JIPI), 18(2), 109–114.

Hooke, R. L. (2012). Land transformation by humans: A review. GSA Today, 22(12).

Houghton, R. A. (2008). Carbon flux to the atmosphere from land use changes: 1850–2005. In: A Compendium of Data on Global Change. Carbon Dioxide Information Analysis Center. Oak Ridge National Laboratory, US Department of Energy, Oak Ridge, TN, USA.

Huebener, H., Cubasch, U., Langematz, U., Spangehl, T., Niehörster, F., Fast, I., & Kunze, M. (2007). Ensemble climate simulations using a fully coupled ocean-troposphere-stratosphere general circulation model. Philosophical Transactions of the Royal Society A: Mathematical, Physical and Engineering Sciences, 365(1857), 2089–2101.

Hunt, J. D., Stilpen, D., & de Freitas, M. A. V. (2018, May 1). A review of the causes, impacts and solutions for electricity supply crises in Brazil. Renewable and Sustainable Energy Reviews. Elsevier Ltd.

ICALRRD. (1993). Laporan hasil penelitian optimalisasi penggunaan lahan daerah aliran sungai (DAS). Departemen Pertanian, Badan Penelitian dan Pengembangan Pertanian.

Ines, A. V. M., & Hansen, J. W. (2006). Bias correction of daily GCM rainfall for crop simulation studies. Agricultural and Forest Meteorology, 138(1–4), 44–53.

IPCC. (2014). Summary for Policy Maker, Climate Change 2014: Impacts, Adaptation and Vulnerability -. IPCC (Intergovernmental Panel on Climate Change).

Jepson, P., & Whittaker, R. J. (2002). Ecoregions in Context: a Critique with Special Reference to Indonesia. Conservation Biology, 16, 42–57.

Julian, M. M., Fink, M., Fischer, C., Krause, P., & Flügel, W.-A. (2013). Implementation of J2000 hydrological model in the Western part of Java Island, Indonesia. The Journal of MacroTrends in Applied Science, 1(1), 1–25.

Julien, P., & Rojas, R. (2002). Upland erosion modeling with CASC2D-SED. International Journal of Sediment Research, 17(4), 265–274.

Julien, P. Y. (2010). Erosion and sedimentation (2nd ed.). Cambridge: Cambridge University Press.

Khan, N., Shahid, S., Ahmed, K., Ismail, T., Nawaz, N., & Son, M. (2018). Performance assessment of general circulation model in simulating daily precipitation and temperature using multiple gridded datasets. Water (Switzerland), 10(12).

Khoi, D. N., & Suetsugi, T. (2014). The responses of hydrological processes and sediment yield to land-use and climate change in the Be river catchment, Vietnam. Hydrological Processes, 28(3), 640–652.

Kiersch, B. (2000). Land Use Impact on Water Resources: A Literature Review. Land and Water Development Division. Rome.

Kilinc, M., & Richardson, E. (1973). Mechanics of soil erosion from overland flow generated by simulated rainfall.

Kim, J., Choi, J., Choi, C., Park, S. (2013). Impacts of changes in climate and land use/land cover under IPCC RCP scenarios on streamflow in the Hoeya River Basin, Korea. Elsevier Enhanced Reader.

Klein Goldewijk, K., Beusen, A., van Drecht, G., De Vos, M. (2011). The HYDE 3.1 spatially explicit database of human-induced land-use change over the past 12,000 years. Glob Ecol Biogeogr, 20(1), 73–86

Klemes, V. (1986). Operational testing of hydrological simulation models. Hydrological Sciences Journal, 31(1), 13–24.

Kottegoda, N., & Rosso, R. (2008). Applied statistics for civil and environmental engineers (Second). Milan, Italy: The McGraw-Hill Companies, Inc.

Kundzewicz, Z. W., Mata, L. J., Arnell, N., Döll, P., Kabat, P., Jiménez, B., … Shiklomanov, I. (2007). Freshwater resources and their management. In: Parry, M.L., Canziani, O.F., Palutikof, J.P., van der Linden, P.J., Hanson, C.E. (Eds.),. In C. ambridge University Press (Ed.), Climate Change 2007: Impacts, Adaptation and Vulnerability. Contribution of Working Group II to the Fourth Assessment Report of the Intergovernmental Panel on Climate Change (pp. 173–210).

Kuntoro, A. A., Cahyono, M., & Soentoro, E. A. (2018). Land cover and climate change impact on river discharge: case study of upper Citarum river basin. Journal of Engineering and Technological Sciences, 50(3), 364–381.

Kusuma, M. S. B., Kuntoro, A. A. and Silasari, R. (2011). Preparedness effort toward climate change adaptation in Upper Citarum river basin, West Java, Indonesia.

Lal, R. (2017). Soil erosion research methods. New York.

Lambert, M. (2017). Impact of sea ice cover and thickness on the regional climate model MAR simulations over the Arctic-CORDEX domain.

Leander, R., Adri Buishand, T., Van Den Hurk, B. J. J. M., & De Wit, M. J. M. (2008). Estimated changes in flood quantiles of the river Meuse from resampling of regional climate model output. Journal of Hydrology, 351, 331–343.

Leander, R., & Buishand, T. A. (2007). Resampling of regional climate model output for the simulation of extreme river flows.

Legesse, D., Coulumb, C. V., & Gasse, F. (2003). Hydrological response of a catchment to climate and land use changes in Tropical Africa: case study South Central Ethiopia. Journal of Hydrology, 275(1–2), 67–85.

Leh, M., Bajwa, S., & Chaubey, I. (2013). Impact of land use change on erosion risk: an integrated remote sensing, geographic information system and modeling methodology. Land Degradation & Development, 24(5), 558-572.

Lenderink, G., Buishand, A., & Deursen, W. van. (2007). Estimates of future discharges of the river Rhine using two scenario methodologies: direct versus delta approach.

López-Moreno, J. I., Zabalza, J., Vicente-Serrano, S. M., Revuelto, J., Gilaberte, M., Azorin-Molina, C., … Tague, C. (2014). Impact of climate and land use change on water availability and reservoir management: Scenarios in the Upper Aragón River, Spanish Pyrenees. Science of The Total Environment, 493, 1222–1231.

Lubis, N. H. (2000). Sejarah kota-kota lama di Jawa Barat. Alqaprint Jatinangor.

M.A. Nearing. (2001). Potential changes in rainfall erosivity in the U.S. with climate change during the 21st century. Journal of Soil and Water Conservation, 56, 229–232.

Ma, X., Xu, J., Luo, Y., Aggarwal, S. P., & Li, J. (2009). Response of hydrological processes to land-cover and climate changes in Kejie watershed, south-west China. Hydrological Processes, 23(8), 1179–1191.

Ma, X., Xu, J., & van Noordwijk, M. (2010). Sensitivity of streamflow from a Himalayan catchment to plausible changes in land cover and climate. Hydrological Processes, 24(11), 1379–1390.

Maeda, E. E., Pellikka, P. K. E., Siljander, M., & Clark, B. J. F. (2010). Potential impacts of agricultural expansion and climate change on soil erosion in the Eastern Arc Mountains of Kenya. Geomorphology, 123(3–4), 279–289.

Mal, S., Singh, R. B., & Huggel, C. (Eds.). (2018). Climate Change, Extreme Events and Disaster Risk Reduction. Cham: Springer International Publishing.

Marhaento, H., Booij, M. J., & Hoekstra, A. Y. (2018a). Hydrological response to future land-use change and climate change in a tropical catchment. Hydrological Sciences Journal, 1368–1385.

Marhaento, H., Booij, M. J., & Hoekstra, A. Y. (2018b). Hydrological response to future land-use change and climate change in a tropical catchment. Hydrological Sciences Journal, 1368–1385.

M Syahril Badri, K., Kuntoro, A. A., & Silasari, R. (2011). Preparedness Effort toward Climate Change Adaptation in Upper Citarum River Basin, West Java, Indonesia.

Mauliana, P. (2016). Prediksi kemungkinan prediksi banjir sungai Citarum dengan logika fuzzy hasil algoritma particle Swarm optimization. Jurnal Informatika, 3(2), 269–276.

Maximillian, J., Brusseau, M. L., Glenn, E. P., & Matthias, A. D. (2019). Pollution and Environmental Perturbations in the Global System. In Environmental and Pollution Science (pp. 457–476). Elsevier.

McColl, C., & Aggett, G. (2007). Land-use forecasting and hydrologic model integration for improved land-use decision support. Journal of Environmental Management, 84(4), 494–512.

Meiyappan, P. (2013). The Climate Data Guide: Carbon Emissions from Historical Land-Use and Land-Use Change.

Menzel, L., & Bürger, G. (2002). Climate change scenarios and runoff response in the Mulde catchment (Southern Elbe, Germany). Journal of Hydrology, 267(1–2), 53–64.

Miao, C., Ni, J., Borthwick, A. G. L., & Yang, L. (2011). A preliminary estimate of human and natural contributions to the changes in water discharge and sediment load in the Yellow River. Global and Planetary Change, 76(3–4), 196–205.

Miller, C. R. (1953). Determination of the unit weight of sediment for use in sediment volume computations. Denver: Bureau of reclamation.

Ministry of Public Works. (2011). TA 7189-INO: INSTITUTIONAL STRENGTHENING IN THE 6 CI's RIVER BASIN TERRITORY - PACKAGE B FOR INTEGRATED WATER RESOURCES MANAGEMENT (IWRM). Bandung.

Mir, S. I., Ismail, B. S., & Tayeb, M. A. (2016). Hydrology and sediment loading in a degrading natural lake system in Malaysia. Environmental Earth Sciences, 75(3), 231.

Mkankam Kamga, F. (2001). Impact of greenhouse gas induced climate change on the runoff of the Upper Benue River (Cameroon). Journal of Hydrology, 252(1–4), 145–156.

Mohammad, A. G., & Adam, M. A. (2010). The impact of vegetative cover type on runoff and soil erosion under different land uses. CATENA, 81(2), 97–103.

Molina-Navarro, E., Trolle, D., Martínez-Pérez, S., Sastre-Merlín, A., & Jeppesen, E. (2014). Hydrological and water quality impact assessment of a Mediterranean limno-reservoir under climate change and land use management scenarios. Journal of Hydrology, 509, 354–366.

Molion, L. (1993). Amazonian rainfall and its variability. in: Bonell, M., Hufschmidt, M. M., Gladwell, J. S (eds) Hydrology and water management in the humid tropics : hydrological research issues and strategies for water management. Cambridge University Press, 55–62.

Moore, M. R., Schlegel, E. M., Jahn, J.-M., & Packham, C. (2019). SURVEY OF TROPICAL CYCLONE CLIMATE VARIABLES FROM 1974-2017.

Moriasi, D. N., Arnold, J. G., Van Liew, M. W., Bingner, R. L., Harmel, R. D., & Veith, T. L. (2007a). Model evaluation guidelines for systematic quantification of accuracy in watershed simulations. Transactions of the ASABE, 50(3), 885–900.

Moriasi, D. N., Arnold, J. G., Van Liew, M. W., Bingner, R. L., Harmel, R. D., & Veith, T. L. (2007b). Model evaluation guidelines for systematic quantification of accuracy in watershed simulations. Transactions of the ASABE, 50(3), 885–900.

Moss, R. H., Edmonds, J. A., Hibbard, K. A., Manning, M. R., Rose, S. K., Van Vuuren, D. P., … Wilbanks, T. J. (2010, February 11). The next generation of scenarios for climate change research and assessment. Nature.

Mukundan, R., Pradhanang, S. M., Schneiderman, E. M., Pierson, D. C., Anandhi, A., Zion, M. S., … Steenhuis, T. S. (2013). Suspended sediment source areas and future climate impact on soil erosion and sediment yield in a New York City water supply watershed, USA. Geomorphology, 183, 110–119.

Mushtaq, F., & Lala, M. G. N. (2017). Assessment of hydrological response as a function of LULC change and climatic variability in the catchment of the Wular Lake, J&K, using geospatial technique. Environmental Earth Sciences, 76(22), 760.

Naabil, E., Lamptey, B. L., Arnault, J., Kunstmann, H., & Olufayo, A. (2017). Water resources management using the WRF-Hydro modeling system: Case-study of the Tono dam in West Africa. Journal of Hydrology: Regional Studies, 12, 196–209.

Nagle, G. N., Fahey, T. J., & Lassoie, J. P. (1999). Profile management of sedimentation in tropical watersheds. Environmental Management, 23(4), 441–452.

NASA. (1976). U.S. Standard Atmosphere, 1976. Washington DC: US Government Printing Office.

Nearing, M. A., Jetten, V., Baffaut, C., Cerdan, O., Couturier, A., Hernandez, M., … Van Oost, K. (2005). Modeling response of soil erosion and runoff to changes in precipitation and cover. In Catena (Vol. 61, pp. 131–154).

Nilawar, A. P., & Waikar, M. L. (2019). Impacts of climate change on streamflow and sediment concentration under RCP 4.5 and 8.5: A case study in Purna river basin, India. Science of The Total Environment, 650, 2685–2696.

Noda, K., Yoshida, K., Shirakawa, H., Surahman, U., & Oki, K. (2017). Effect of Land Use Change Driven by Economic Growth on Sedimentation in River Reach in Southeast Asia-A Case Study in Upper Citarum River Basin. Journal of Agricultural Meteorology, 73(1), 2017–2039.

155

Notebaert, B., Verstraeten, G., Ward, P., Renssen, H., & Van Rompaey, A. (2011). Modeling the sensitivity of sediment and water runoff dynamics to Holocene climate and land use changes at the catchment scale. Geomorphology, 126(1–2), 18–31.

Nunes, J. P., Seixas, J., & Keizer, J. J. (2013). Modeling the response of within-storm runoff and erosion dynamics to climate change in two Mediterranean watersheds: A multi-model, multi-scale approach to scenario design and analysis. Catena, 102, 27–39.

Ogden, F., & Heilig, A. (2001). Two-Dimensional Watershed-Scale Erosion Modeling With CASC2D. In Landscape Erosion and Evolution Modeling (pp. 277–320). Boston, MA: Springer US.

Onen, F., & Bagatur, T. (2017). Prediction of Flood Frequency Factor for Gumbel Distribution Using Regression and GEP Model. Arabian Journal for Science and Engineering, 42(9), 3895–3906.

Orchiston, T. S., Monaghan, R. M., & Laurenson, S. (2013). Reducing overland flow and sediment losses from winter forage crop paddocks grazed by dairy cows.

Pal, R., & Pani, P. (2016). Seasonality, barrage (Farakka) regulated hydrology and flood scenarios of the Ganga River: a study based on MNDWI and simple Gumbel model. Modeling Earth Systems and Environment, 2(2).

Peña, L. E., Barrios, M., & Francés, F. (2016). Flood quantiles scaling with upper soil hydraulic properties for different land uses at catchment scale. Journal of Hydrology, 541, 1258–1272.

Piao, S., Friedlingstein, P., Ciais, P., De Noblet-Ducoudré, N., Labat, D., & Zaehle, S. (2007). Changes in climate and land use have a larger direct impact than rising CO_2 on global river runoff trends. Proceedings of the National Academy of Sciences of the United States of America, 104(39), 15242–15247.

Poerbandono, Julian, M. M., & Ward, P. J. (2014). Assessment of the effects of climate and land cover changes on river discharge and sediment yield, and an adaptive spatial planning in the Jakarta region. Natural Hazards, 73(2), 507–530.

Poerbandono, Ward, P. J., & Julian, M. M. (2009). Set up and calibration of a spatial tool for simulating river discharge of Western Java in recent decades: preliminary results and assessments. Journal of Engineering and Technological Sciences, 41(1), 50–64.

Ramankutty, N., Foley, J. (1999). Estimating historical changes in global land cover: croplands from 1700 to 1992. Global Biogeochem Cycles, 13(4), 997–1028

Rees, H. G., & Collins, D. N. (2006). Regional differences in response of flow in glacier-fed Himalayan rivers to climatic warming. In Hydrological Processes (Vol. 20, pp. 2157–2169).

Render, B., Stair, R. M., & Hanna, M. E. (2012). Quantitative Analysis for Management. New Jersey.

Ribolzi, O., Evrard, O., Huon, S., De Rouw, A., Silvera, N., Latsachack, K. O., … Valentin, C. (2017). From shifting cultivation to teak plantation: Effect on overland flow and sediment yield in a montane tropical catchment. Scientific Reports, 7(1).

Ridwan, F., Ardiansyah, M., & Gandasasmita, K. (2017). Modeling Land Use/Cover Change Using Artificial Neural Network and Logistic Regression Approach (Case Study: Citarum Watershed, West Jawa).

Rodriguez-Lloveras, X., Buytaert, W., & Benito, G. (2016). Land use can offset climate change induced increases in erosion in Mediterranean watersheds. CATENA, 143, 244–255.

Rogger, M., Agnoletti, M., Alaoui, A., Bathurst, J. C., Bodner, G., Borga, M., … Blöschl, G. (2017). Land use change impacts on floods at the catchment scale: Challenges and opportunities for future research. Water Resources Research, 53(7), 5209–5219.

Rojas, R., Feyen, L., Dosio, A., & Bavera, D. (2011). Improving pan-European hydrological simulation of extreme events through statistical bias correction of RCM-driven climate simulations. Hydrology and Earth System Sciences, 15(8), 2599–2620.

Salim, A. G., Dharmawan, I. W. S., & Narendra, B. H. (2019). Pengaruh Perubahan Luas Tutupan Lahan Hutan Terhadap Karakteristik Hidrologi DAS Citarum Hulu. Jurnal Ilmu Lingkungan, 17(2), 333.

Saxton, D. K. E., Willey, M. P. H., & Rawls, D. W. J. (2006). Field and pond hydrologic analyzes with the SPAW model. In ASABE Annual International Meeting. Portland, Oregon.

Saxton, K. E., & Rawls, W. J. (2006). Soil water characteristic estimates by texture and organic matter for hydrologic solutions. Soil Sci Soc Am J, 70, 1569–1578.

Schmidli, J. ¨ U., Frei, C., & Vidale, P. L. (2006). DOWNSCALING FROM GCM PRECIPITATION: A BENCHMARK FOR DYNAMICAL AND STATISTICAL DOWNSCALING METHODS. INTERNATIONAL JOURNAL OF CLIMATOLOGY Int. J. Climatol, 26, 679–689.

Singh, J., Knapp, H. V., & Demissie, M. (2004). Hydrologic Modeling of the Iroquois River Watershed Using HSPF and SWAT.

Sinha, R. K., & Eldho, T. I. (2018). Effects of historical and projected land use/cover change on runoff and sediment yield in the Netravati river basin, Western Ghats, India. Environmental Earth Sciences, 77(3), 1–19.

Siswanto, S. Y. (2010). Land degradation assessment in West Java Island, Indonesia. 2010.

Siswanto, S. Y., & Francés, F. (2019). How land use/land cover changes can affect water, flooding and sedimentation in a tropical watershed: a case study using distributed modeling in the Upper Citarum watershed, Indonesia. *Environmental Earth Sciences, 78*(17).

Solomon, S., Qin, D., Manning, M., Marquis, M., Averyt, K., Tignor, M. M. B., … Chen, Z.

(2007). Climate Change 2007 The Physical Science Basis. LAND USE, LAND COVER AND SOIL SCIENCES.

Suripin, M. (2001). Pelestarian Sumber Daya Tanah dan Air. Jakarta: Andi.

Tardy, Y., N'kounkou, R., & Probst, J. L. (1989). The global water cycle and continental erosion during Phanerozoic time (570my). American Journal of Science.

Tarigan, S. D., & Tukayo, R. K. (2013). Impact of land use change and land management on irrigation water supply in Northern Java coast. J Trop Soils, 18(2), 169–176.

Terink, W., Hurkmans, R. T. W. L., Torfs, P. J. J. F., & Uijlenhoet, R. (2009). Bias correction of temperature and precipitation data Bias correction of temperature and precipitation data for regional climate model application to the Rhine basin Bias correction of temperature and precipitation data. Hydrol. Earth Syst. Sci. Discuss (Vol. 6).

Teutschbein, C., & Seibert, J. (2010). Regional Climate Models for Hydrological Impact Studies at the Catchment Scale: A Review of Recent Modeling Strategies. Geography Compass, 4(7), 834–860.

Teutschbein, C., & Seibert, J. (2012). Bias correction of regional climate model simulations for hydrological climate-change impact studies: Review and evaluation of different methods. Journal of Hydrology, 456–457, 12–29.

Tommi. (2011). Pengaruh perubahan penggunaan lahan terhadap karakteristik hidrologi DAS Citarum Hulu. IPB (Bogor Agricultural University), Bogor.

Trenberth, K. E., Dai, A., Rasmussen, R. M., & Parsons, D. B. (2003). The changing character of precipitation. Bulletin of the American Meteorological Society.

US EPA National Center for Environmental Assessment, I. O. (2009). Land-Use Scenarios: National-scale housing-density scenarios consistent with climate change storylines. Washington, DC.

Vaighan, A. A., Talebbeydokhti, N., & Bavani, A. M. (2017). Assessing the impacts of climate and land use change on streamflow, water quality and suspended sediment in the Kor River Basin, Southwest of Iran. Environmental Earth Sciences, 76(15), 1–18.

van Vuuren, D. P., Edmonds, J., Kainuma, M., Riahi, K., Thomson, A., Hibbard, K., … Rose, S. K. (2011). The representative concentration pathways: An overview. Climatic Change, 109(1), 5–31.

Varis, O., Kajander, T., & Lemmelä, R. (2004, October). Climate and water: From climate models to water resources management and vice versa. Climatic Change.

Verstraeten, G., Poesen, J., de Vente, J., & Koninckx, X. (2003). Sediment yield variability in Spain: a quantitative and semiqualitative analysis using reservoir sedimentation rates. Geomorphology, 50(4), 327–348.

Wang, W. J., Thompson, F. R., He, H. S., Fraser, J. S., Dijak, W. D., & Spetich, M. A. (2018). Population dynamics has greater effects than climate change on tree species distribution in a temperate forest region. Journal of Biogeography, 45(12), 2766–2778.

Watung, R. L., Tala'ohu, S. H., & Dariah, A. (2005). Change and flood mitigation in Citarum and Kaligarang watersheds. Prosiding Multifungsi Pertanian.

Wheater, H., & Evans, E. (2009). Land use, water management and future flood risk. Land Use Policy, 26, 251–264.

Wibowo, M. (2011). Pemodelan statistik hubungan debit dan kandungan sedimen sungai contoh kasus di DAS Citarum-Nanjung. Jurnal Teknologi Lingkungan, 2(3), 255–260.

Wilson, C. O., & Weng, Q. (2011). Simulating the impacts of future land use and climate changes on surface water quality in the Des Plaines River watershed, Chicago Metropolitan Statistical Area, Illinois. Science of The Total Environment, 409(20), 4387–4405.

Wischmeier, W. H., Johnson, C. B., & Cross, B. V. (1971). A soil erodibility nomograph for farmland and construction sites. Journal of Soil and Water Conservation, 26(189–193).

Wischmeier, W. H., & Smith, D. D. (1961). A universal equation for predicting rainfall-erosion losses: an aid to conservation farming in humid regions. Washington, D.C.: Agricultural Research Service, United States Department of Agriculture.

Wohl, E., Barros, A., Brunsell, N., Chappell, N. A., Coe, M., Giambelluca, T., … Mcdonnell, J. (2012). The hydrology of the humid tropics. Nature Climate Change, 2, 655–662.

Wolf, L., & Collins, J. (2015). Putting Regional Climate Prediction in Reach. Computing in Science and Engineering, 17(5), 49–51.

Xu, C. (2002). Hydrologic models. Sweden: Uppsala University.

Yu, B., Zhang, G., & Fu, X. (2015). Transport capacity of overland flow with high sediment concentration. J. Hydrol. Eng., 20(6), 1–10.

Yulianto, F., Maulana, T., & Khomarudin, M. R. (2018). Analysis of the dynamics of land use change and its prediction based on the integration of remotely sensed data and CA-Markov model, in the upstream Citarum Watershed, West Java, Indonesia. International Journal of Digital Earth, 12(10), 1151–1176.

Yulianto, F., Suwarsono, S., & Sulma, S. (2019). Improving the accuracy and reliability of land use/land cover simulation by the integration of Markov cellular automata and landform-based models a case study in the upstream Citarum watershed, West Java, Indonesia. Journal of Degraded and Mining Lands Management, 6(2), 1675–1696.

Yusuf, S. M., Murtilaksono, K., Hidayat, Y., & Suharnoto, Y. (2018). Analysis and prediction

of land cover change in upstream Citarum watershed. Jurnal Pengelolaan Sumberdaya Alam Dan Lingkungan (Journal of Natural Resources and Environmental Management), 8(3), 365–375.

Zare, M., Panagopoulos, T., & Loures, L. (2017). Simulating the impacts of future land use change on soil erosion in the Kasilian watershed, Iran. Land Use Policy, 67, 558–572.

Zhang, L., Dawes, W. R., & Walker, G. R. (2001). Response of mean annual evapotranspiration to vegetation changes at catchment scale. Water Resources Research, 37(3), 701–708.